NASA CR-145103

National Aeronautics and Space Administration

CONFIGURATION DEVELOPMENT STUDY OF THE X-24C HYPERSONIC RESEARCH AIRPLANE -PHASE III

H G Combs, et al
Lockheed Aircraft Corporation
Advanced Development Projects

January 1977

Prepared for

NATIONAL AERONAUTICS AND SPACE ADMINISTRATION
Langley Research Center
Hampton, Virginia 23665

SUPPLEMENTAL DATA

NASA CR-145103

X77.10016

CONFIGURATION DEVELOPMENT STUDY OF THE X-24C HYPERSONIC RESEARCH AIRPLANE

- PHASE III -

H. G. Combs, et al
Lockheed Aircraft Corporation
Advanced Development Projects
January 1977

Page 54, Aerodynamic Analysis, Supplemental Information

Nozzle Flap Used in Aerodynamic Analysis

The Phase III configuration on which the longitudinal aerodynamic analysis was performed included a deflected nozzle flap not shown in the report. The nozzle flap used for this analysis extends from the scramjet nozzle surface at fuselage station 896 parallel to the lower surface of the wing (-5° to WL 100) to fuselage station 925.

Analysis indicated that the scramjet half-nozzle may act as a very large "elevon," developing excessive nose-up pitching moments along with high trim drag and poor spanwise lift distribution, giving rise to high vortex drag. Analytically, it was found that the "elevon" effect of the nozzle can be corrected by adding the deflected trailing edge flap. It should also be noted that the calculated performance data in the report includes the base drag contribution of the nozzle flap.

NASA CR-145103

National Aeronautics and
Space Administration

CONFIGURATION DEVELOPMENT STUDY OF THE X-24C HYPERSONIC RESEARCH AIRPLANE -PHASE III

H G Combs, et al
Lockheed Aircraft Corporation
Advanced Development Projects
January 1977

Prepared for

NATIONAL AERONAUTICS AND SPACE ADMINISTRATION
Langley Research Center
Hampton, Virginia 23665

FOREWORD

This Analytical Study Report is submitted to the National Aeronautics and Space Administration in accordance with NASA Contract NAS-1-14222. The work reported herein was performed between May 1976 through August 1976 culminating in oral presentations at NASA LRC on 24 August 1976, to USAF personnel at Wright Patterson AFB on 26 August 1976 and at NASA, Dryden on 27 September 1976. The study was performed by the Advanced Development Projects "Skunk Works" of the California Company, a Division of Lockheed Aircraft, under the supervision of Mr. H.G. Combs, Study Manager. Engineering graphics and supporting text were developed under the direction of Messrs. D.H. Campbell (Propulsion and Thermodynamics), M.D. Cassidy (Aerodynamics), C.D. Sumpter (Structures), E.B. Seitz (Weights), and G.J. Kachel and R.P. James (Vehicle Design). The program monitor for NASA was Mr. J.D. Watts.

The three phased study was a co-operative effort between the contractor and NASA in which data and frequent consultation, as well as program direction were provided by NASA.

SUMMARY

Results of the conclusions which evolved from the three phased study on the configuration development of the X-24C Hypersonic Research Airplane make it evident that it is practical to design and build the high performance National Hypersonic Flight Research Facility airplane with todays state of the art within the cost and operational constraints established by NASA.

This final study phase covers the refinement of the vehicle, selected from the prior Phase II Study, into a vehicle which met the constraints, performance and cost requirements as projected by the Phase II Study.

The vehicle launched at 31.75 Mg from the B-52 can cruise for 40 seconds at Mach 6.78 on scramjets, has the off design capability of approaching Mach 8 with a 453.6 kg payload, or 70 seconds of cruise at Mach 6 with a 2.27 Mg payload, without scramjets.

Costs of a two vehicle program can be ketp within $70M in January 1976 dollars, including spares, AGE, and data, but excluding engines and other GFE. A reduced program costs can be achieved by a vehicle scaled to a lesser launch mass and lesser capability.

The International System of Units, NASA-SP-7012, was used in deriving all units of measurement used in this report.

TABLE OF CONTENTS

LIST OF FIGURES

LIST OF FIGURES (Continued)

LIST OF FIGURES (Continued)

LIST OF FIGURES (Continued)

LIST OF FIGURES (Continued)

LIST OF TABLES

INTRODUCTION

As a result of the conclusions evolved from the three phased study on the configuration development of the X-24C Hypersonic Research Airplane, it is evident that it is practical to design and build the high performance NHFRF airplane with todays state of the art within the cost and operational constraints established by NASA.

This report covers the last segment, Phase III, of the study to refine the vehicle, selected from the Phase II study, into a vehicle meeting the constraints, performance and cost requirements as projected by the Phase II Study.

The Phase II Study, covered in Reference 1, examined the performance growth, of the design concepts, and attendant costs associated with the increase in performance of the vehicle concepts derived from the Phase I Study. The Phase II configuration definition selected for the Phase III Study included: (1) a launch mass of 31751 Kg maximum, (2) a propulsion system consisting of an LR-105 Atlas engine and 12 LR-101 Sustainer engines, and (3) a Lockalloy heat-sink structure/thermal protection system.

The Phase I Study, Reference 2, concluded: (1) the LR-105 engine with 12 LR-101 Sustainers, using RP fuel and LOX to be significantly better than the LR-99 for the X-24C on a performance basis, (2) the Lockalloy heat-sink vehicle and elastomeric Ablator covered aluminum vehicle to be approximately equal in acquisition cost and mass, (3) the LI-900 RSI Space Shuttle type insulator covered aluminum vehicle to be more expensive and lighter in mass than the Lockalloy or elastomeric Ablator vehicle, (4) that the risks using Lockalloy material were procurement oriented and would be pretty well out of the way before X-24C flight, (5) risks, in using elastomeric Ablator, would continue throughout the life use cycle, and (6) Phase II could be done satisfactorily without coming to a firm selection on the type of thermal protection system; all types resulted in approximately the same vehicle mass. Subsequently, Phase I recommended the Phase II Study

carry both the Lockalloy heat-sink and the elastomeric Ablator into the performance growth evaluation in conjunction with the propulsion system consisting of the LR-105 with 12 LR-101 engines. The latter, due to its better growth potential over the LR-99 with 2 LR-11 engines.

This report on the Phase III Study reflects the configuration refinement of concepts and requirements, emanating from the Phase I and II studies, which actually resulted in relatively complete redesign of the Phase II configuration, in order to accomplish all the compromises necessary to establish validity in the Phase III configuration.

BASIS FOR DESIGN REFINEMENT

The objective of the last phase of the X-24C Development Study was to refine the vehicle concept selected at the end of the Phase II study into a vehicle which can meet the constraints, performance and cost requirements as projected by the Phase II Study results.

The requirement is actually a relatively complete redesign, of the Phase II configuration, in order to accomplish all the compromises necessary to establish validity in the vehicle.

As noted in the previous studies the detail analysis and designs, produced in this study, were of sufficient depth to support the conclusions and results of the study, but would necessitate further design and analysis to support a manufacturing effort.

The study was performed on the vehicle configuration and cost constraints emerging from the Phase II Study, Reference 1, which meet the requirements of the NASA Statement of Work (SOW), Reference 3, and the following salient variances.

Aerodynamic Configuration - The aerodynamic configuration, Figure 1, evolved from the NASA baseline configuration, Figure 2 and include the following refinements:

- Deletion of the centerline vertical fin and increase the size of the two side fins to enhance vehicle stability.
- Use of curved sides in lieu of the flat surfaces to aid in carrying longitudinal axial loads in the Lockalloy Monocoque shell construction. This requirement evolved from the Phase I Study, Reference 2.

Research Requirements - The physical constraints dictated by the B-52 launch vehicle necessitated the following payload bay refinements:

- Increase the payload bay from 3.05 meter to 3.66 meter length to provide the scramjet fuel volume and improve the aerodynamic fineness ratio.
- A "single covered" structure rather than the "double covered" structure as used in Phase I and II trades studies is recommended. Performance and payload bay volume, for this vehicle, are so important that the vehicle cannot afford to carry the mass penalty, of the double structure, on missions not requiring the double structure. However, the structure, ahead and behind the payload bay joints, are configured so that a payload bay with a double wall structure can be accommodated if future requirements indicate the need.

Vehicle Operation - B-52 physical constraints were established using B-52 data and B-52 launch station center of gravity limits coordinated with the Boeing Company, in lieu of the constraints dictated by the X-15-2 vehicle.

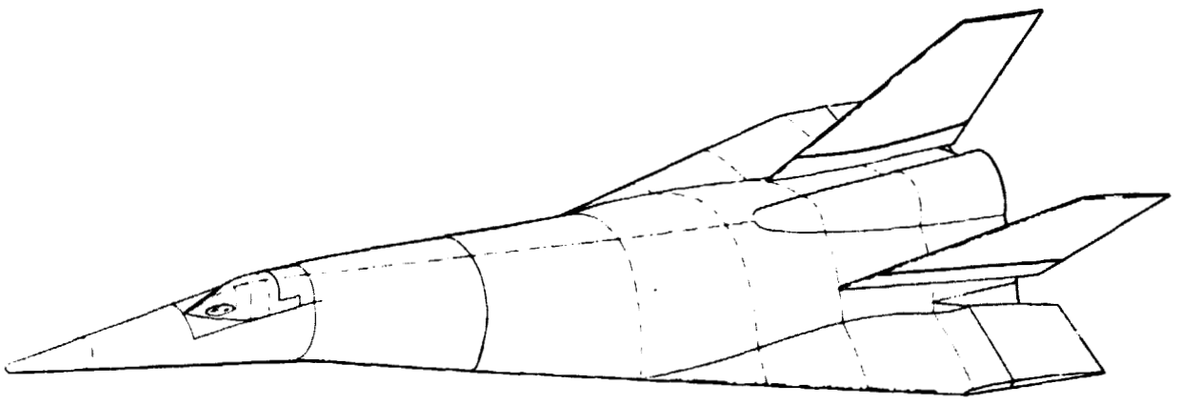

Figure 1 - Phase III Aerodynamic Configuration

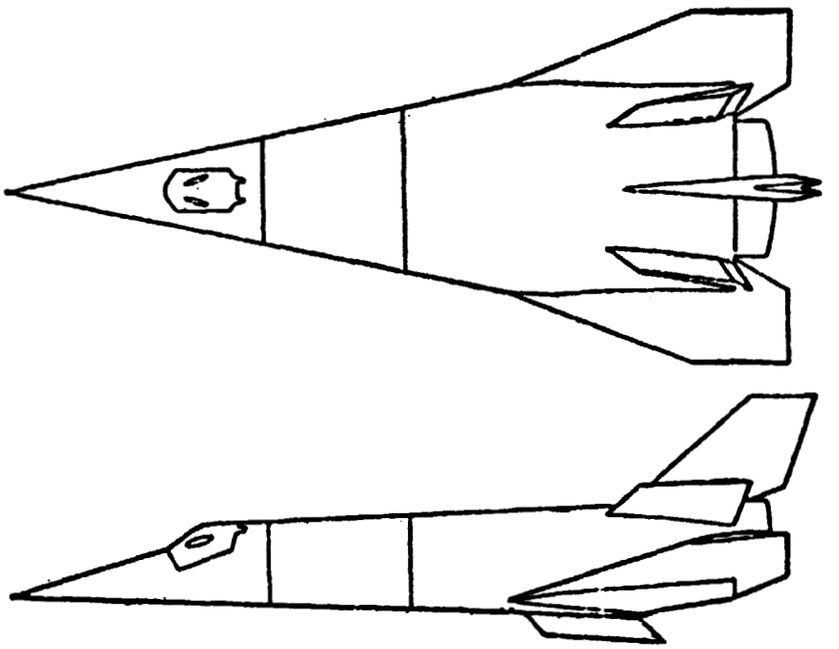

Figure 2 - Baseline Aerodynamic Configuration

CANDIDATE VEHICLE

The vehicle concept selected for Phase III refinement envelopes the various possible vehicles which can accomplish the mission for the NHFRF.

By demonstrating feasibility of the maximum vehicle which can be handled on the B-52 launch platform, it follows that other lesser vehicles can certainly be accommodated. On this basis the concept carried into this study phase and which emanated from the Phase II recommendations include:

- Launch mass of 31.75 Mg with a B-52 launch vehicle
- Lockalloy heat sink structure
- LP-105 plus 12 LR-101 engines as basic propulsion
- Configured to cruise for 40 seconds at q = 47.9 kPa on scramjets (with a 20% thrust margin)
- An interchangeable payload bay for scramjet hydrogen fuel and variety of other experiments
- Configured to be a good test vehicle without scramjets or with other type of propulsion test units.

TECHNICAL APPROACH

A systematic refinement analysis was conducted on the candidate vehicle consisting of the following major task elements:

(1) Refined the aerodynamic configuration considering the design criteria established by NASA and other constraints emanating from the Phase I and II studies.

(2) Developed mission profiles, maximum allowable zero fuel mass and vehicle detail mass in similar manner to the methods employed in the Phase I and II studies.

(3) Refined and updated the structural and system concepts with particular emphasis on:

- Mass
- Performance
- Cost constraints

(4) Produced a recommended version of the X-24C conceptual design utilizing the results from the preceding effort and prior studies (Reference 1 and 2).

(5) Designed and fabricated a 1/30 scale precision wind tunnel model of the final X-24C version.

REALISTIC CONCEPT

The refinement of the Phase III vehicle concept was achieved through a systematic program involving the interactions between the technical disciplines, shown in Figure 3, in conjunction with the results of the two prior studies.

The NASA Baseline configuration was used in Phase I and II as a basis for trade studies involving propulsion, thermal protection, performance and cost. The Baseline Configuration served its purpose and led to valid trade study results. These results can be applied to a refined configuration which is more realistic as a practical research vehicle.

Basic problems, noted during the Phase I and II studies, which handicap the Baseline Configuration include:

o The Baseline Configuration has high cruise drag. This requires a relatively large scramjet package for scramjet cruise.

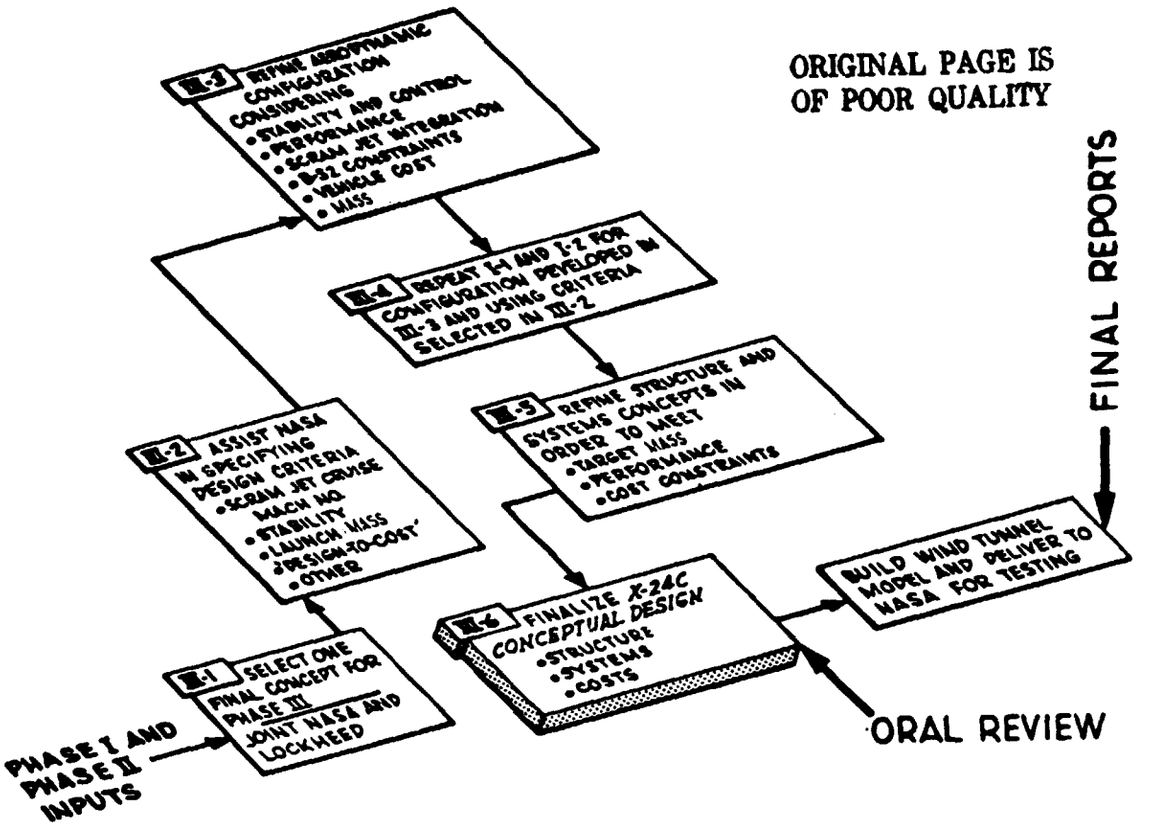

Figure 3 - Program Disciplines

- The scramjet required to cruise the Baseline Configuration will not satisfy the B-52 ground clearance requirements.
- If the Baseline Configuration were kept small enough to allow room for the scramjets, then the internal volume is insufficient to contain the fuel required to accelerate the vehicle to scramjet speeds of Mach 6 or better.
- The Baseline Configuration lift/drag ratio , in landing configuration, is less than needed for handling characteristics at landing.

In order to overcome the problems associated with the Baseline Configuration, it was necessary to significantly redefine the configuration. The principal considerations, affecting the vehicle refinement, included the following:

- The vehicle must be designed for maximum capability at a cost established in the Phase II Study. (Two vehicles, $63.4M, January 1976 Dollars, including spares, AGE, and data but excluding engines and GFE.)
- Vehicle size and mass must fit the B-52 constraints as defined by current Boeing Aircraft studies (Reference NASA Contract NAS4-2319).
- Cross-section area must be minimized in order to reduce drag.
- Length must be sufficient to provide the fuel volume required and improve the fineness ratio.
- Scramjet exit nozzle must be behind the vehicle body so as to not cause additional frontal area drag.
- The aerodynamic shape must be configured so as to keep the aerodynamic "center" aft of the "center of gravity" in order to maintain a stable vehicle.
- The scramjet mass is a very significant part of the vehicle mass empty and will cause a large "center of gravity" shift when removed, unless it can be located near the airplane "center of gravity."

Development of mission profiles and maximum fuel loadings and integration of the scramjet modules with the airframe proceeded simultaneously with the evolution of the final airframe configuration depicted in Figure 4. Characteristic differences between the final configuration and Baseline Configuration is possible by comparing the two superimposed configurations, Figure 5.

Analysis and design details leading to the final X-24C configuration produced by this study are discussed below.

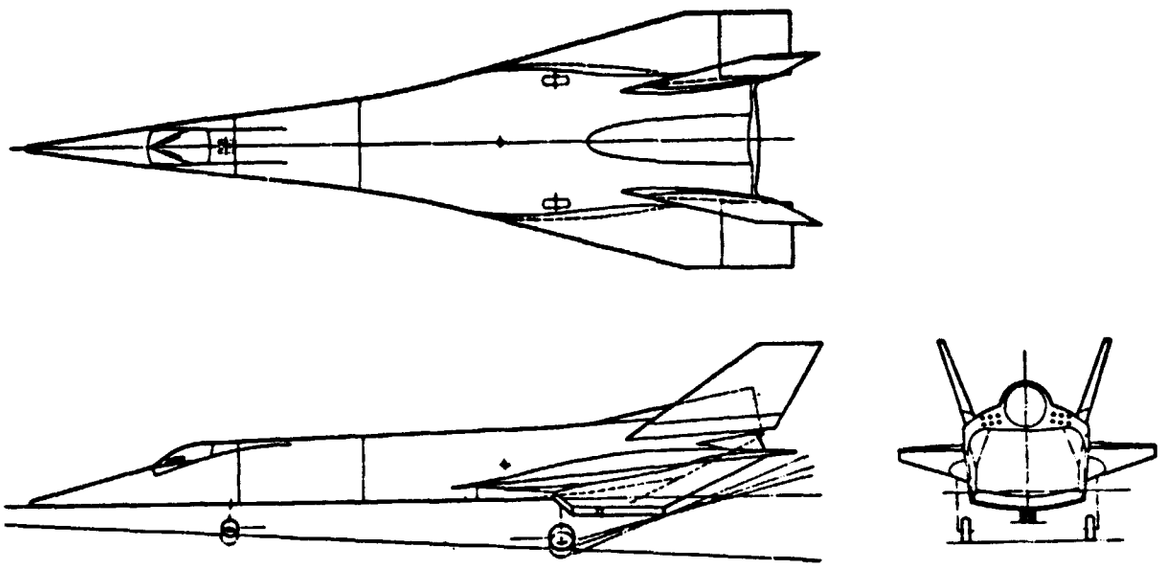

Figure 4 - Airframe Configuration - Final

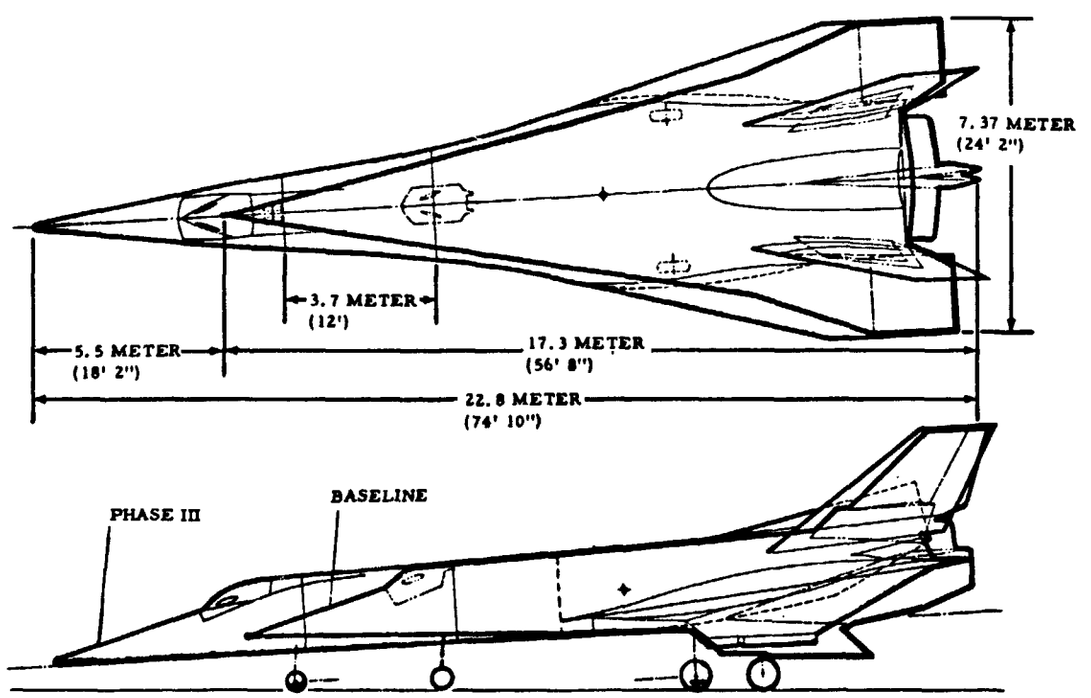

Figure 5 - Baseline and Phase III Configurations - Size Comparison

B-52 Interface

The constraints of the X-24C/B-52 interface are very important in determining a practicable X-24C configuration. The size of the X-24C cross-section is limited to the space available under the wing of the B-52. The length of the X-24C is the primary variable which can be used to satisfy fuel volume and X-24C "fineness ratio" requirements. Figure 6 provides an overview of the B-52 constraints the X-24C was required to accommodate.

Positioning of the X-24C under the B-52, Figure 7, is very critical. The X-24C center of gravity must be located so as to minimize the adverse effects on the B-52 pitch trim. The angle of incidence of the X-24C, on the B-52, was selected to allow scramjet ground clearance with a minimum aerodynamic loading effect on the B-52. X-24C wing span was limited by clearance to the fuselage and the jet wake plume from the B-52 engine pod. Static ground line was determined with the B-52 leaned over with one gear/tire fully compressed.

General Arrangement

The X-24C configuration, Figure 4, is 22.81 meters long, 7.37 meters wing span and 6.27 meters high in ground attitude. The interchangeable payload bay is 3.7 meters long as compared to the 3.05 meters on the Baseline configuration. The length increase compensates for the more slender forebody of the final configuration, and provides the volume required for scramjet hydrogen fuel. The main landing gear is located close enough to the center of gravity so as to protect the nose gear from excessive "slam down."

The scramjet location is positioned to take advantage of the efficient exit nozzle angle, while satisfying ground clearance.

Vertical tails (side fins) are all-moving surfaces and are used as speed brakes, when required, by moving them symmtrically inward at the leading edges.

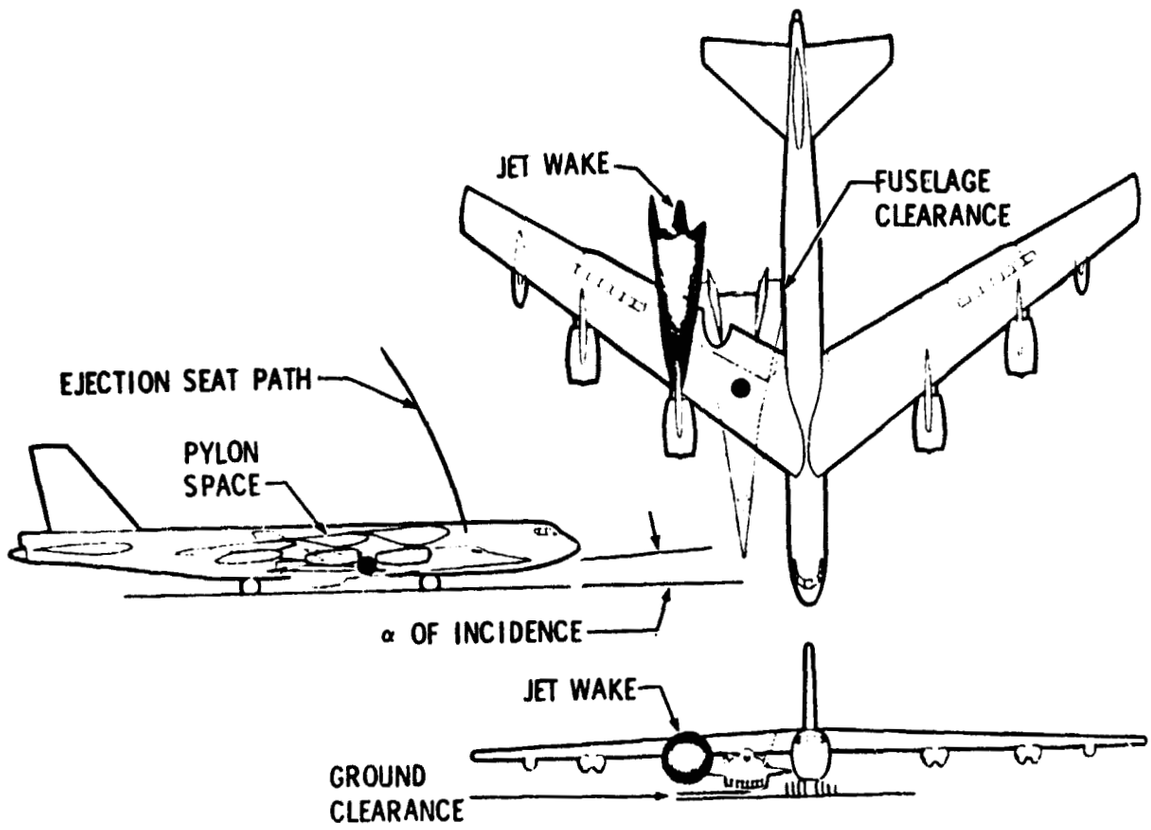

Figure 6 - B-52 Physical Constraints

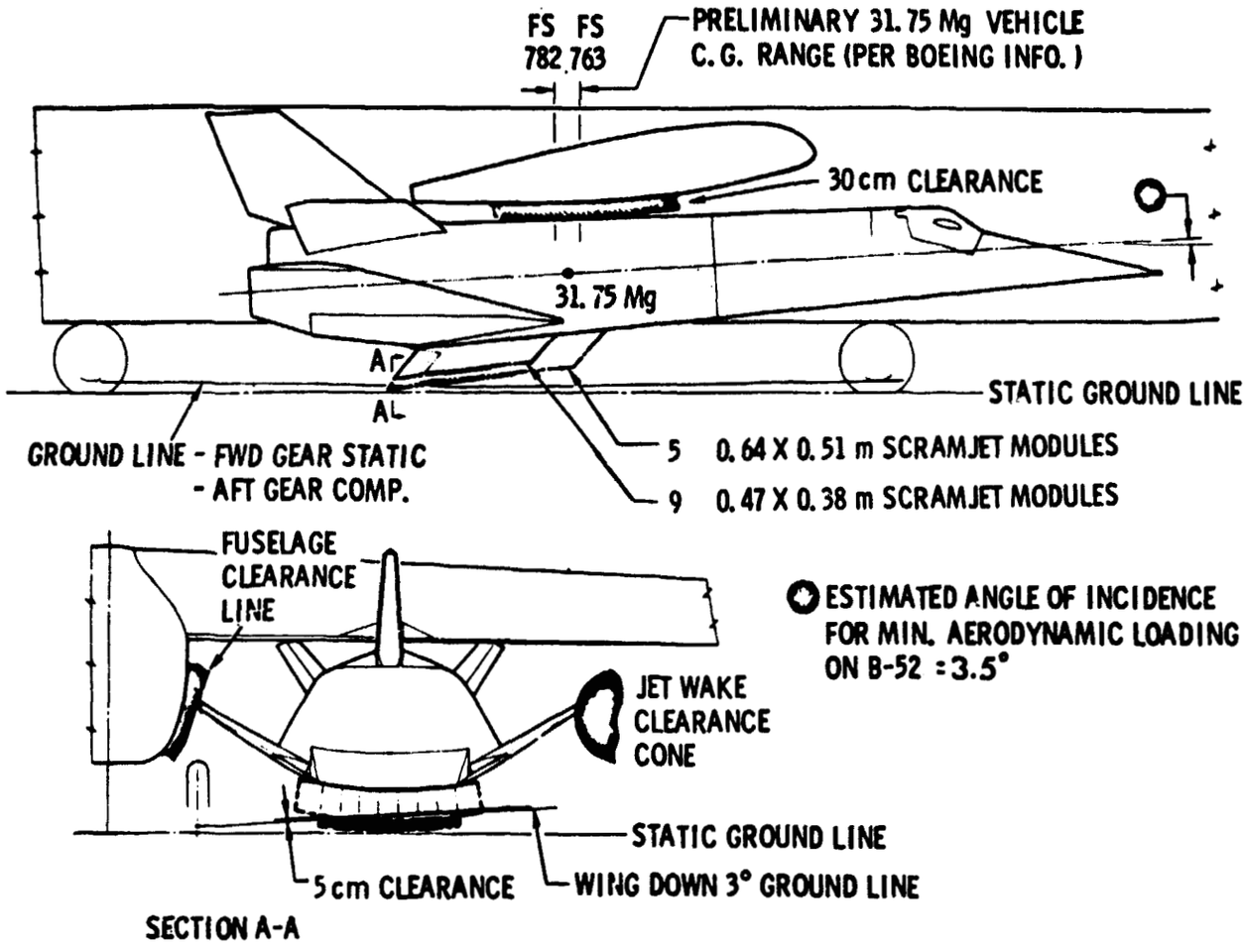

Figure 7 - B-52/X-24C Phase III Interface

The internal arrangement, Figure 8, is established so as to be compatible with its anticipated long life as a research vehicle. The interchangeable payload bay is dept available for a great variety of hypersonic research experiments. The fuel cells are dept separate from the fuselage shell structure in order to allow space for anticipated equipment as well as the unanticipated equipment and test items that will be undoubtedly needed during the life of the vehicle.

Wings, vertical tails (side fins), elevons and payload bay are removable so as to be candidates for becoming special test items.

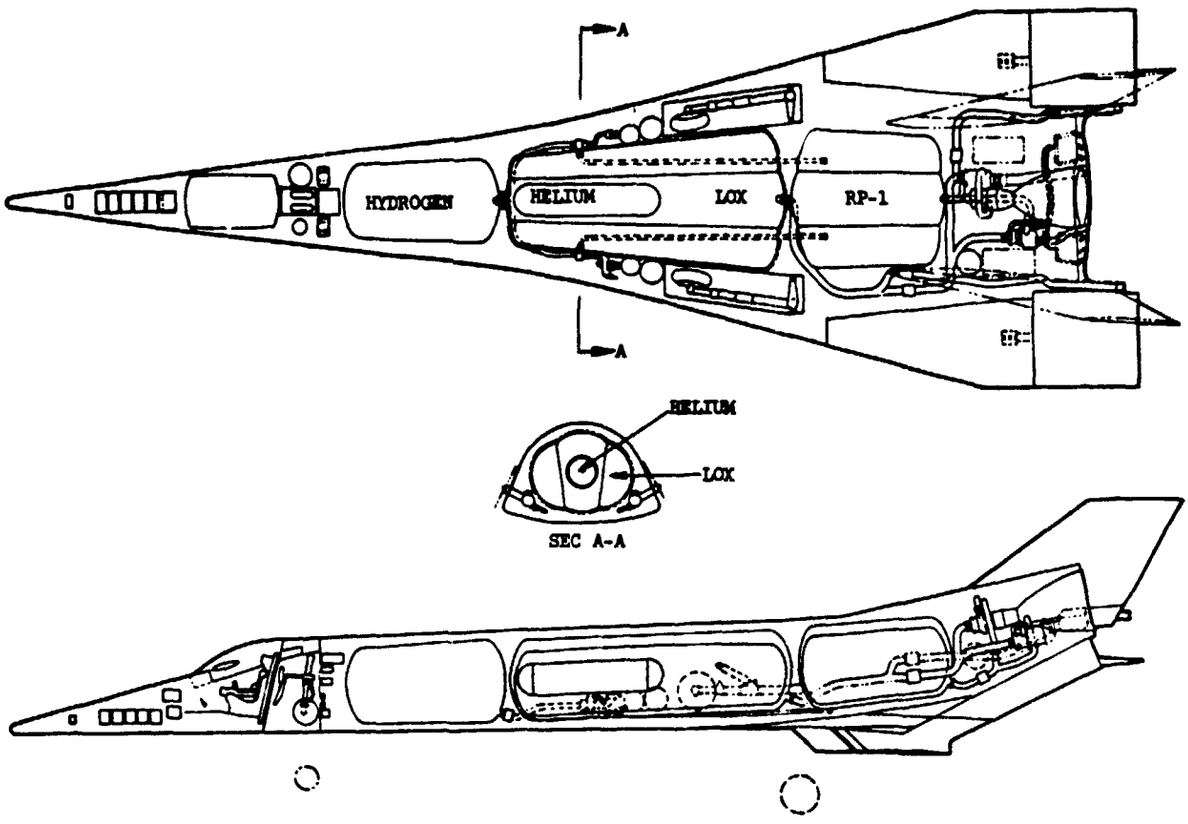

Figure 8 - Internal Arrangement

Structural Arrangement

The X-24C structure is conventional shell structure. The only unusual feature is that Lockalloy is used for the shell covering and as such becomes adequate heat sink for X-24C thermal loads.

The working temperature limit for the Lockalloy is selected as 588.7 K. This means that the Mach 3+ technology already demonstrated by the USAF/ LOCKHEED SR-71 airplane can be directly applied as "state of the art."

The high modulus of elasticity and the low density of Lockalloy make it practical to use a structure of shell and frames with very few longitudinal stringers. This results in a significant part count reduction and associated cost savings.

The Lockalloy skin is installed as removable panels, approximately 0.5 meter by 1.02 meter in size, covering the space from one frame to the adjacent frame. Use of the relatively small panels does not significant increase tooling and production costs, while providing complete access to any part of the vehicle. Thermal stresses in the various components of the shell and frames are kept within limits by selection of proper substructure materials and detail design.

Fuselage - The structural configuration, Figure 9, consists of thick, load-carrying Lockalloy skin supported by frames at (0.48 ±0.025 meter) spacing. The skin panels are spliced together with screws, and screws are used to fasten the surfaces to the substructure. This enables the removal of many of the fuselage surface panels, providing access to the interior.

Main frames are provided at the forward face of the cockpit, forward and aft ends of the payload bay, at the rear attachment points (to the launch vehicle), at the vertical tail rudder post, and the wing rear beam attachment. Longitudinal beams extend along the inboard edge of the lower ventral fins and extend forward as edge members for the main landing gear well inboard wall. On top side, longitudinal beams are provided from the rear attachment points forward, extending over two frames, and rearward for main engine pickup.

Frames from the payload bay aft are configured using the truss concept identified in the Phase I Study, Reference 2. This concept depicted in Figure 10, uses a series of aluminum links bridging between a titanium cap member, attached to the Lockalloy skin panel, and an aluminum cap member opposite the skin inner surface.

Frames forward of the payload bay, depicted in Figure 11, will employ stainless steel or titanium zee section frames as identified in the Phase I Study.

Payload Bay - The 3.7 meter long payload bay, Figure 13, is structurally similar to the main fuselage. Attachment of the bay to the forward and aft fuselage is accomplished through a series of fitting/bolt combinations, located near the inboard skin surface, around the perimeter of the frames. Access for bolt installation or removing is possible by removal of skin panels.

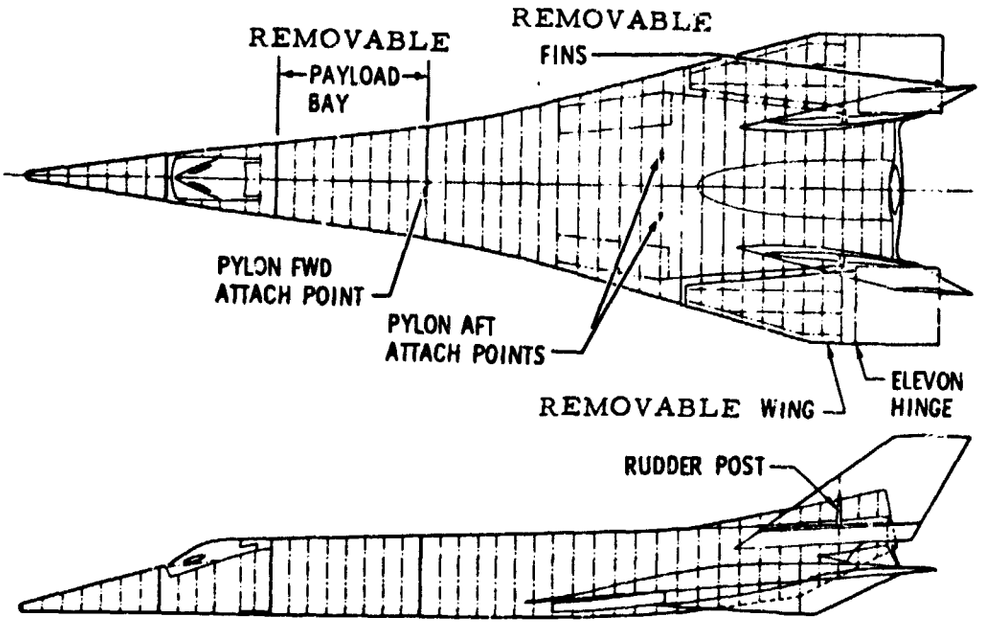

Figure 9 - Structural Arrangement

The payload bay is configured as a "single covered" structure rather than the "double covered" structure as used in the previous studies. Performance and payload volume for this vehicle are so important that it cannot be afforded to carry approximately 190.5 kg of double structure for missions which do not require the double structure. The mass and cost savings, brought about by the "single cover" payload bay, are used to help affect the added size and complexity of the X-24C configuration.

However, the structure, ahead and behind the payload joints, is designed, Figure 12, so that a payload bay with recessed structure can be used if future requirements indicate the need.

Cockpit Structure - The aerodynamic refinement of the vehicle forebody eliminates the need for the cockpit pressure shell used for the Baseline configuration in Phase I and II. A conventional shell structure, Figure 11, will be used.

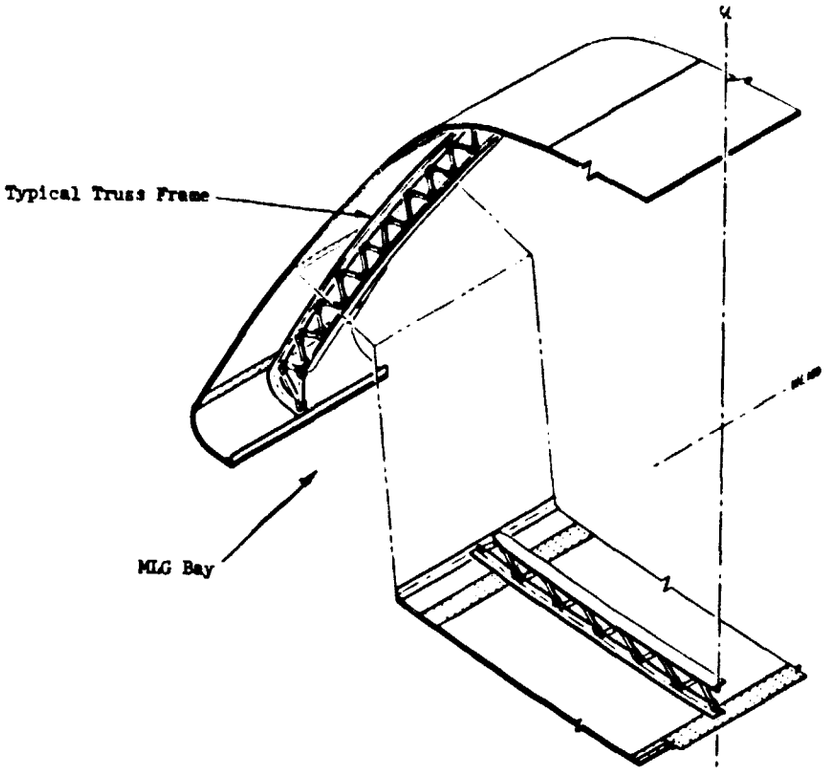

Figure 10 - Typical Frames - Aftbody

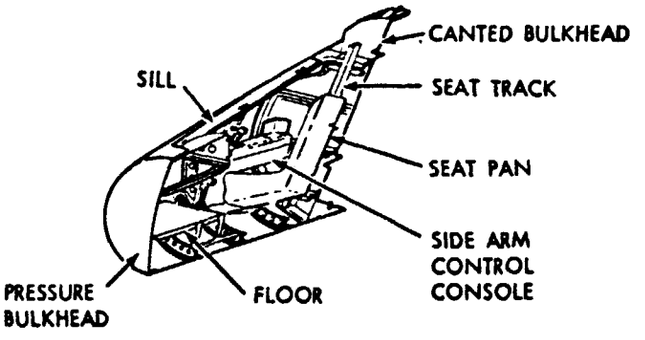

Figure 11 - Typical Structure - Forebody

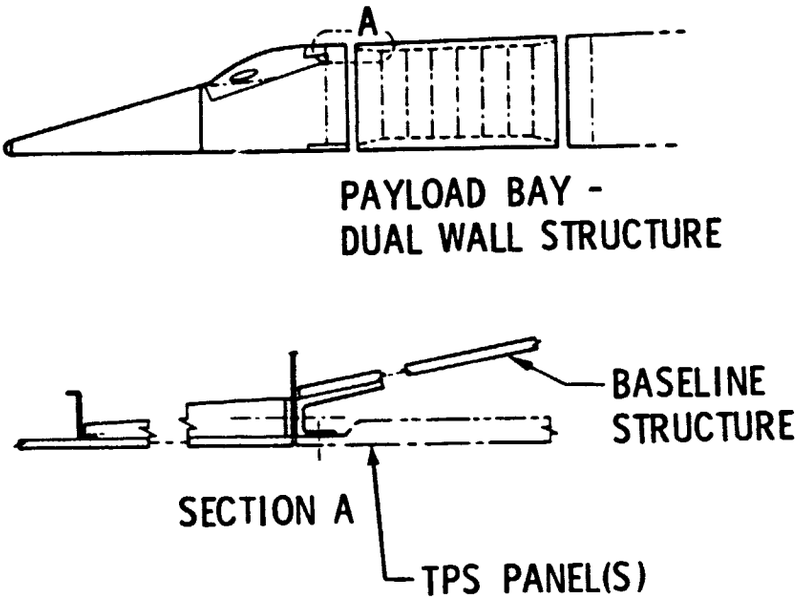

Figure 12 - Payload Bay, Double Wall Concept

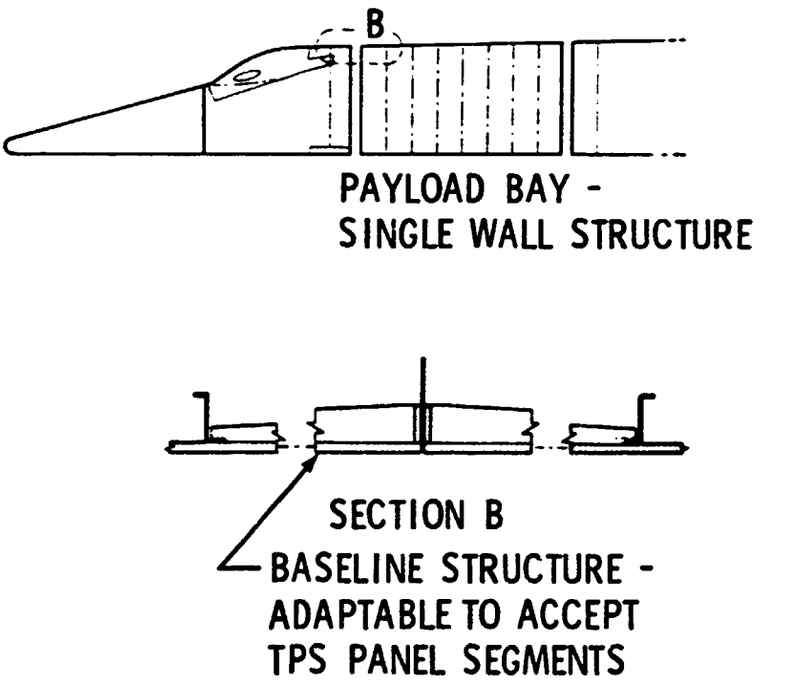

Figure 13 - Payload Bay, Single Wall Concept

Canopy - The canopy concept will be similar to the Lockheed SR-71 design using latching and actuating components where possible. Window panels will be the X-15 high-temperature panels positioned to provide the pilot an optimum viewing point.

Due to the criticalness of pilot vision it is essential that further consideration be given to developing a concept that expands the visibility in the forward sector, especially during the landing approach.

Wings - Wing assemblies, Figure 14, with their elevon control surfaces, will utilize the structural concept used in the YF-12 Ventral Fin, Reference 4. The assembly attaches to the main fuselage through a series of links, Figure 14, allowing for rapid wing replacement and thermal deflections resulting from replacement wings.

Vertical Rudders - The twin all-movable vertical tails are outboard and tilted in order to maintain effectiveness to as high an angle of attack as possible. By rotating them symmetrically inward additional directional stability is achieved and they become effective speed brakes as well.

The vertical tails are structural configured similar to the wing assemblies, Figure 15. Mounting to the vehicle will utilize the same concept employed for the USAF/LOCKHEED SR-71 rudders. A single rudder post extending from the fuselage, Figure 9, is used for attachment of the vertical tail(s) and as the pivot point about which the tail assembly is operated. This design permits rapid replacement for future test vertical tails.

Ventral-Lower - The two ventrals, Figure 15, have been integrated into the aft fuselage to enhance directional stability. In the scramjet role they act as portions of the scramjet module side walls, improve nozzle performance and protect the inboard end of the elevons against turbulence associated with the scramjet exit nozzle. Integration of the ventrals into the scramjet role are described under the Scramjet Installation herein.

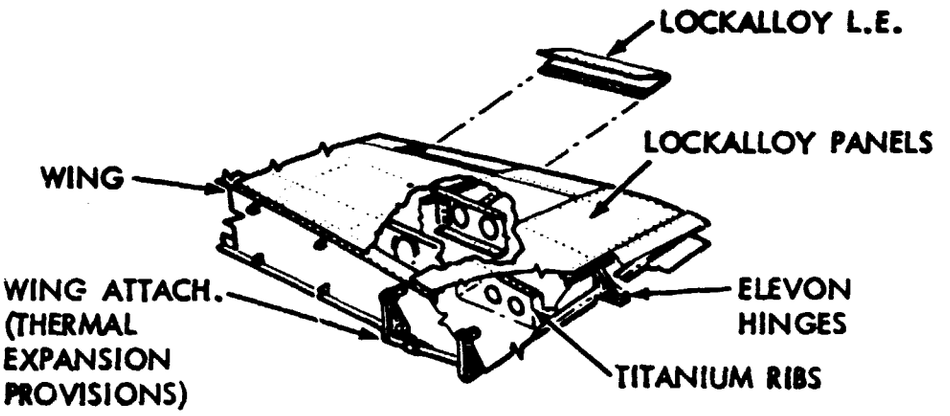

Figure 14 - Wing Installation

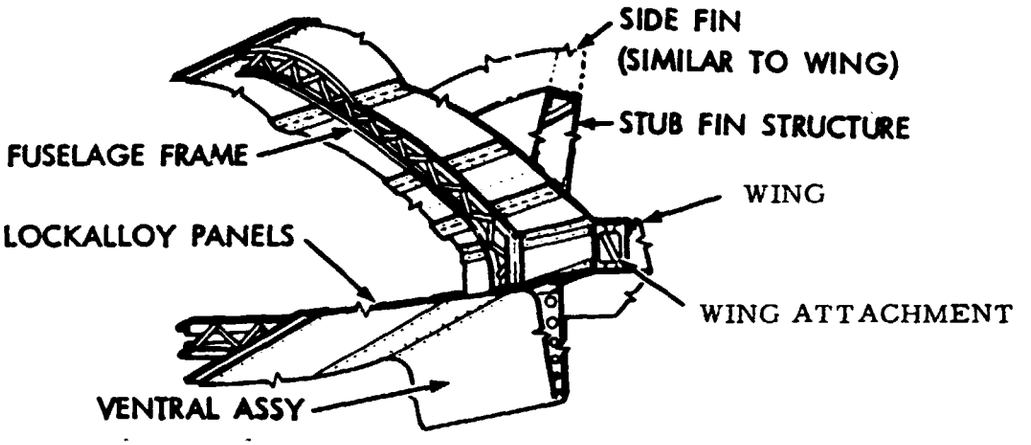

Figure 15 - Wing, Ventral and Side Fin

Nose Landing Gear - Nose gear installation, Figure 16, reflects the C-140A gear selected in the Phase I Study, as off-the-shelf hardware. Retraction, of the nose gear, vertically behind the pilots is accomplished with no effect on the vehicle frontal area. Employment on the X-24C will require a new outer cylinder to provide trunnion pins and extention mechanism attachments compatible with the X-24C.

Main Landing Gear - Main gear installation, Figure 17, reflects the F-106 gear identified in the Phase I Study. While the arrangement is generally similar to

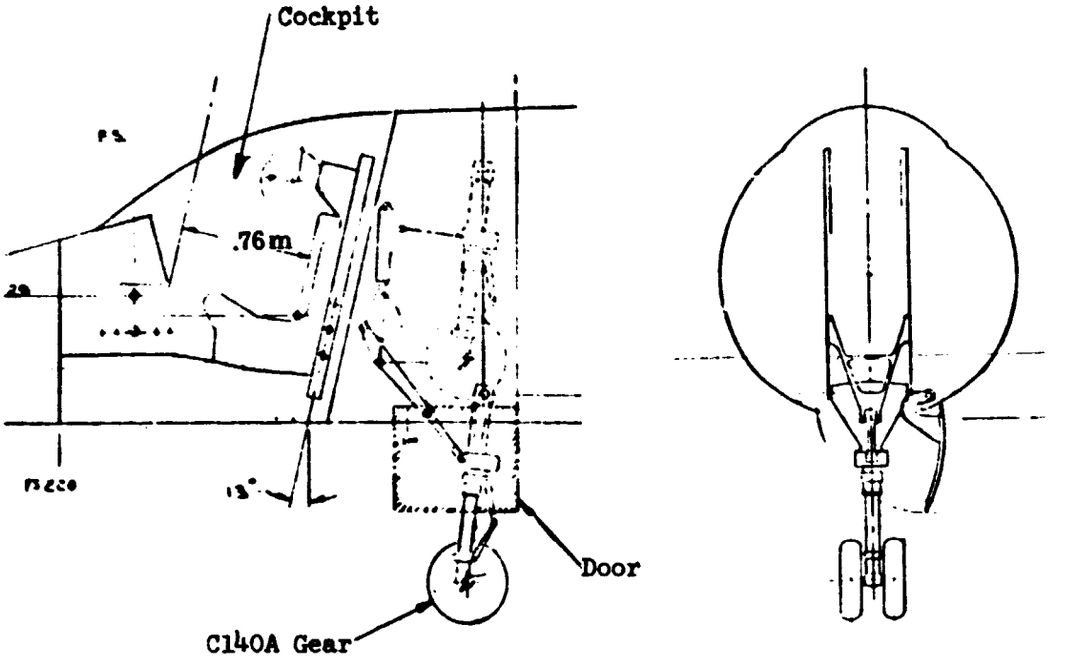

Figure 16 - Nose Landing Gear

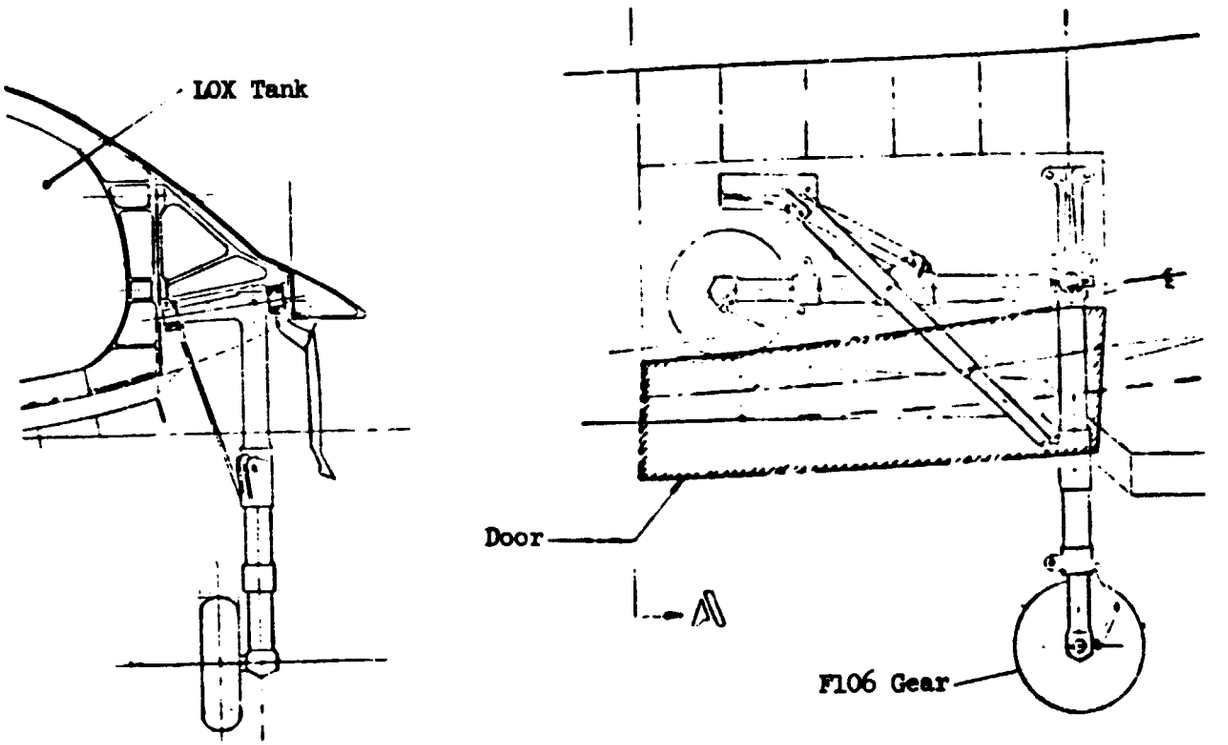

Figure 17 - Main Landing Gear

the arrangement described in Phase I, the gear was moved outboard, approximately 0.25 meters to optimize the propellant tank configuration. Wing-fuselage contour blending has been used to house the forward swinging main landing gear. Aircraft structure, Figure 17, has been configured to transmit the gear trunnion points directly into the vehicle main frames.

Propulsion System

LR-105 Rocket Engine Installation - Engine installation represents a compromise between scramjet exhaust nozzle position, nozzle fixed ramp angle and B-52 clearance requirements.

Engine installation, Figure 18, follows the concept developed in Phase I except for a higher mounting position on the vehicle. This higher position was a consequence of the scramjet nozzle design. The mounting structure consists of two structural beams, criss-crossing in front of the engine, for engine attachment using the same mount provisions used in the Atlas Rocket Configuration. Due to the horizontal engine position, as opposed to the vertical position on the Atlas installation, a new mount towards the engine nozzle end must be provided on the engine to pin the engine to the vehicle engine shroud and reduce the complexity of sealing at this interface which engine deflection, without the support, will produce.

LR-101 Sustainer Engine Installation - Sustainer installation, Figure 18, mounts adjacent to the main engine. Excepting for the higher position of main engine, noted above, the sustainer engines are mounted in the same manner developed in Phase I.

Scramjet Integration

Integration of the scramjet of sufficient size to cruise the vehicle and still remain within the B-52 size constraints was a major driving factor in the X-24C configuration evolution. The X-24C height constraint led to a modular scramjet package which is almost half the allowable vehicle span.

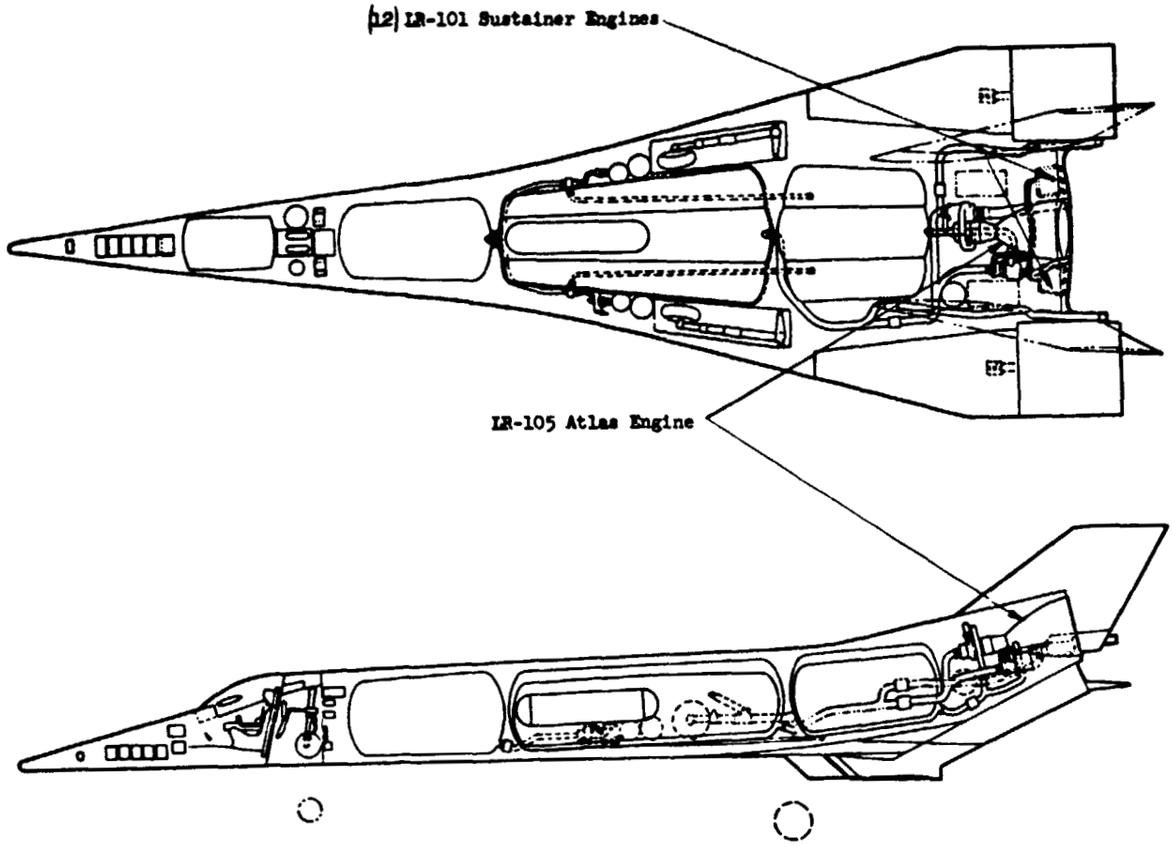

Figure 18 - Propulsion System

The compression surface, Figure 19, forward of the scramjet requires additional width. This compression surface must be of sufficient length and shape to attain flow conditions at the scramjet inlet which are uniform as practical.

To attain the highest level of thrust and minimize the aft center of gravity shift, from the scramjet, a large integrated half nozzle, Figure 19, takes up most of the aft end of the vehicle. The only base area is that required by the main rocket and vernier engines.

Nozzle side walls, Figure 19, doubling as ventrals, in the non-scramjet role, for directional stability improve nozzle performance and protect the inboard end of the elevons.

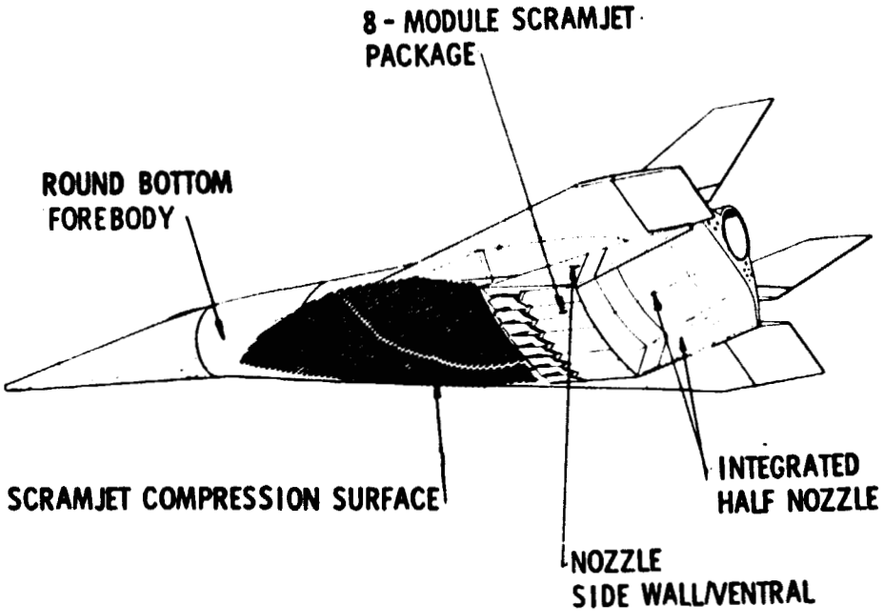

Figure 19 - Scramjet System

The forebody lower surface is rounded rather than extending the scramjet compression surface to the nose to reduce its destabilizing effect on longitudinal stability at hypersonic speeds.

Results of the scramjet studies leading to the final concept can be found in Scramjet Integration and Performance Studies herein.

Scramjet Installation - The scramjet module configuration, based on definitions coordinated between the Garrett Corporation and members of the Lockheed Study Team, attaches to the bottom surface of the vehicle, Figure 20, using a series of truss links between vehicle hardpoints and scramjet module structure, Figure 20. To eliminate the discontinuity in slope at the module/airframe interface, the lower vehicle surface ahead and behind the scramjet module is recon toured in the following manner:

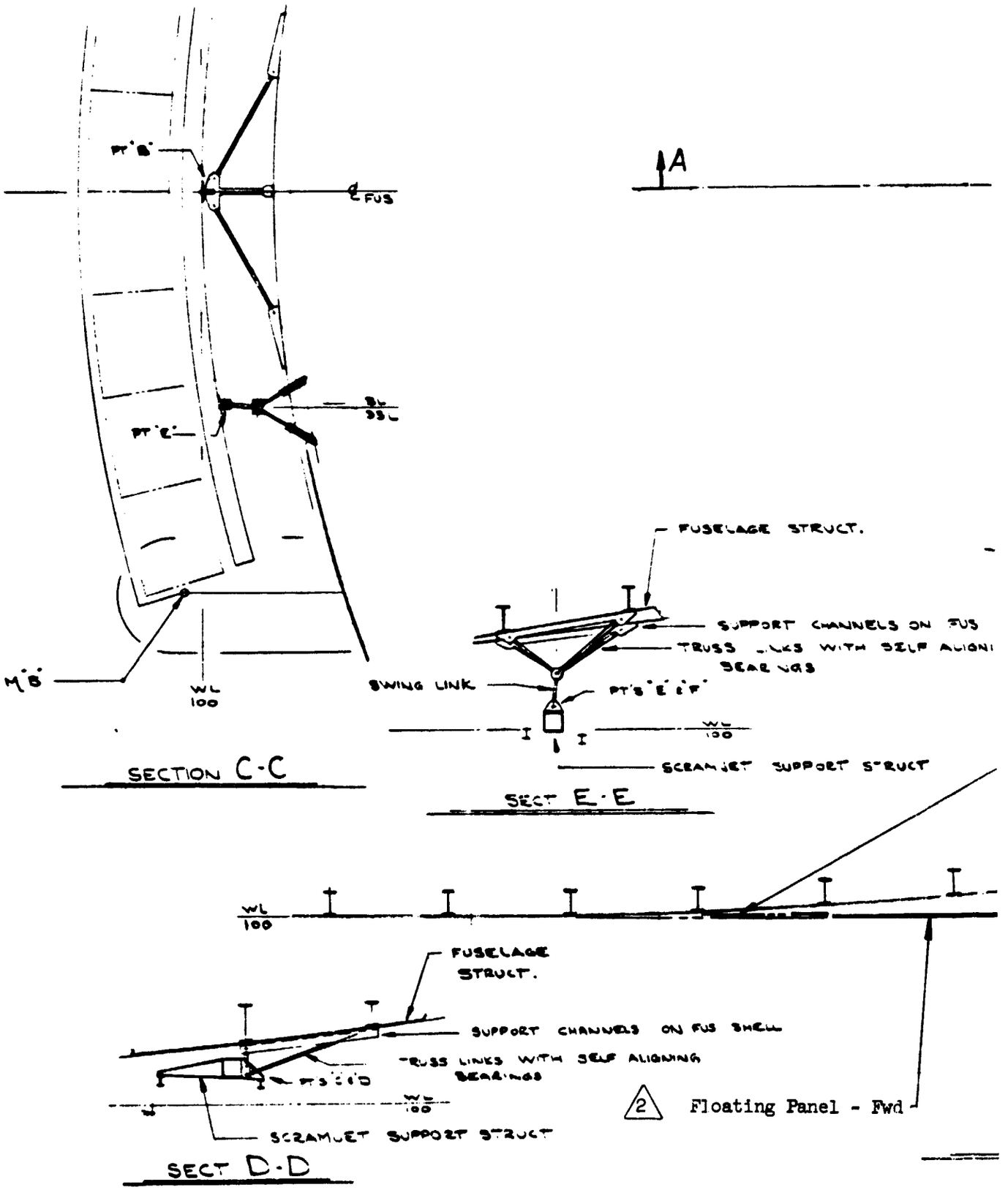

FOLDOUT FRAME 1

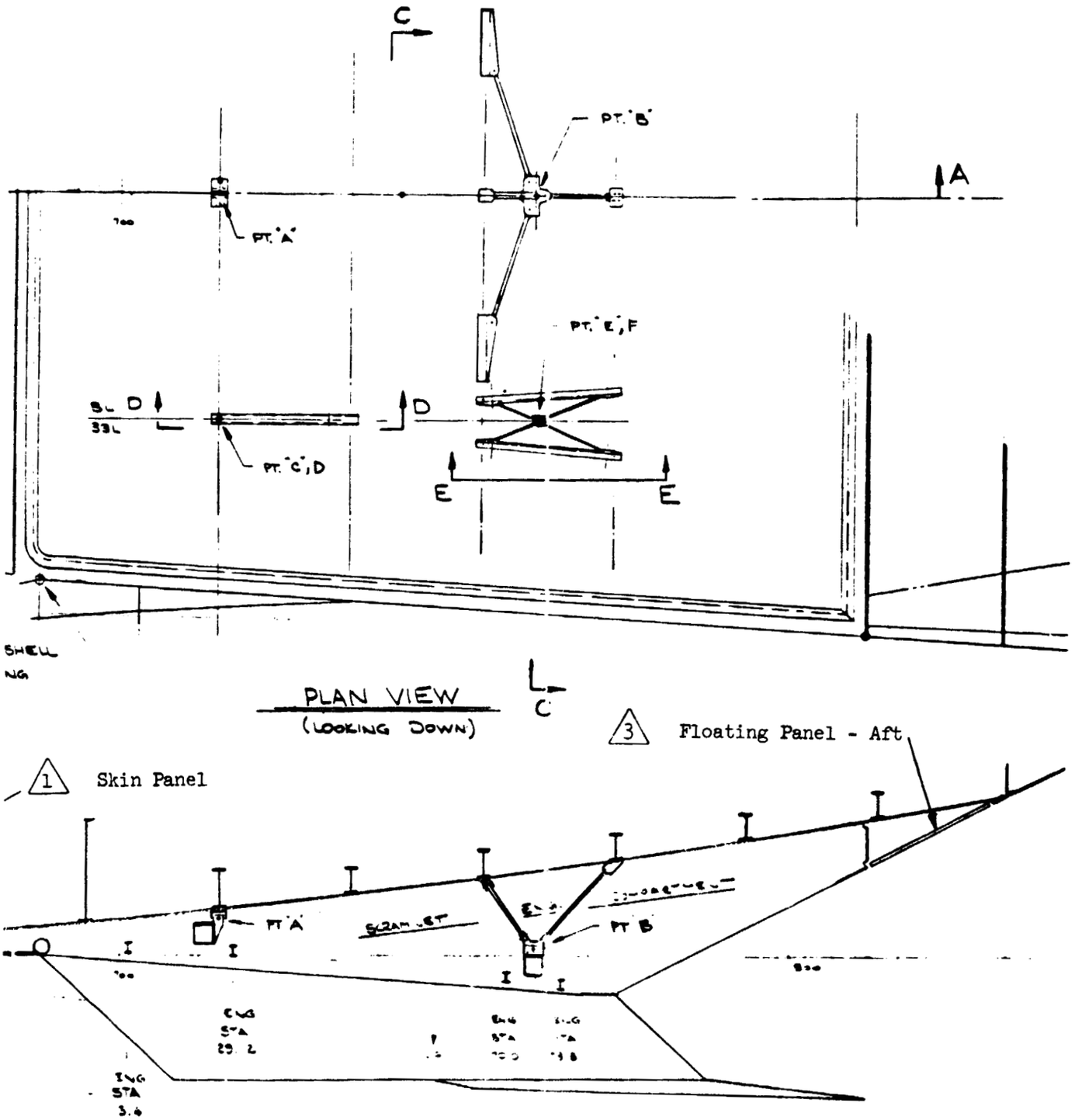

Figure 20 - Scramjet Installation

FOLDOUT FRAME 2

ORIGINAL PAGE IS OF POOR QUALITY

- Skin panel, item (1) on Figure 20, is replaced with a new panel repositioned to the required contour using a series of spacers between the skin panel and existing structural frames.
- A floating panel, item (2) on Figure 20, completes the recontouring between the repositioned panel and scramjet nozzle inlet.
- On the scramjet backside, a floating panel, Figure 20, incorporating ventral segments, completes the blending between the scramjet module and vehicle integrated nozzle and ventral fins.

  (Note: Floating as noted above denotes panel capable of accommodating thermal expansion/contraction between the scramjet module and vehicle.)

Vehicle Change - Scramjet - The inclusion of the scramjet module to the vehicle, tailored for the non-scramjet mission, requires the following changes for the scramjet role:

- The ventrals, item (1) on Figure 21, are removed. The sides of the scramjet module are configured to perform as scramjet nozzle side walls and double as ventrals for directional stability.
- The skin plane, item (2) on Figure 21, representing the integrated half nozzle, sized to accommodate the aerodynamic heat rates in the non-scramjet configuration, must be replaced with a panel sized to accommodate the temperature and turbulence associated with the scramjet exit nozzle.
- Previous structural analysis, identified the need for sizing the vehicle skin panels to provide as close to a linear temperature gradient, between the upper and lower surfaces of the fuselage to minimize the thermal stresses. The most critical thermal loading condition occurs with the scramjet module installed, when the lower vehicle surface, Figure 21, under the scramjet is considerably cooler than the remainder of the shell. To compensate for the change in temperature gradients the skin panel will be replaced with an aluminum panel.

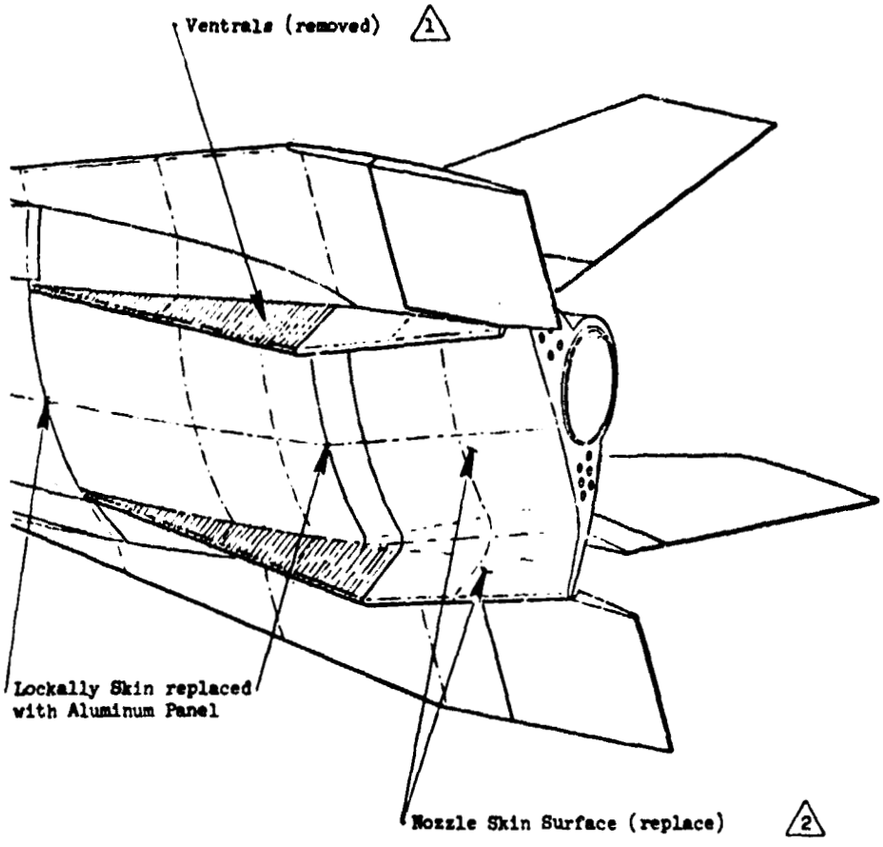

Figure 21 - Vehicle Change for Scramjets

Scramjet System - Approximately 1.6 m^3 of volume exists between the top surface of the scramjet module and vehicle under surface, Figure 20. This volume is partially taken up by the structural mounts for the scramjet. The remaining volume will be used for installation of the coolant and fuel manifolds, coolant regulating valves, fuel valves, bypass valve, pump valve, purge valve, etc., and their associated plumbing lines. Volume efficienty was based on the given state of scramjet system design by NASA and AiResearch.

Better utilization of this volume can be achieved by reviewing the method of scramjet mounting, i. e., making the truss links part of scramjet module and providing the main attach points on the vehicle.

Scramjet/Vehicle Sealing - Previous studies identified sealing between the scramjet module and vehicle as a difficult requirement due to deflections and thermal expansion/contractions which could be expected from the scramjet module. The requirements, Figure 22, are met by the conceptual designs depicted in Figures 23, 24 and 25.

Propellant and Fuel System Installation

Fuel system depicted in Figure 26, is essentially identical to the system described in the Phase I and II studies. Capacity of the fuel tanks has been adjusted to accommodate the mission fuel requirements of the vehicle. Additionally all tanks have been recontoured to fit the vehicle shape resulting from this study.

Fuel Tanks - All tanks are constructed of aluminum. The tanks are installed using a series of truss links to transfer tank loads into the vehicle shell, and which, accommodate vehicle and tank deflections without increasing tank stresses. Termination of the truss links are designed to occur at the main frame and as close to the skin surface as possible. Those links that cannot be terminated on a frame will require an intercostal between frames. The intercostal will be capable

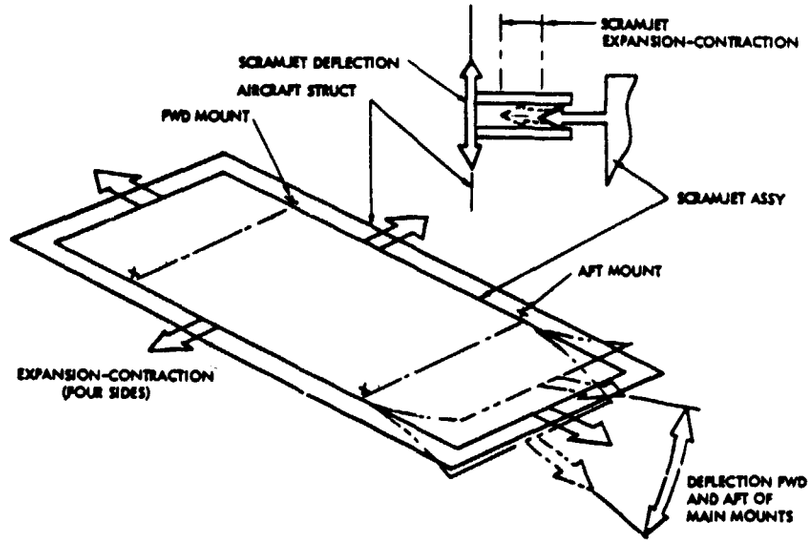

Figure 22 - Scramjet/Vehicle Sealing Requirement

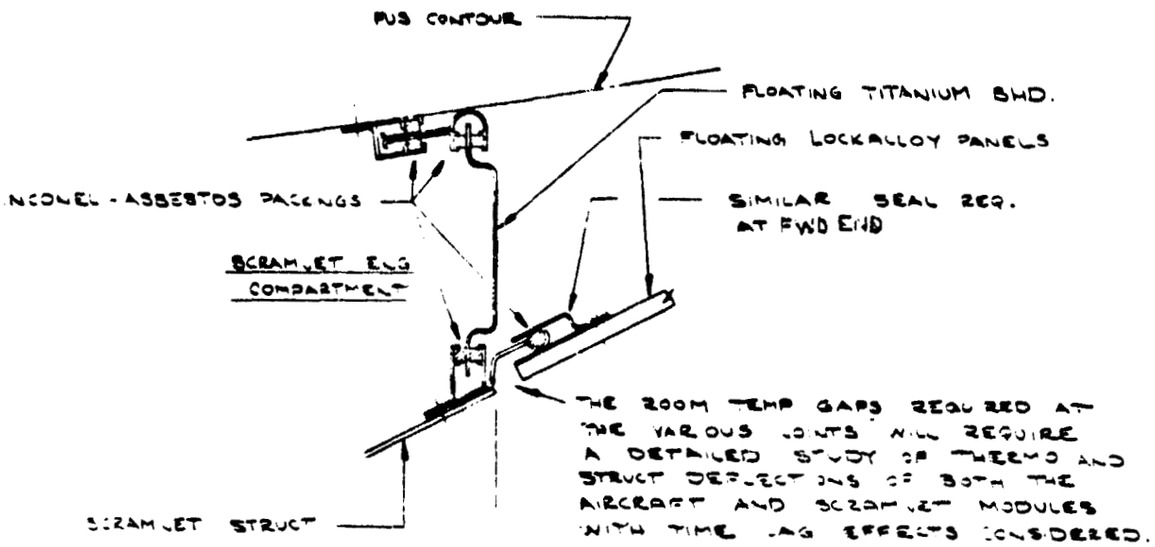

Figure 23 - Sealing - Aft End Scramjet

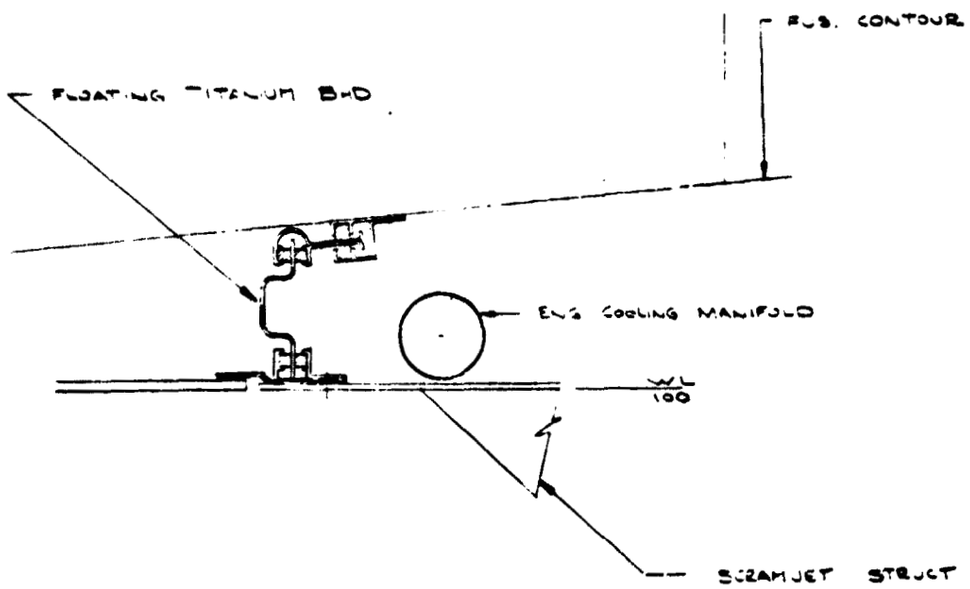

Figure 24 - Seal - Forward End Scramjet

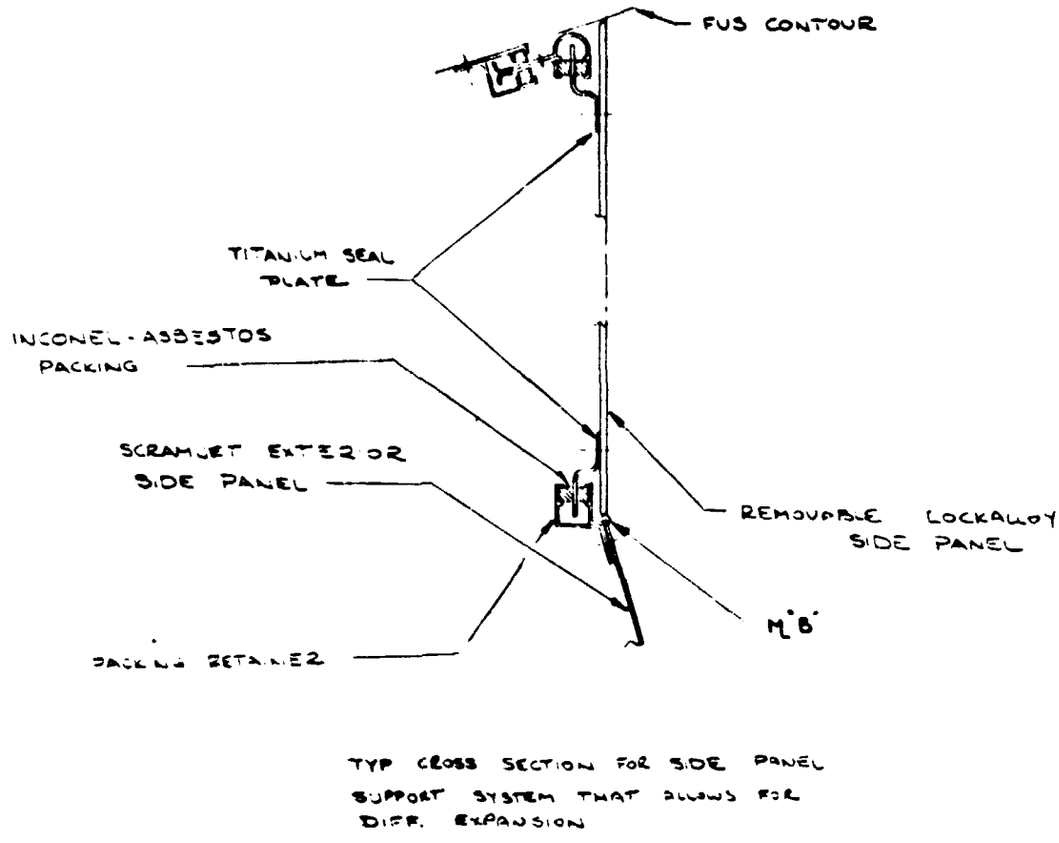

Figure 25 - Sealing - Scramjet Sides

of transferring shear loads into the skin surface and still permit skin thermal expansion without increasing the thermal stress.

In addition to the sizing of tanks for the fuel required for the mission, adjustments were made for a 5 percent ullage and ten percent for hydrogen boil off. Externally, the lox tank is provided with 30 mm of insulation, and the hydrogen tank with approximately 6 mm of insulation as defined in Hydrogen Tank Insulation herein. Additionally, all tanks are provided with 30 mm of clearance, between the insulation and vehicle structure to allow for vehicle and tank deflections.

(Note: Boil off, noted above, is minimum estimated loss of hydrogen from time of tank top off to when X-24C launch occurs.)

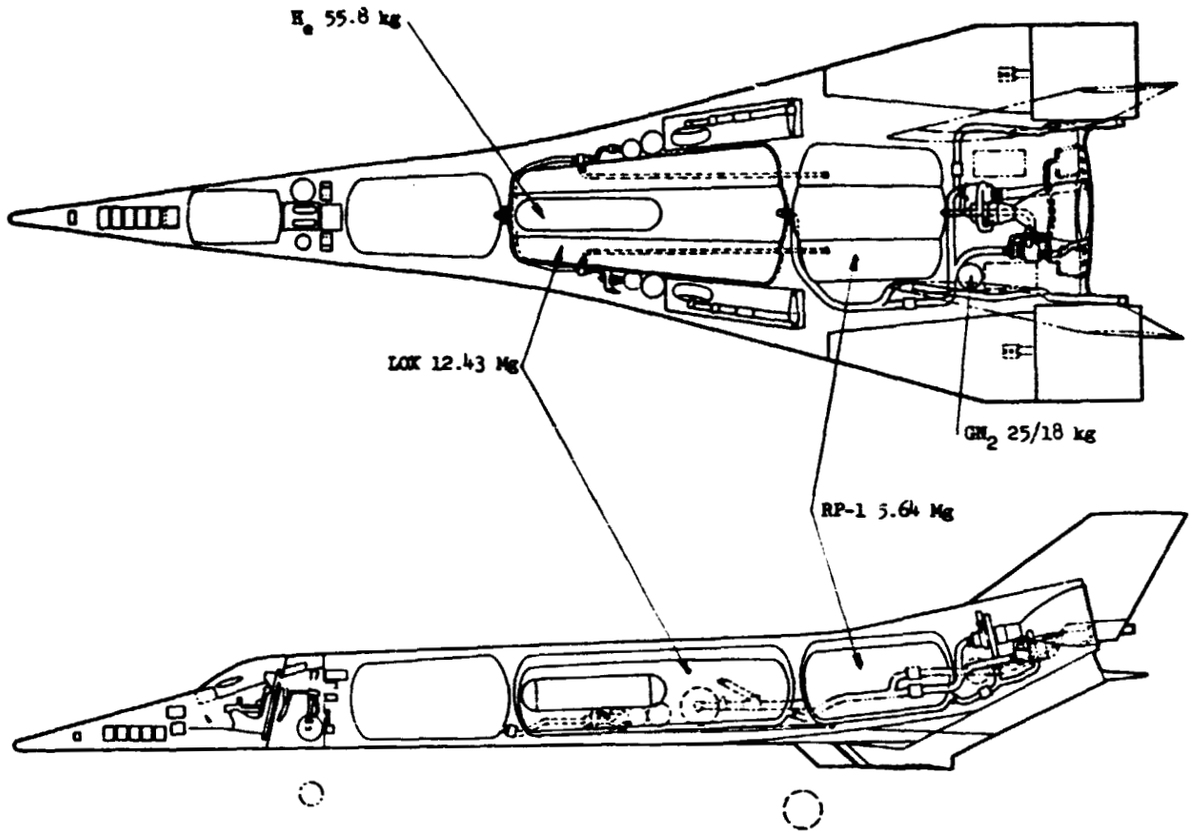

Figure 26 - Fuel System

Functional Systems

A major study requirement was the identification of equipment and systems that are available in Government stores, or as an alternative those available from existing programs which can be adapted, at reasonable cost, to the X-24C program.

The electrical system, depicted in Figures 27 and 28, consists of five silver-zinc batteries available from theX-15/X-24B programs. Three of the batteries are used exclusively for the flight control system. The fourth provided power for communications, instruments, engine needs, etc. The fifth battery for flight test instrumentation power.

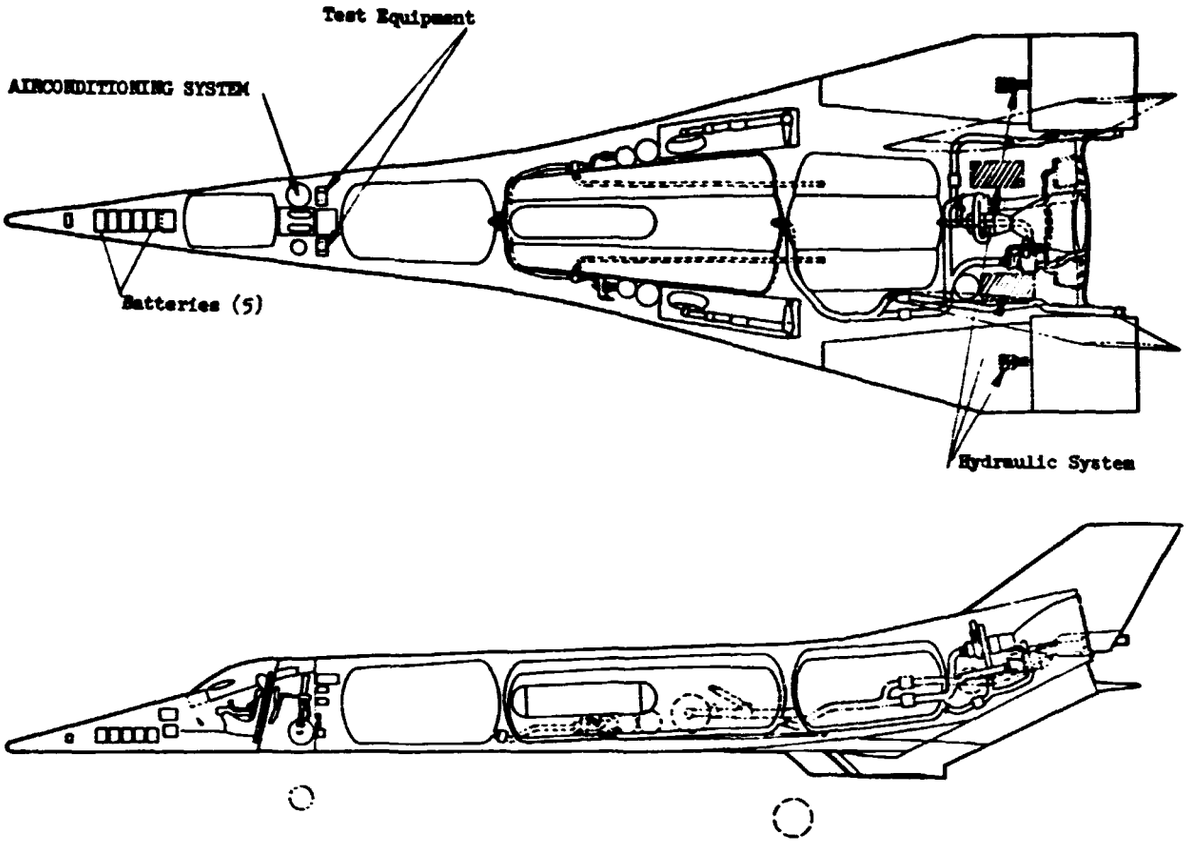

Figure 27 - Electrical/Hydraulic System

Three hydraulic systems, shown in Figures 27 and 28, are required. The number 1 and 2 systems are 30.684 MPa systems used for surface actuation. The number 3 system is a 10.34 MPa system and is for the third channel of the flight control system. Pumps, regulator, reservoir for the number 1 and 2 systems are from the X-15/X-24B programs. The third hydraulic system, because of its lower pressure rating will be Contractor Furnish Equipment (CFE).

Also shown in Figure 27 are the air conditioning system, consisting of the liquid nitrogen system and the pilots oxygen system, which are from the X-15 program.

The C-140A nose and F-106 main landing gears, described previously, herein, were identified in the Phase I Study as GFE. Both gears have sufficient

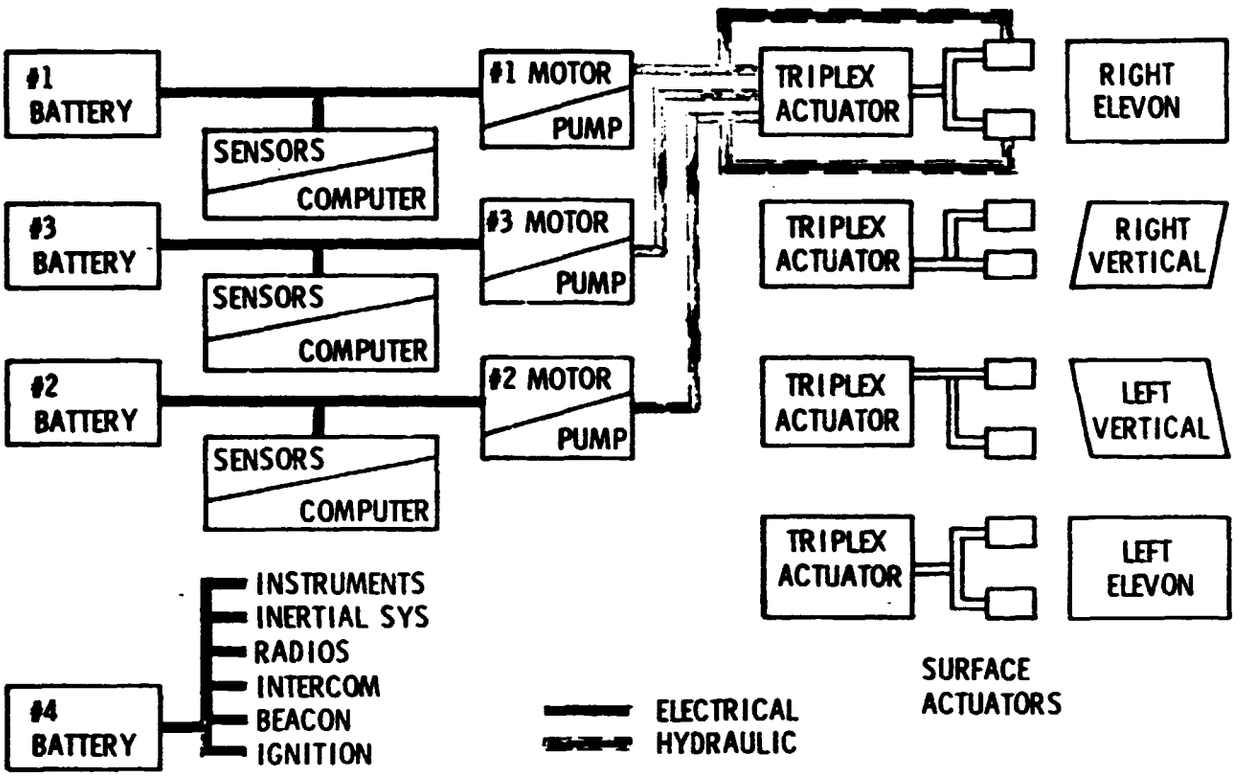

Figure 28 - Electrical/Hydraulic System Schematic

margin to handle the higher loads of the Phase III Configuration. Minor modification, is required for X-24C adaptation, but not to the extent requiring requalification or drop tests.

The UHF/EVHF radios, the AN/ARC-159 radios are items presently stocked at the NASA Dryden Flight Research Center. Intercom and Radar Beacon, also used on the X-24C, are available from the X-15/X-24B programs.

Systems which were developed for other programs which can be easily modified for X-24C application were identified. The flight control system, Figure 29, is an all fly-by-wire system with three channel redundancy. Surface actuators are the left and right elevons for pitch and roll control and the two all-movable vertical tails for yaw and speed control. The heart of the flight control system is the use

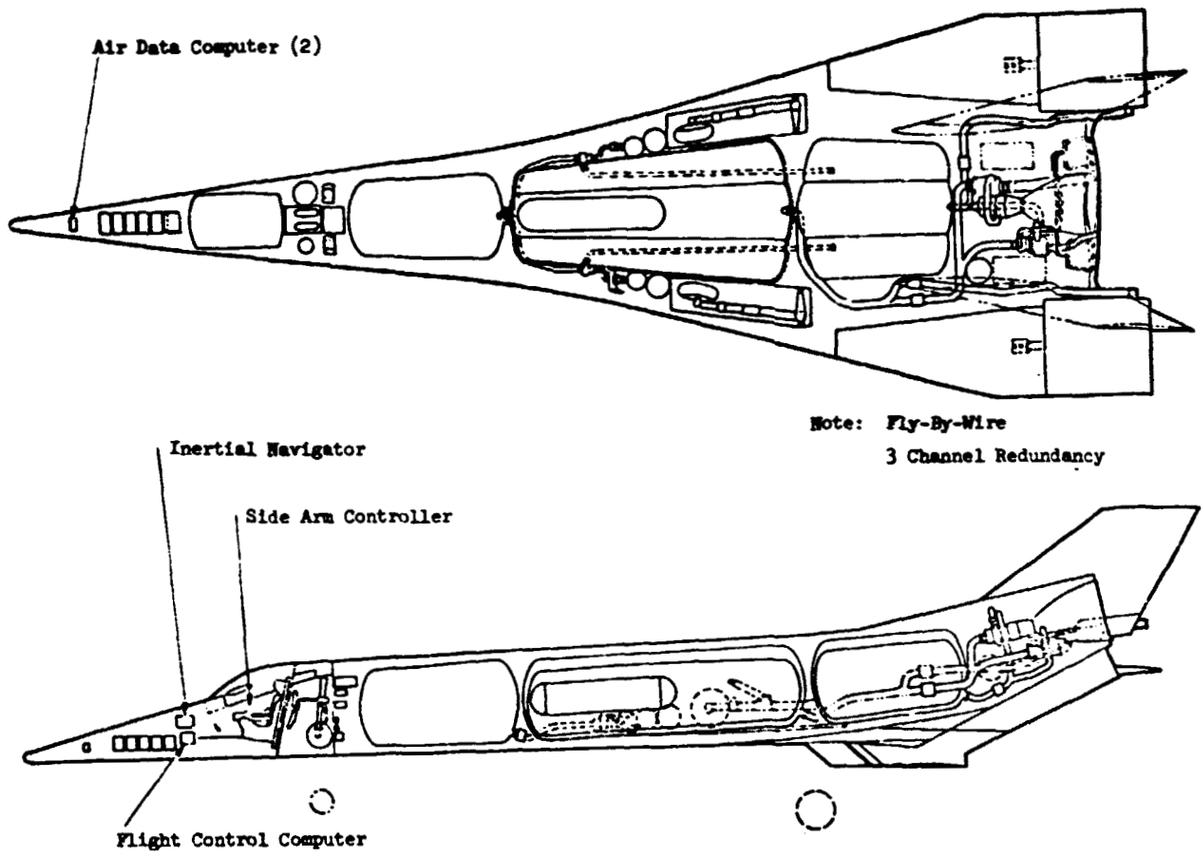

Figure 29 - Flight Control System

of four triplex actuators, Figure 28, which are located in the fuselage and interface the flight control computer with the surface actuators. The triplex actuator was developed for the Heavy Lift Helicopter program and as such, is a flight qualified component. The electro-mechanical components of the system, i.e., side-arm controller, flight control computer, rate and acceleration sensors are a fallout of the F-15 programs. A modified version of the F-5E Inertial Navigation System is planned for the X-24C. These modifications consist of software changes to permit outputting of attitude, heading and inertial velocities and accelerations. The latter in analog format for pilot display. The air data system consists of a fixed hemispherical probe located in the nose of the vehicle, and dual transducers which output Mach, q, altitude, angle-of-attack, side-slip angle and speed. Excepting for the surface actuators, the above system component are all located in the nose/cockpit region easily accessible for maintenance. The triplex actuators are located adjacent to the surface actuators.

The X-24C employs the LR-105 engine for boost and 12 LR-101's for cruise when not on scramjets. The fuel system, Figure 26, is shown schematically in Figure 31. All engines use RP-1 for fuel and liquid oxygen (LOX) as the oxidizer. Helium is employed to pressurize the fuel tanks as depicted in Figure 30. The LOX tank is pressurized at ignition at 530.9 kPa and running 289.58 kPa. The RP-1 tank is initially pressurized at 365.42 kPa dropping to 206.05 dPa during operation. The helium tank is submerged within the LOX tank. Helium is contained at a pressure of 20.684 MPa for purging requirements of the LR-105 and LR-101 engines before ignition and following cut-off, following the schedule reflected by Figure 32. Helium is also used to "cold start" the two turbo pumps installed on the X-24C. The use of two turbo pumps is a departure from the Phase I and II studies where only one was used. Loss of the LR-105 pump will not inhibit LR-101 engine operation. This capability will permit powered flight on sustainer engines, at a reduced speed, to more favorable landing sites. The addition of the second turbo pump did increase the vehicle mass approximately 204 kg plus an additional 45.4 kg for the gaseous nitrogen for purge and cold start. Placement of the tanks was predicted on minimizing center-of-gravity travel during propellant burn-off.

The X-24C requires 0.46 meter deep scramjet modules for cruise. The scramjet fuel and coolant system, Figure 33, shown schematically in Figure 34 included the hydrogen tank (located in the payload bay), two hydrazine fuel pumps (located forward of the main wheel wells), two hydrazine and two helium tanks (in the same area as the pumps), a computer (in the payload bay) in addition to the scramjet modules on the bottom of the vehicle. The hydrogen is pressurized at 344.74 kPa. The hydrazine, employed to run the two turbo pumps, is pressurized at 3.03 kPa. Helium used for purging the hydrogen lines as well as the scramjet compartment is pressurized at 20.684 MPa. Hydrogen flows for the scramjet configured vehicle at Mach 6 and a "q" of 47.88 kPa are 0.59 kg/second/module or a total of 4.85 kg of hydrogen per second.

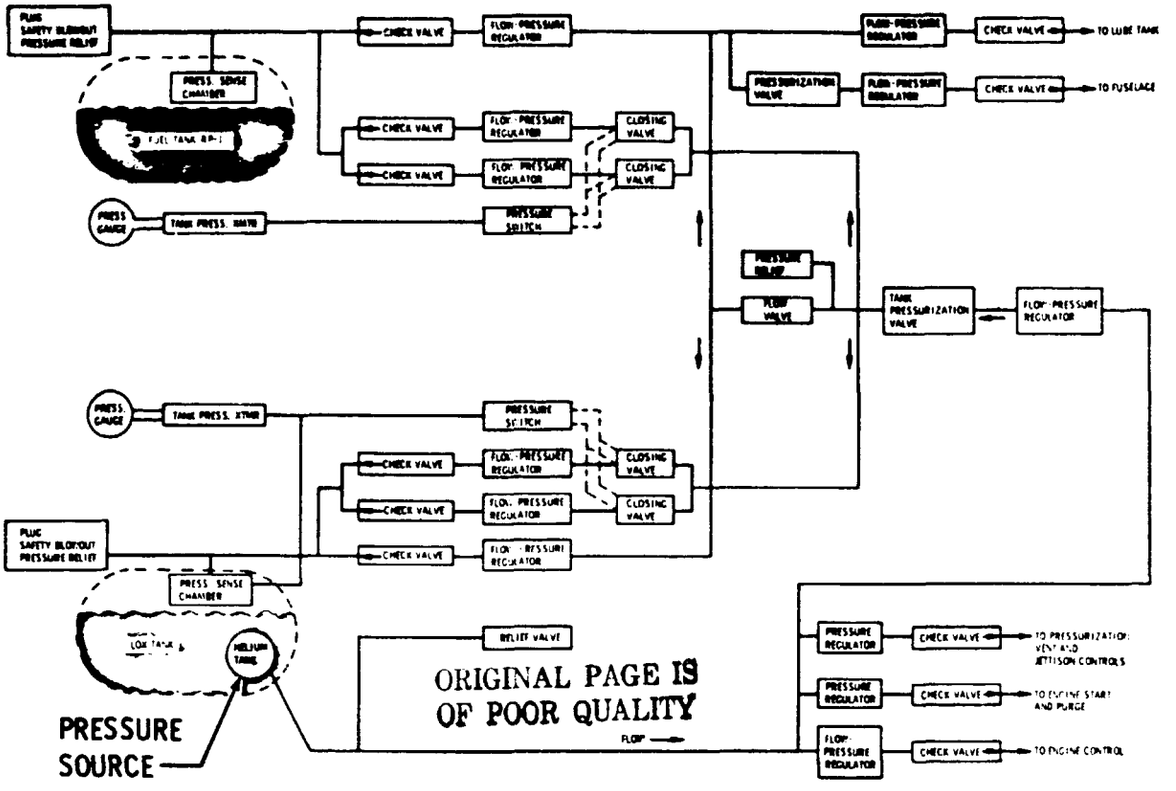

Figure 30 - Pressurization System

Thermal Analysis

Thermal analysis was performed to size the Lockalloy skin surface and provide temperature for stress calculations. Studies to determine the feasibility of sealing expansion gaps between Lockalloy skin panels, method of splice Lockalloy panels, and effects of shock wave/boundary layer interaction were also performed.

Additional thermal analysis on tank insulation requirements and vehicle pressurization were also made. All analysis, plus their results, are described below:

Skin Thickness Calculations - The calculations of Lockalloy thickness requirement were made for the two basic missions; (1) Mach 6.6 cruise for 40 seconds,

NOTE: Base Unit = U.S. Standards

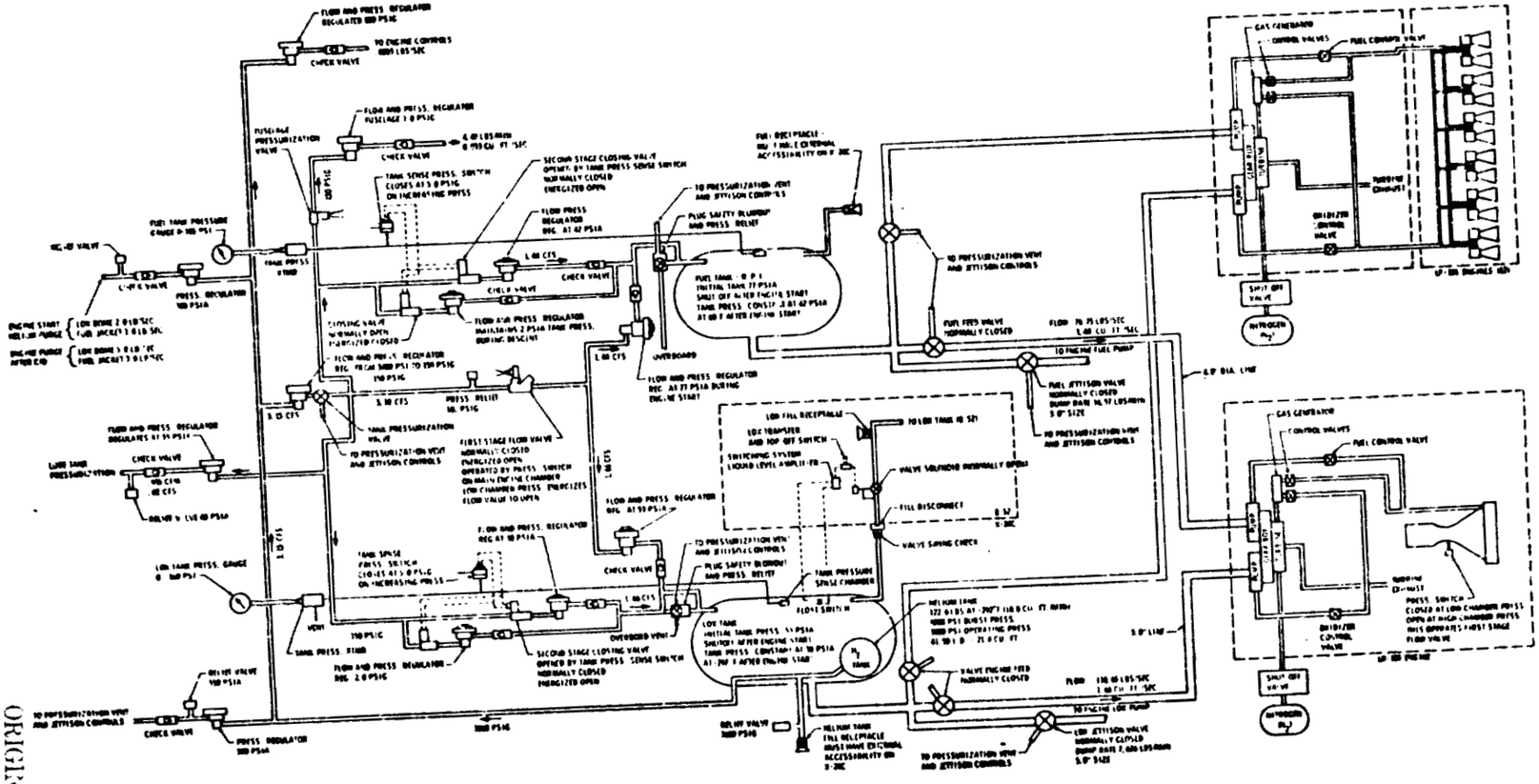

Figure 31 - Propellant System Schematic

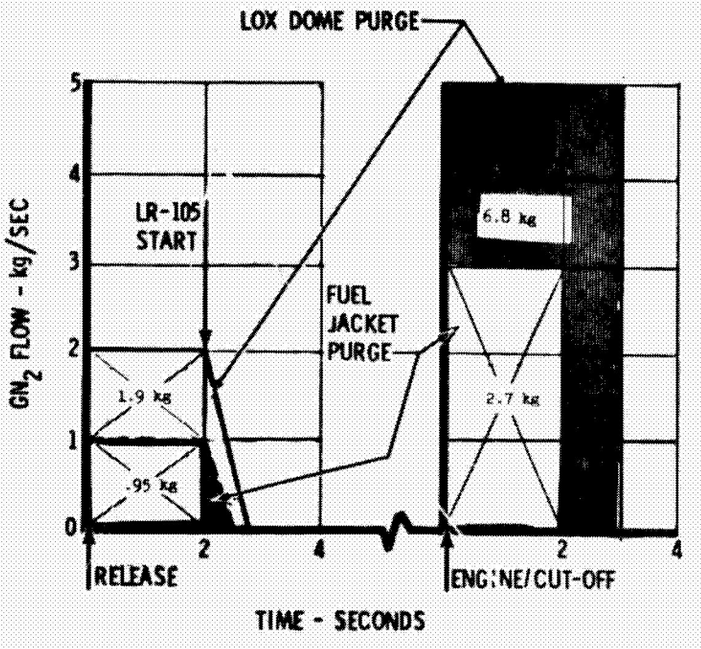

Figure 32 - LR-105 Purge Schedule

and (2) dash to Mach 7.8 with no cruise. As in the first phase of the study, the Lockalloy skin temperature history at each location was computed for multiple skin thicknesses. A curve was then prepared showing the variation of peak Lockalloy temperature versus Lockalloy thickness. Figures 36 through 44 show these curves for a vehicle in its "clean" configuration (no scramjet). The curve designations can be referred to Figure 35 for location identification. These curves were used to support analysis activity by the stress and weight organizations to establish the final Lockalloy panel thicknesses.

Figures 45 and 46 were prepared to show the thickness distribution which satisfies the 588.7 K maximum temperature Lockalloy requirement for the Mach 6.6,

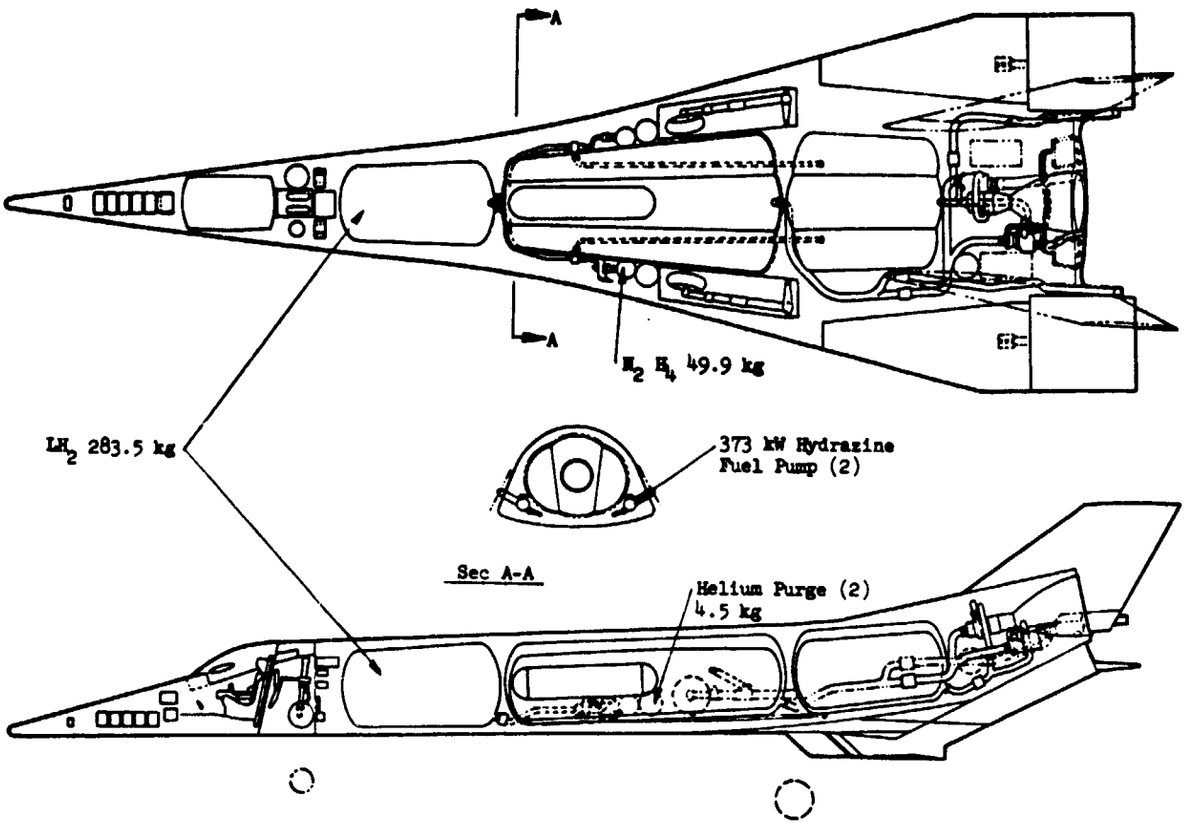

Figure 33 - Scramjet Fuel System

forty second cruise mission. Lower temperatures will result during the Mach 7.8 dash mission.

Lockalloy thicknesses for the scramjet nozzle, for scramjets operating, were computed on a peak temperature of 588.7 K, and constant heating for forty seconds. Figure 47 presents these results as a function of distance from the start of the nozzle intersection with w.l. 100.

Leading edges were assumed also constructed of Lockalloy. The combination of leading edge radius and sweep angle results in heating rates low enough to enable the use of Lockalloy with a 588.7 K maximum. The leading edge design did not change for that identified in Phase I. However, the side fin leading edge radius was reduced to 12 mm which necessitated a new analysis. Various length

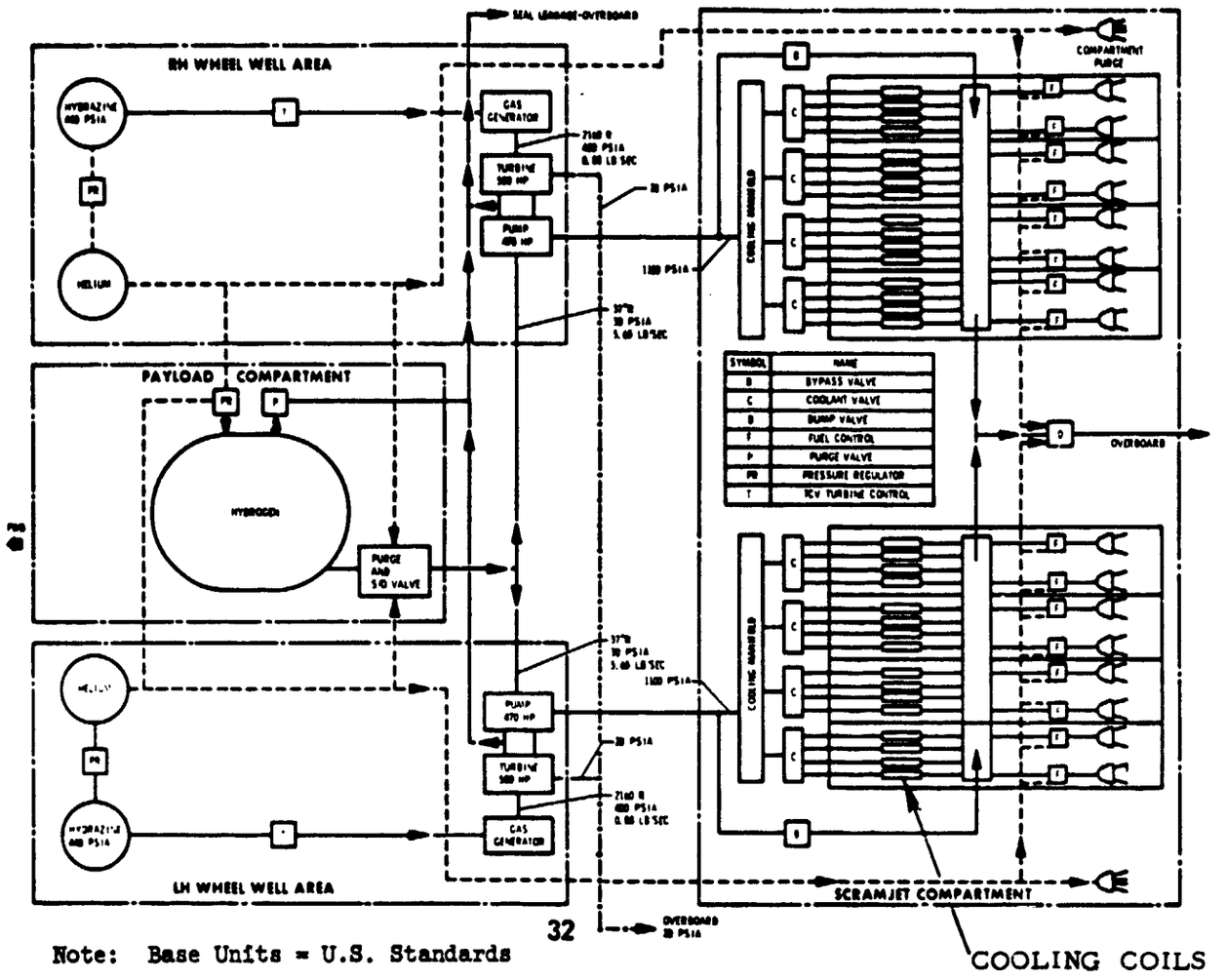

Figure 34 - Scramjet/Coolant System Schematic

solid Lockalloy leading edges were investigated. The results are presented in Figure 48 and show that a 588.7 K peak can be maintained if a 51 mm minimum length solid section is provided.

Lockalloy Expansion Joints - A study was made to determine the feasibility of sealing gaps between adjacent structures differing greatly in temperature, i.e., around the scramjet module. The sealing of the gap is desirable to prohibit the flow of boundary layer air into the vehicle interior.

The sealing method investigated consisted of a titanium or stainless steel strip which could be attached to one side and allowed to slide on the adjacent side.

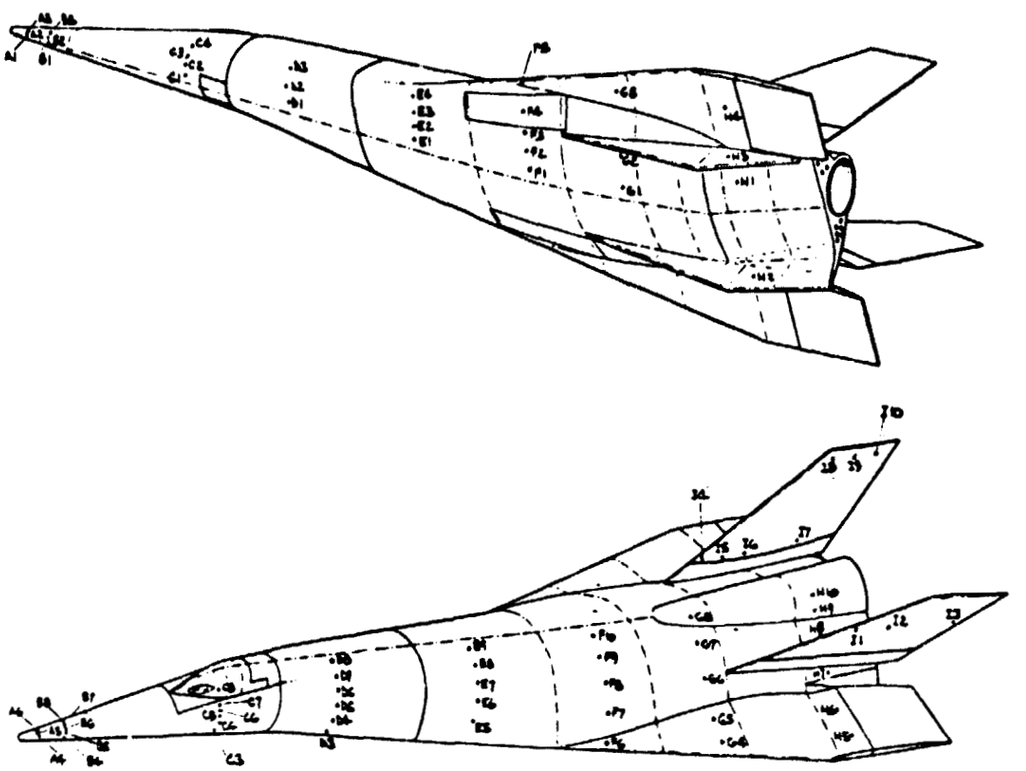

Figure 35 - Thermal Analysis Locations

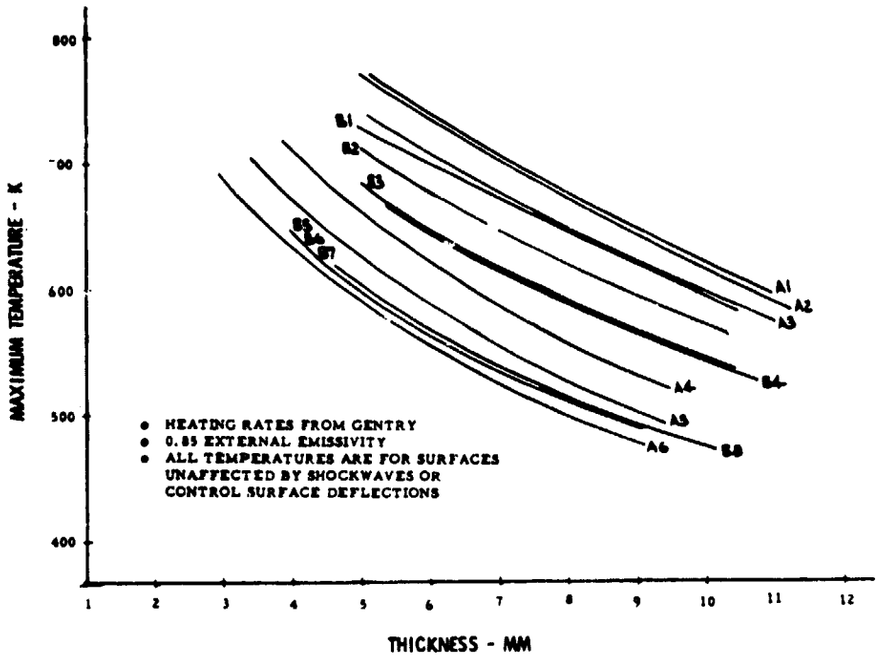

Figure 36 - Lockalloy Peak Temperature vs Thickness - Mach 6.6, Nose Region

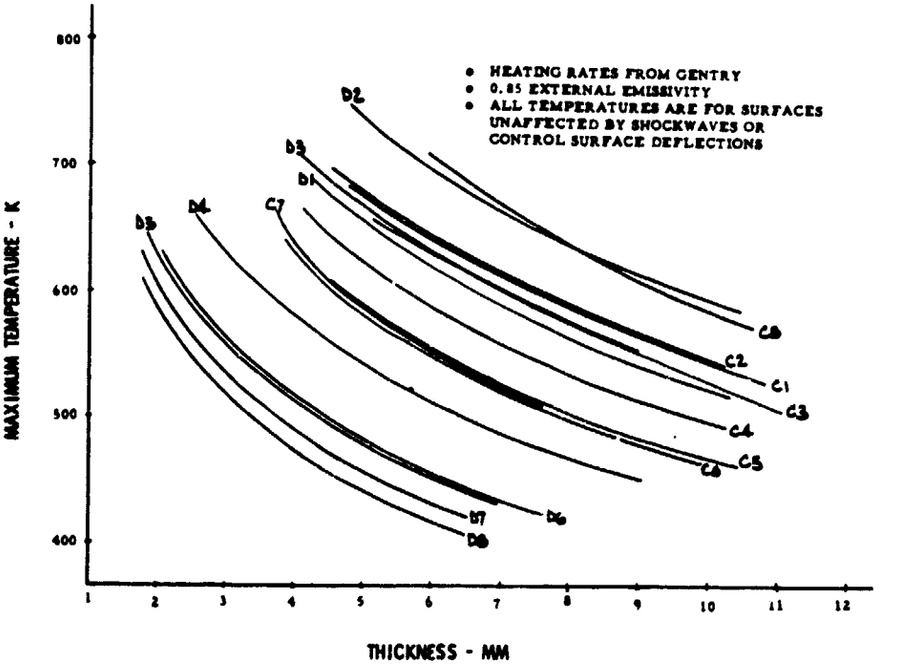

Figure 37 - Lockalloy Peak Temperature vs Thickness - Mach 6.6, Forebody Region

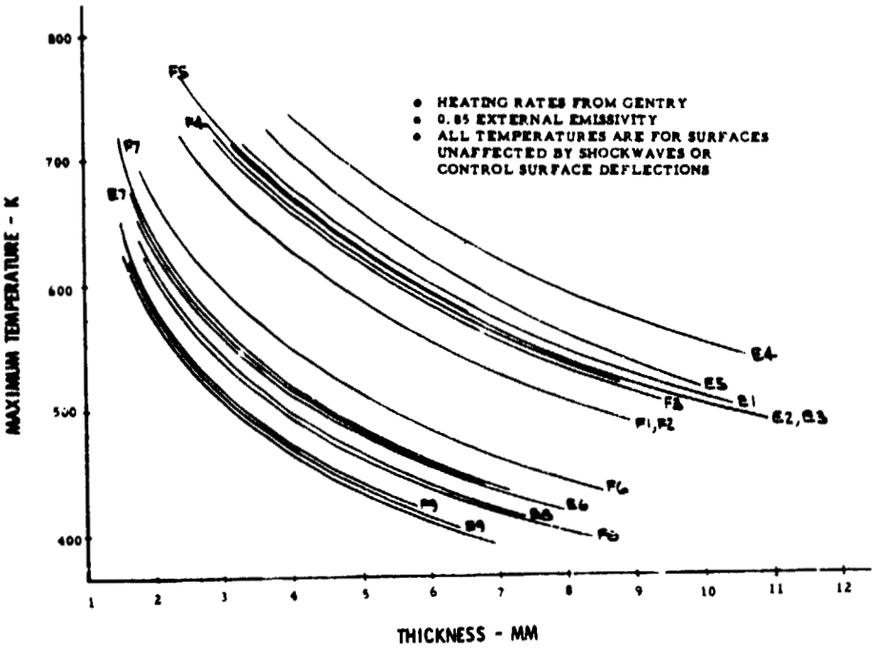

Figure 38 - Lockalloy Peak Temperature vs Thickness - Mach 6.6, Midbody Region

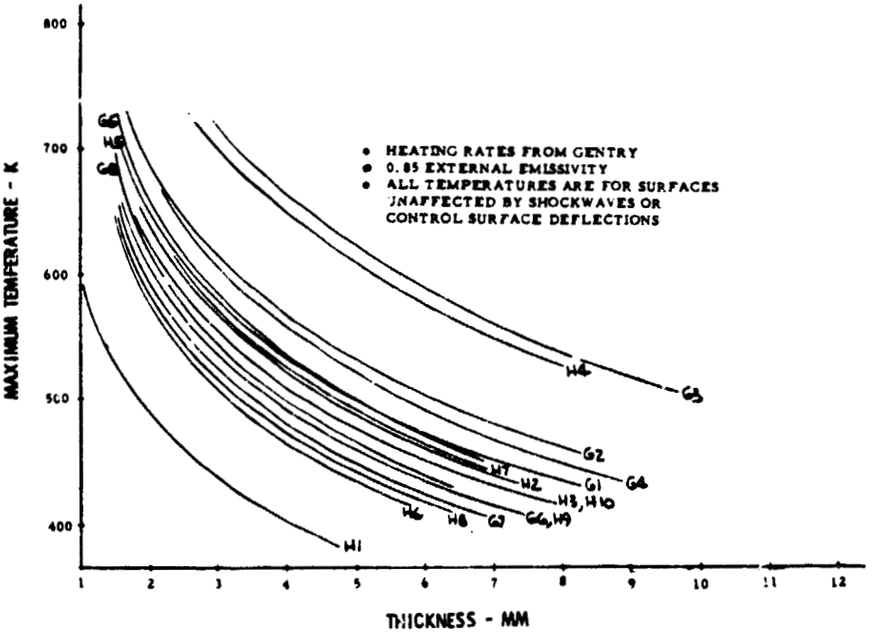

Figure 39 - Lockalloy Peak Temperature vs Thickness - Mach 6.6, Aftbody Region

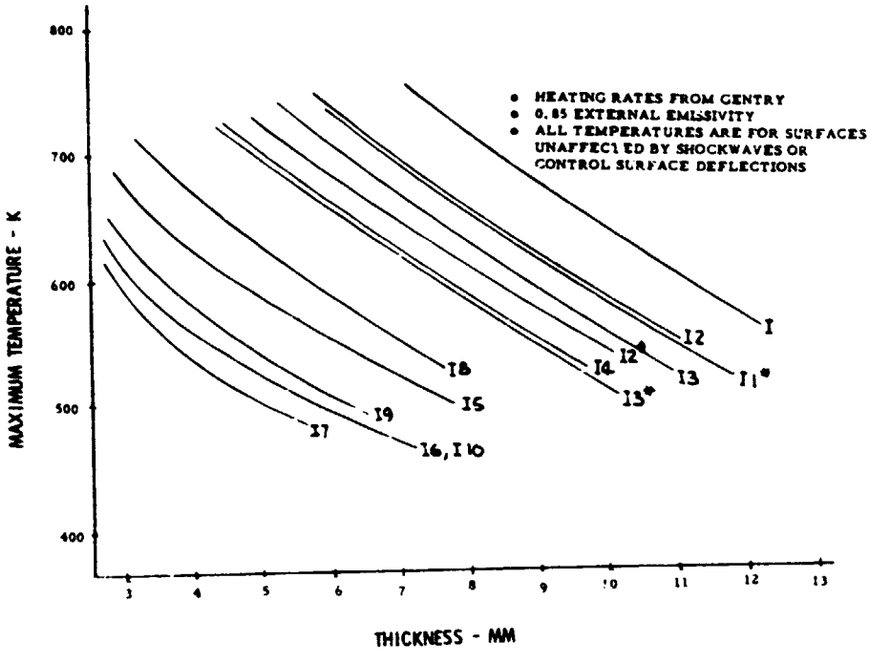

Figure 40 - Lockalloy Peak Temperature vs Thickness - Mach 6.6, Fins Region

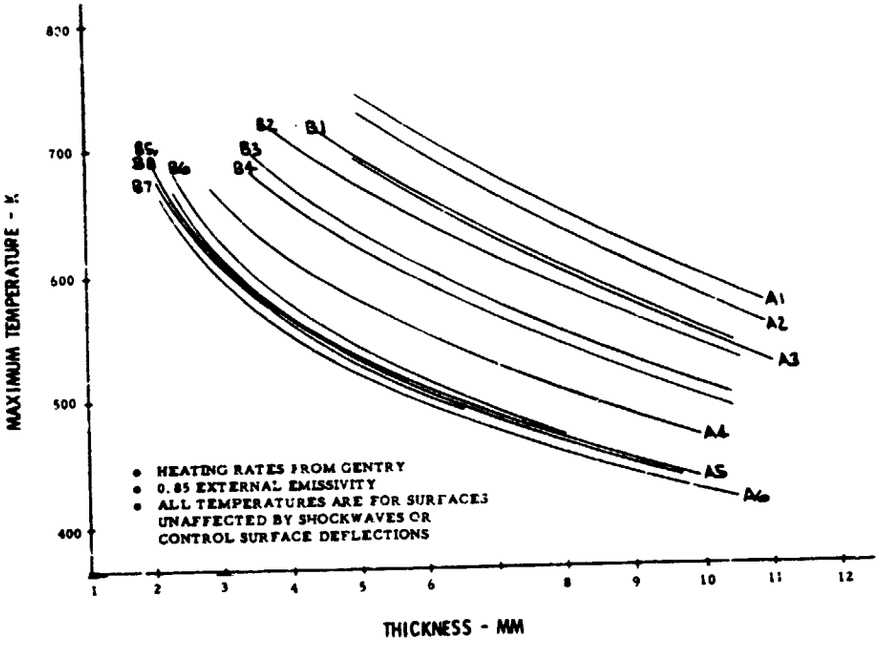

Figure 41 - Lockalloy Peak Temperature vs Thickness - Mach 7.8, Nose Region

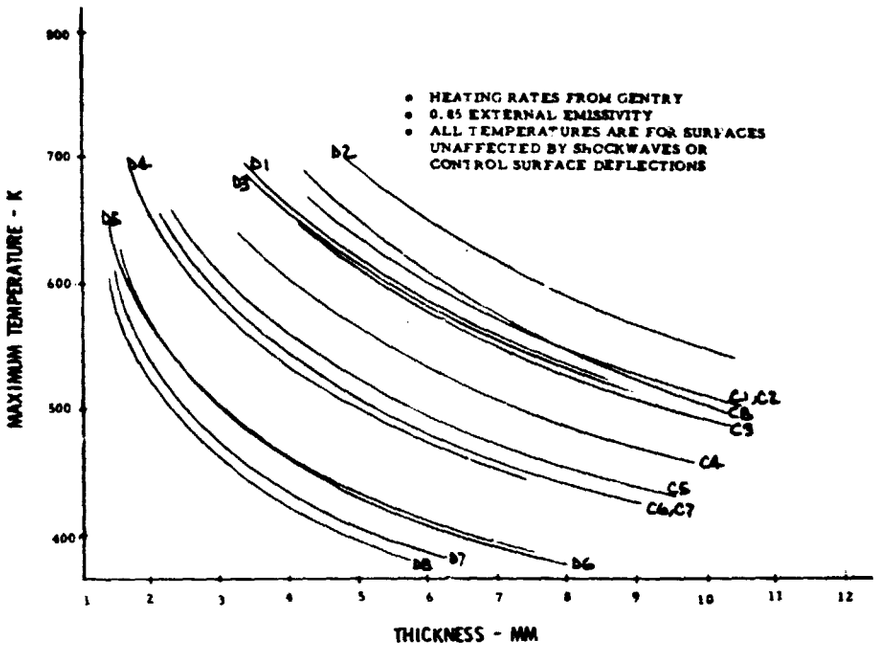

Figure 42 - Lockalloy Peak Temperature vs Thickness - Mach 7.8, Forebody Region

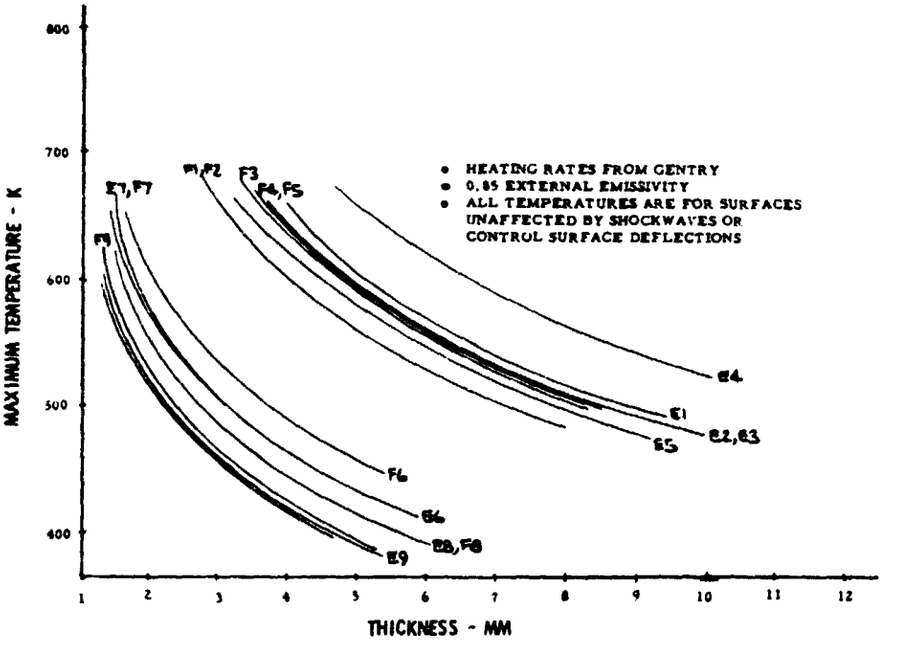

Figure 43 - Lockalloy Peak Temperature vs Thickness - Mach 7.8, Midbody Region

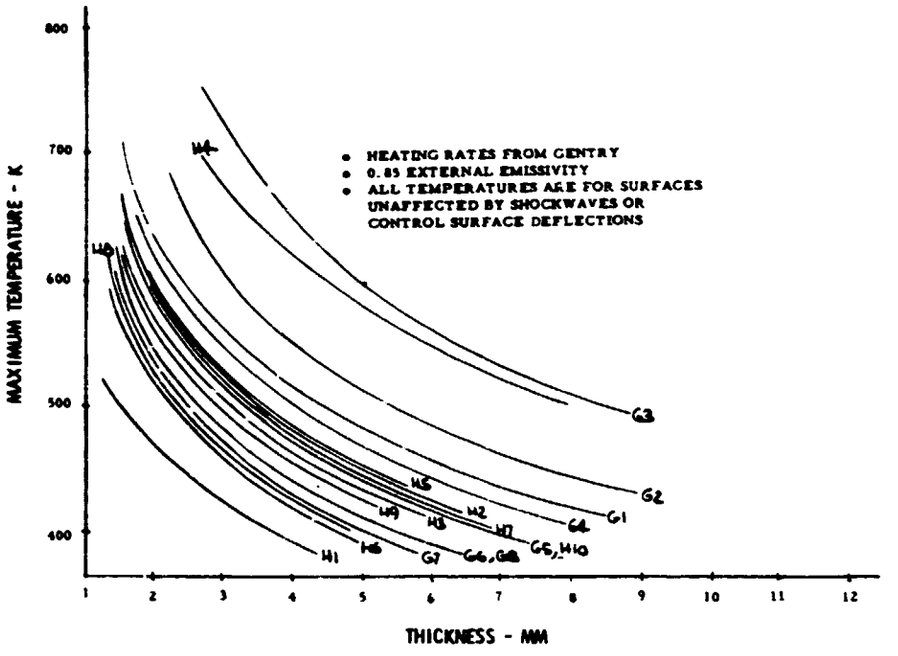

Figure 44 - Lockalloy Peak Temperature vs Thickness - Mach 7.8, Aftbody Region

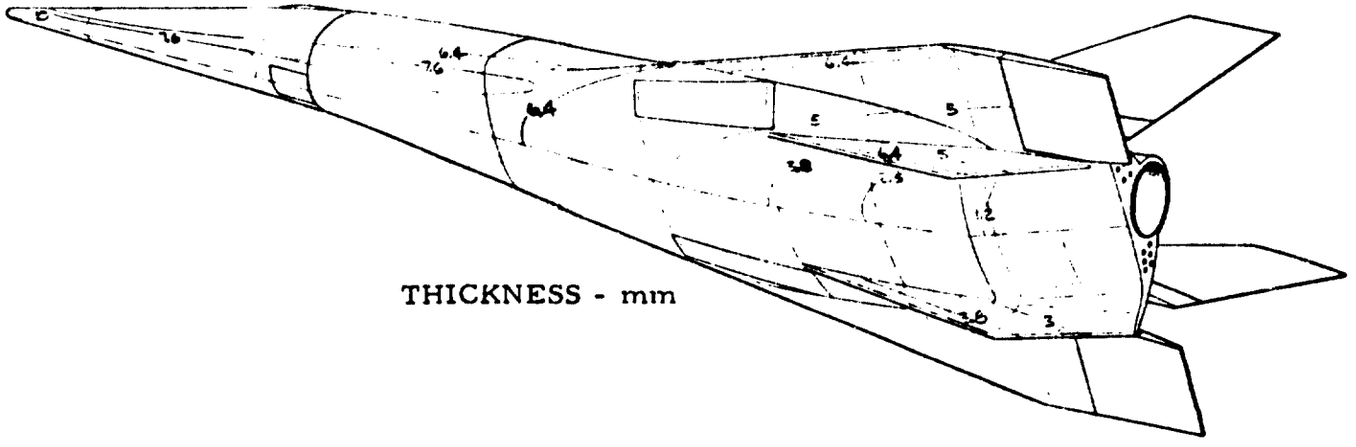

Figure 45 - Skin Thicknesses Requirements for Thermal Protection Only - Lower Body

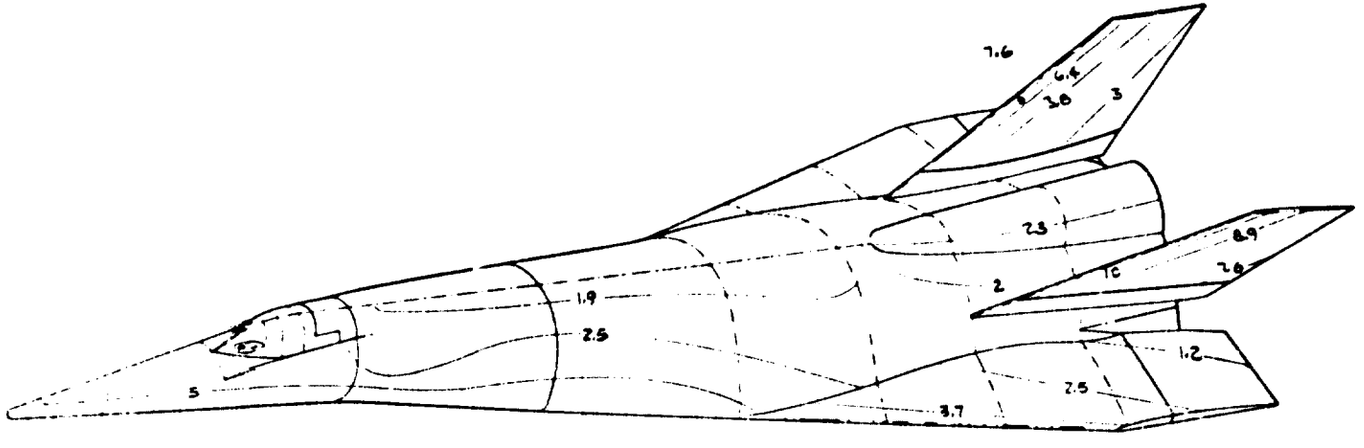

Figure 46 - Skin Thicknesses Requirements for Thermal Protection Only - Upper Body

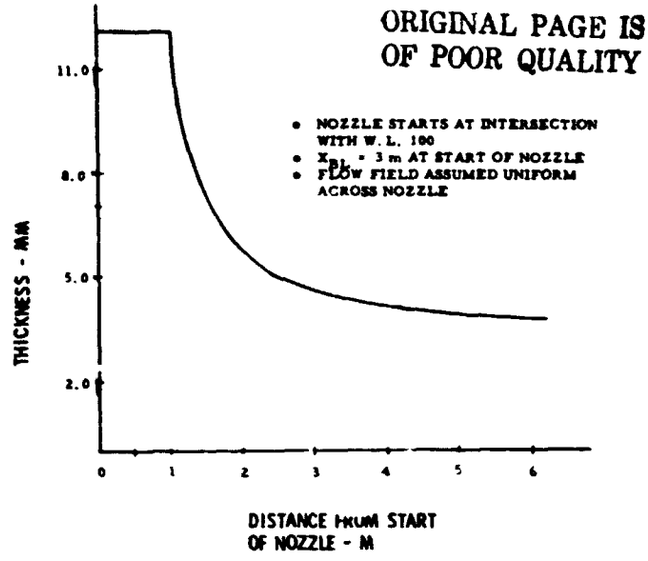

Figure 47 - Skin Thickness on Scramjet Nozzle for 40 Second Scramjet Operation @ M = 6.6

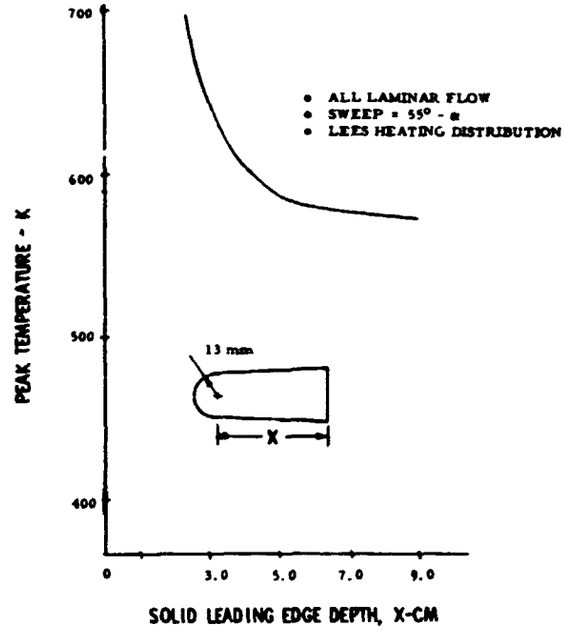

Figure 48 - Fin Leading Edge Peak Temperature @ M = 6.6, 40 Second Cruise

The desired gap in the cold vehicle condition was estimated to be as much as 25 mm. The thermal response of the thin strip had to be estimated to verify the feasibility of the design concept.

A thermal circuit was set up for a transient solution on the Lockheed Thermal Analyzer program. The strip was assumed attached to a Lockalloy panel whose temperature history reached a peak of 588.7 K. Thermal contact was ignored between the strip and the adjacent structure on which it would slide. The heating rate to the metal sealing strip was estimated from the Mach 7 gap heating test results of Wieting, Reference 9. An average value of one-half the local heat transfer coefficient was used in conjunction with the local adiabatic wall temperature. The results are shown in Figure 49. They indicate that there is sufficient heat sink involved to allow the use of this sealing method. Painting the metal strip (ϵ = 0.85) was found to be beneficial if a thin strip is used in conjunction with a large gap.

Lockalloy Splices - The possibility of excessive thermal gradients in Lockalloy at splice joints was considered a potential problem due to the local reduction in Lockalloy thickness at the joints. Although attachment or support straps will be used at these joints, it was desired to consider the worst thermal gradient which could be expected if heat transfer between the Lockalloy and attached strap was ignored. Both tapered and strapped reductions in Lockalloy were investigated on a transient basis. Figures 50 and 51 show that maximum of 336 K gradient would be produced in the stepped configuration, but only 300 K in the tapered. Neither gradient is prohibitive, however, and both should be considerably less than the predicted valves with the actual presence of the support straps.

Shock Wave/Boundary Layer Interaction - A study was conducted during Phase I, Reference 2, to determine the best estimate of heating increase due to the intersection of fin shock waves with the fin adjacent surface. It was concluded that an increase of 30 percent in local film coefficient was the minimum which would be used for highly swept fins, oriented at small angles with the local air flow.

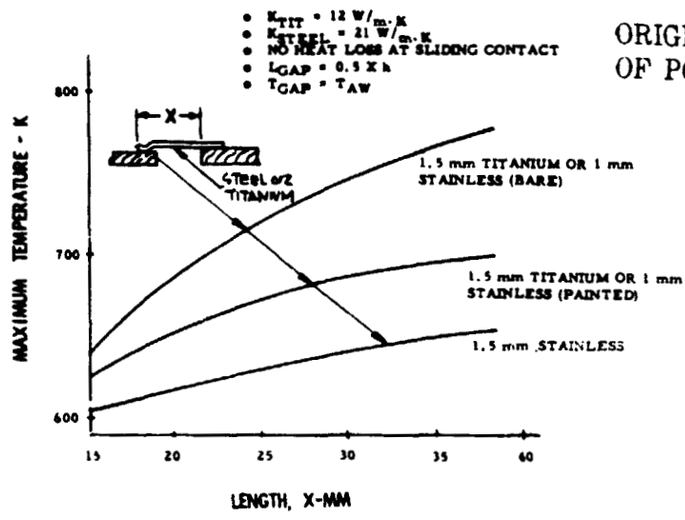

Figure 49 - Estimated Seal Temperatures in Skin Joint Areas Around Scramjet

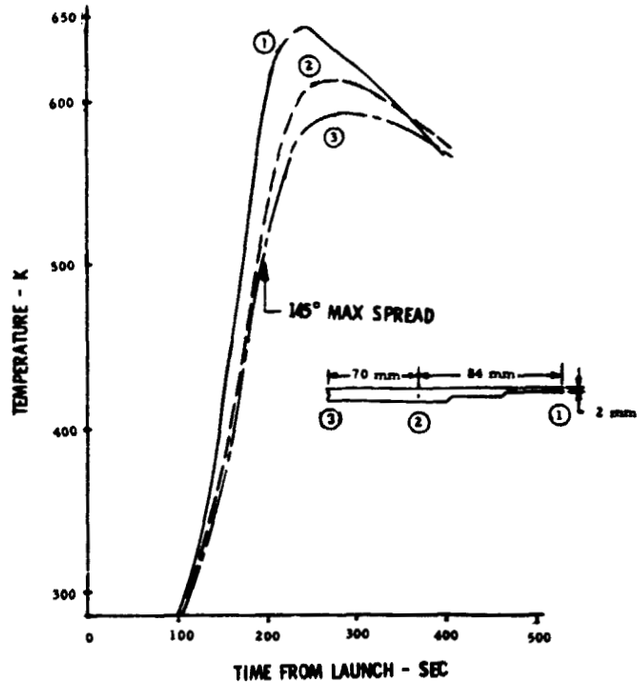

Figure 50 - Thermal History of Typical Skin Splice Area - Stepped

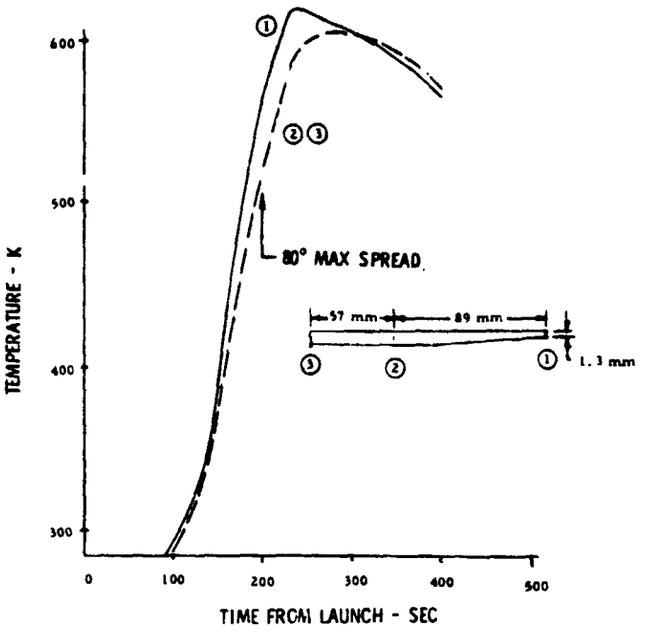

Figure 51 - Thermal History of Typical Skin
Splice Area - Tapered

This increase would be maximum along an angle of 2.25 degrees away from the fin surface. Therefore, a first approximation to the mass increase for the canted fin (side fin) shock was made by increasing all adjacent fuselage panels influenced by this included angle by 30 percent. It should be noted that this is a fixed angle determined by the position of the fixed stub fin. The stub fin height is assumed to be sufficiently large to eliminate fuselage coundary layer/rudder shock wave intersection.

Since the wing leading edge intersects the fuselage in an area where the fuselage/wing angle is very obtuse, the shock wave/boundary layer interaction was assumed weak enough to ignore in this area. However, further aft on the wing the fuselage becomes more nearly normal with the wing. This occurs in the area of the elevons where the shock produced by the elevons (when deflected) will also intersect the fuselage. Since the elevons will deflect up or down most of the

flight, a 30 percent increase in heating on the adjacent fuselage panels above and below the elevons was assumed for one-half the duration of the total heating period.

These heating increase estimates were made for the purpose of approximating Lockalloy panel thickness sizing only. The exact selection of thicknesses in shock interference areas will require wind tunnel tests to better define the heating distributions.

Hydrogen Tank Insulation - An insulation system study for the liquid hydrogen fuel tank was made. It was concluded that the results of the tank insulation research program presented in References 5 through 8 are still essentially current. Basically, two insulation schemes were considered. These are a helium-nitrogen purged plastic foam and fiberglass insulation and a vacuum-fiberglass insulation.

The helium-nitrogen purge system is relatively simple and reliable and uses a 25 mm layer of styrofoam and a 38 mm layer of fiberglass. Mylar barriers are placed such that flow channels are created. Helium is forced through the styrofoam and nitrogen through the fiberglass to effectively prevent air from permeating the insulation and liquifying.

The vacuum-fiberglass system is more difficult to construct than the helium-nitrogen system. Two layers of 3 mm thick fiberglass, with the fibers directionally oriented, and an outer flexible layer of mylar make up this insulation. The sealing of the cover and the prevention of leaks is very critical since the thermal conductivity is a function of the vacuum pressure.

Selection of the vacuum-fiberglass system over the helium-nitrogen purge system was made on the basis that it permitted hydrogen tank sizing within the volumetric constraints of the payload bay structural envelope.

Vehicle and Tank Pressurization - To prevent hot ram air from infiltrating the airplane and heating internal structure and equipment, it was decided to pressurize the whole airplane to 6.9 kPa (g). Based on current airframe assembly

techniques, with a maximum effort at sealing, a total effective leakage area of 45 cm^2 was estimated. To further reduce the pressurization requirements, it was decided to pressurize only during the flight regime between Mach 2 on acceleration and Mach = 2 on deceleration.

Helium was selected as the pressurizing fluid and will be stored within the LOX tank at 20.7 MPa to take advantage of the volume reduction at cryogenic temperatures. In addition to airframe pressurization, helium will also be used to pressurize the LOX and the RP-1 fuel tanks and to provide a source of pressure for the engine controls.

Main engine fuel line purge is provided by a 0.06 m^3 tank of gaseous nitrogen at 20.7 MPa.

Aerodynamic Analysis

The Phase III configuration, shown in Figure 4, was analyzed throughout the flight envelope to determine its aerodynamic characteristics. The purposes were: 1) to verify that the configuration has acceptable stability and control characteristics, 2) to provide drag data for performance studies, and 3) to identify possible problem areas in the basic design. Several computer programs were used to obtain the necessary data. Subsonic, transonic and supersonic lift, stability and control data were estimated by the vortex lattice method with leading edge vortex effects added. A vortex lattice computer program, vorlax, was developed at the Lockheed California Company. Side edge vortex effects were computed by hand using the method of NASA TR R-428. Skin friction drag up to Mach 3 was estimated by the Sommer and Short T' Method. Wave drag up to Mach 3 was computed by the NASA Wave Drag Program empirically modified for use to higher values of Mach numbers. Aerodynamic data for Mach 3 to 8 were generated by the Hypersonic Arbitrary Body Aerodynamic Computer Program developed by the McDonnell Douglas Corporation. All of the aerodynamic data presented are based on the following reference values:

$S = 73.1\ m^2$

$l_b = 21.3\ m$

$b = 7.37\ m$

$\bar{x} = 0.65\, l_b$

$\bar{z} =$ W. L. 140

Some other basic geometric characteristics of this vehicle with scramjet modules off are:

Wetted area excluding base area	$233\ m^2$
Maximum normal cross-sectional area	$6.98\ m^2$
Base area	$2.97\ m^2$

Subsonic, Transonic and Supersonic Data - Figures 53 through 60 show estimated lift and pitching moment data from Mach 0.2 to 3.0 for three elevator deflections. Figures 61 and 62 show estimates sideslip characteristics for the Mach 0.2 to 3.0 range at three angles of attack with and without vertical stabilizers. Drag data for the same Mach range were computed for the untrimmed aircraft by the methods listed above. Trimmed drag data which were used in performance calculations are presented in Aerodynamic Data for Performance herein.

Hypersonic Data - The high supersonic and hypersonic Mach number aerodynamic characteristics, both viscous and inviscid, were calculated with the "Hypersonic Arbitrary - Body Aerodynamic Computer Program "Reference 10." A number of hypersonic theories were used to determine the inviscid forces. Modified Newtonian theory was used on the hemispherical nose as well as the leading edges of the fuselage, wings, and vertical tails. Tangent wedge theory was used on the flat outboard surface of the vertical tail. All other compression surfaces were calculated using tangent cone theory. Fuselage base pressures were computed using $C_p = -1/m^2$. The pressures on the aft fuselage scramjet expansion surface were estimated from X-15 empirical data, Reference 11. All remaining

Figure 52 - Inviscid Aerodynamic Configuration

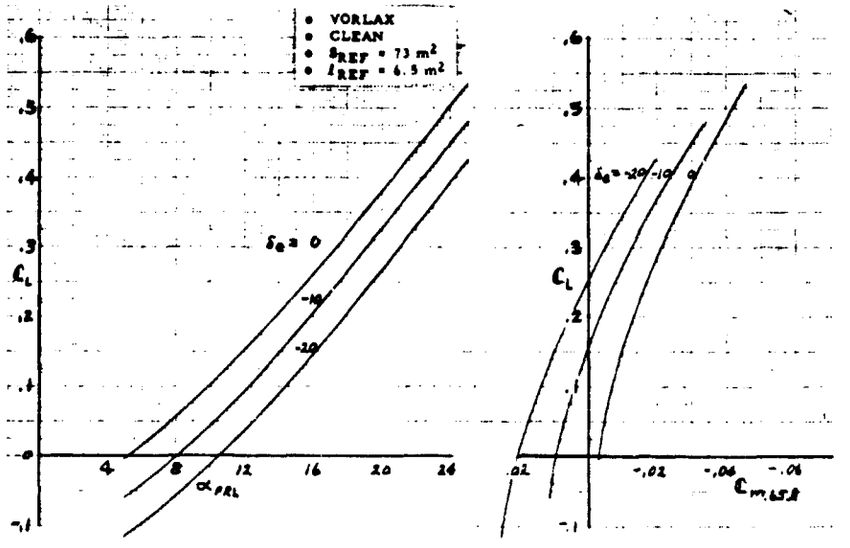

Figure 53 - Pitch Data - M = 0.2

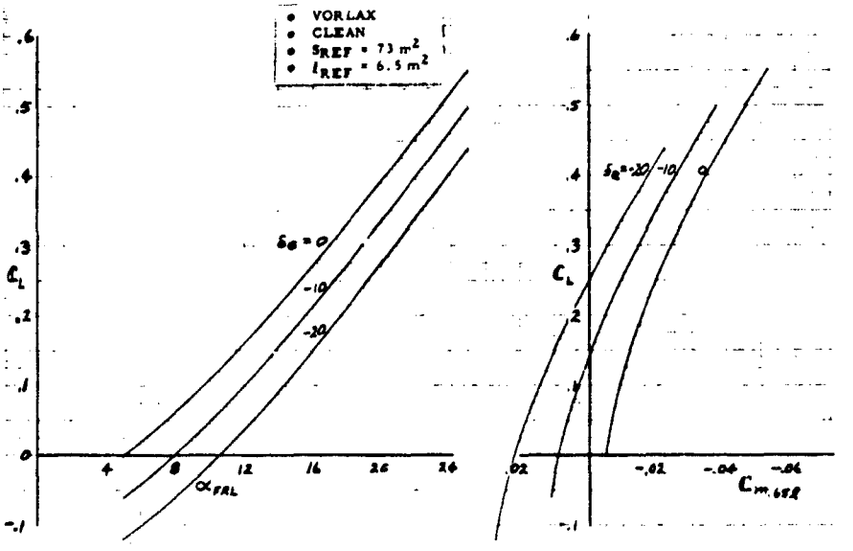

Figure 54 - Pitch Data - M = 0.7

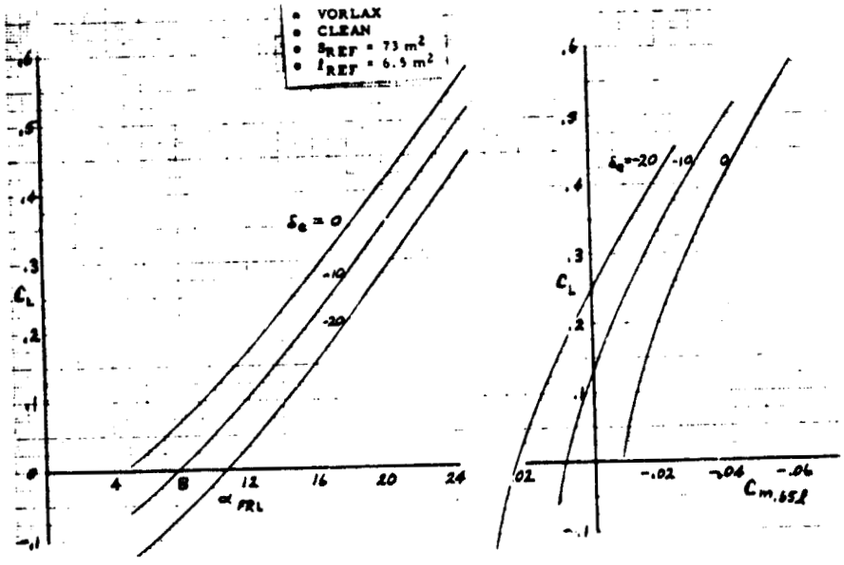

Figure 55 - Pitch Data - M = 0.9

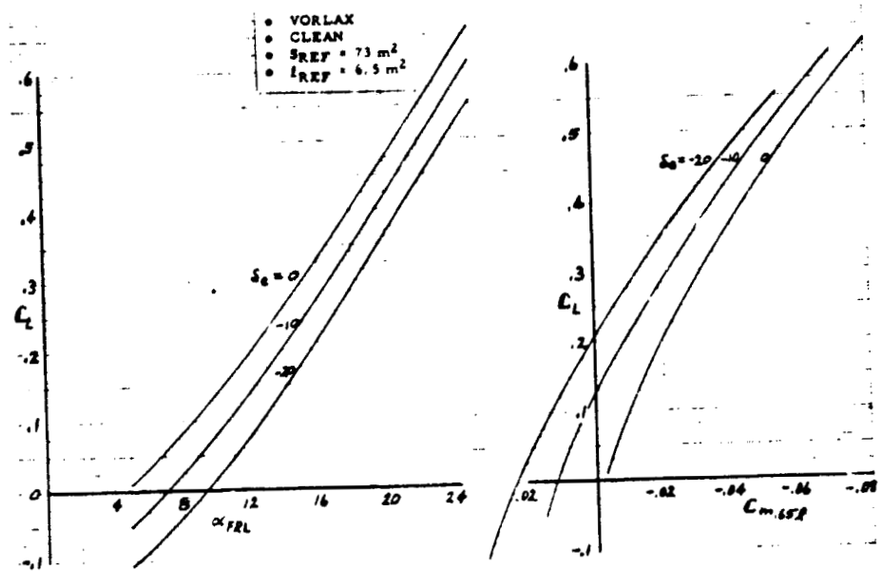

Figure 56 - Pitch Data - M = 1.2

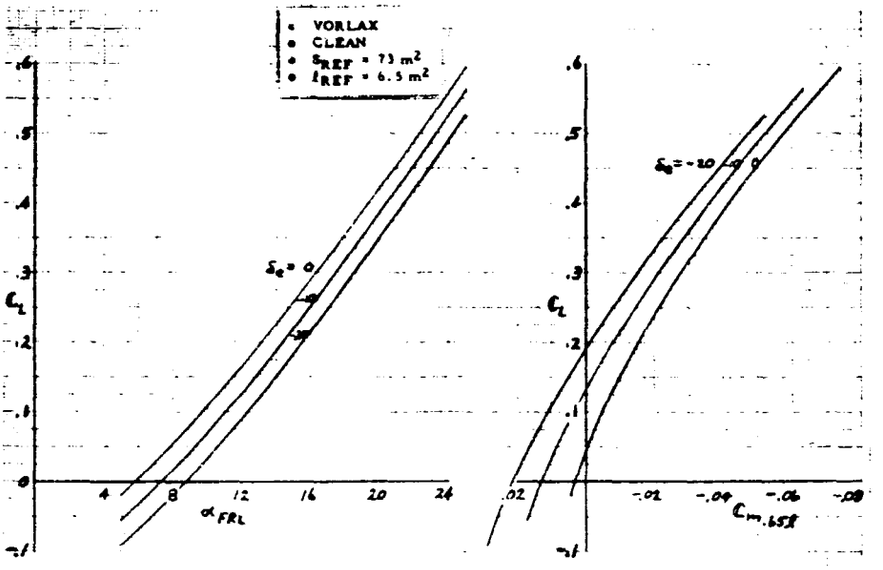

Figure 57 - Pitch Data - M = 1.6

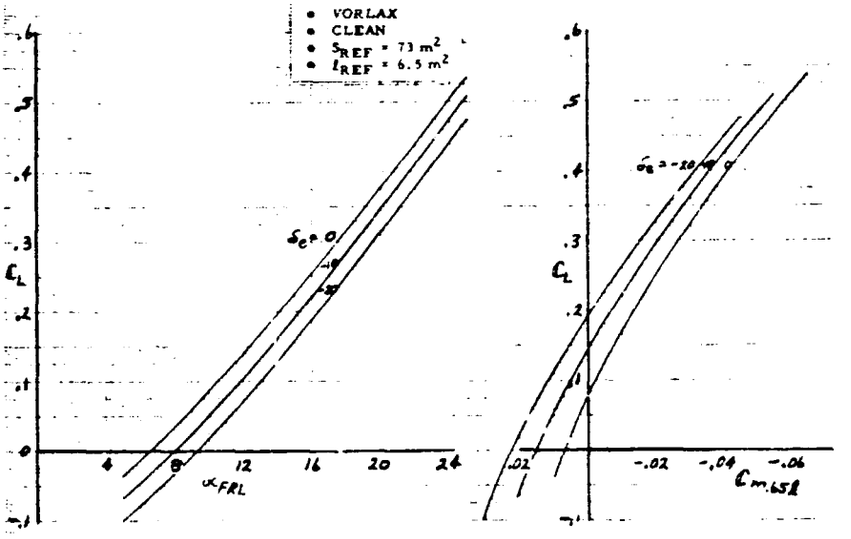

Figure 58 - Pitch Data - M = 2.0

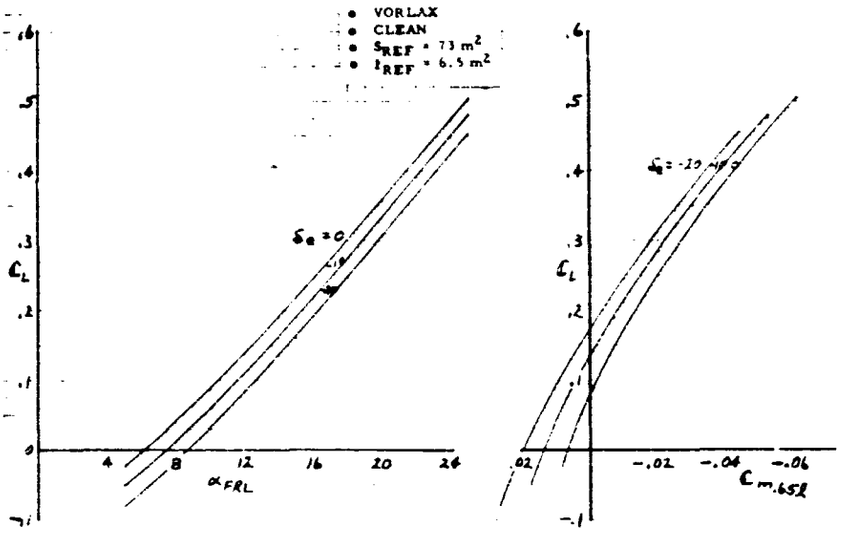

Figure 59 - Pitch Data - M = 2.4

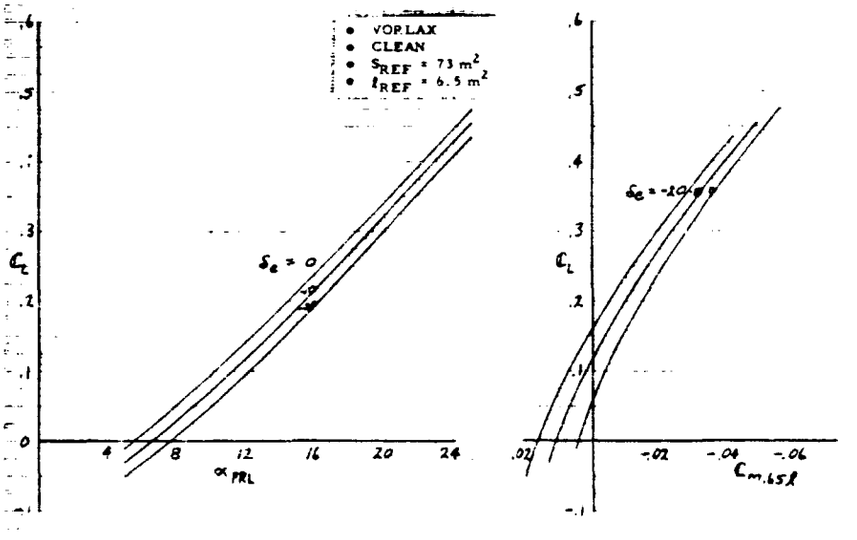

Figure 60 - Pitch Data - M = 3.0

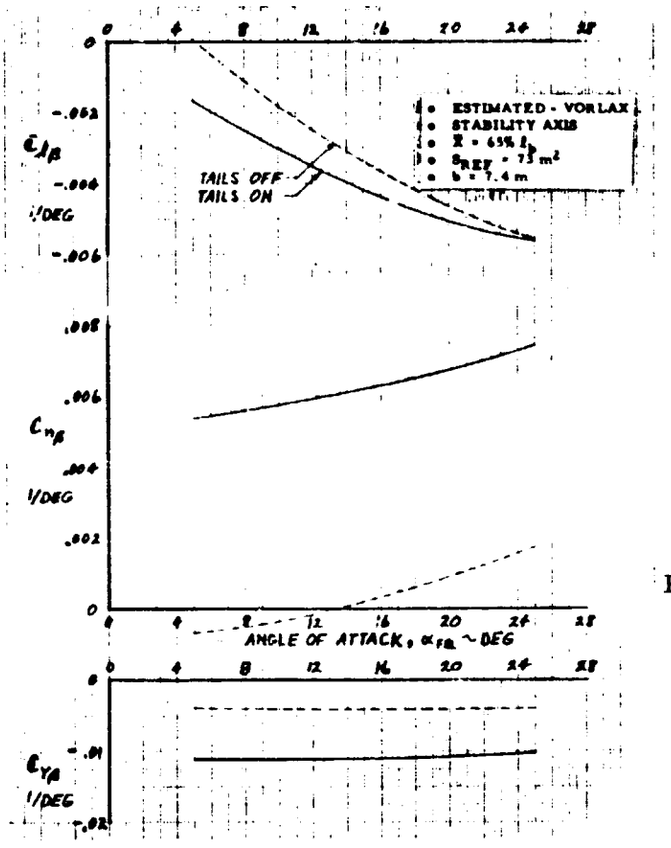

Figure 61 - Low Speed Sideslip Data

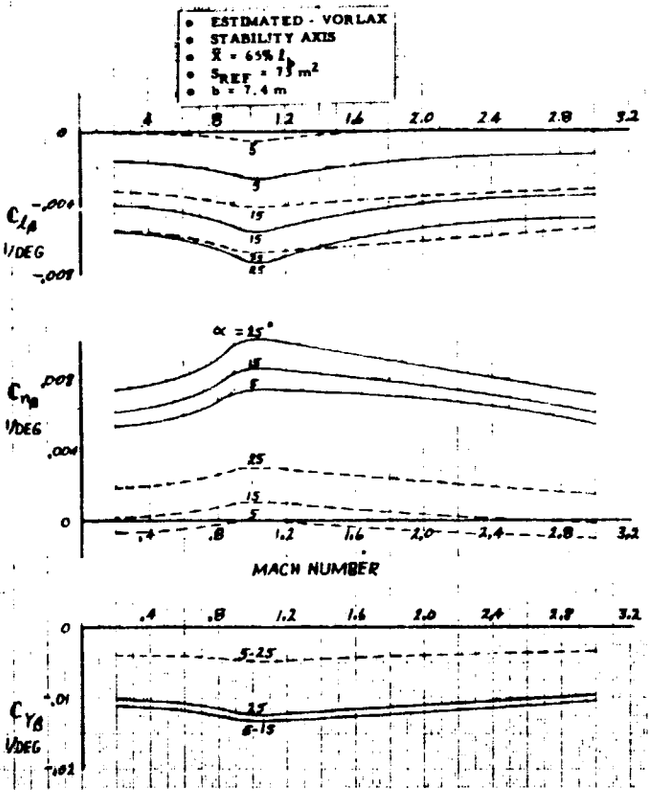

Figure 62 - Sideslip Characteristics

expansion surfaces were computed with a Prandtl-Meyer expansion from free stream. Computer generated drawings of the inviscid aerodynamic configuration are shown in Figure 52.

The viscous forces were calculated by the Spalding-Chi method using a wall temperature of 444.4 K. A fully turbulent boundary layer was assumed. Lift and pitching moment for five elevon positions at Mach 3.0, 4.0, 6.0 and 8.0 are shown in Figures 63 through 66. The corresponding untrimmed drag polar are shown in Figures 67 through 70. Hypersonic sideslip characteristics are shown in Figure 71 as a function of angle of attack.

Stability and Control Summary Data - Longitudinal stability, elevator effectiveness, and lateral-directional stability are summarized throughout the Mach number range from 0.2 to 8.0 in Figures 72, 73 and 74 respectively. Figure 73 shows the vehicle to be statically stable in pitch across the Mach number range. However, for high angles of attack at low speed the vehicle is excessively stable and experiences large lift loss due to trim. In addition to showing lateral and directional

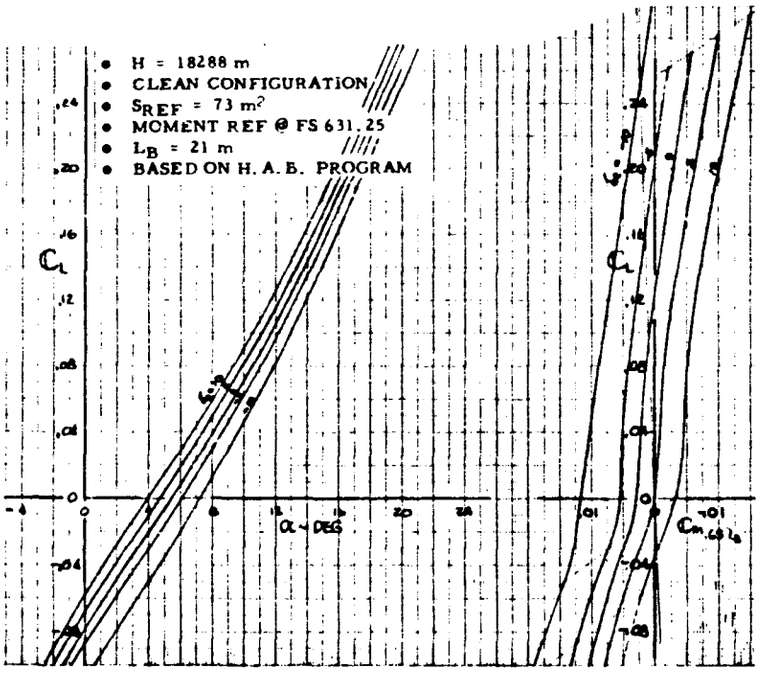

Figure 63 - Pitch Characteristic - M = 3.0

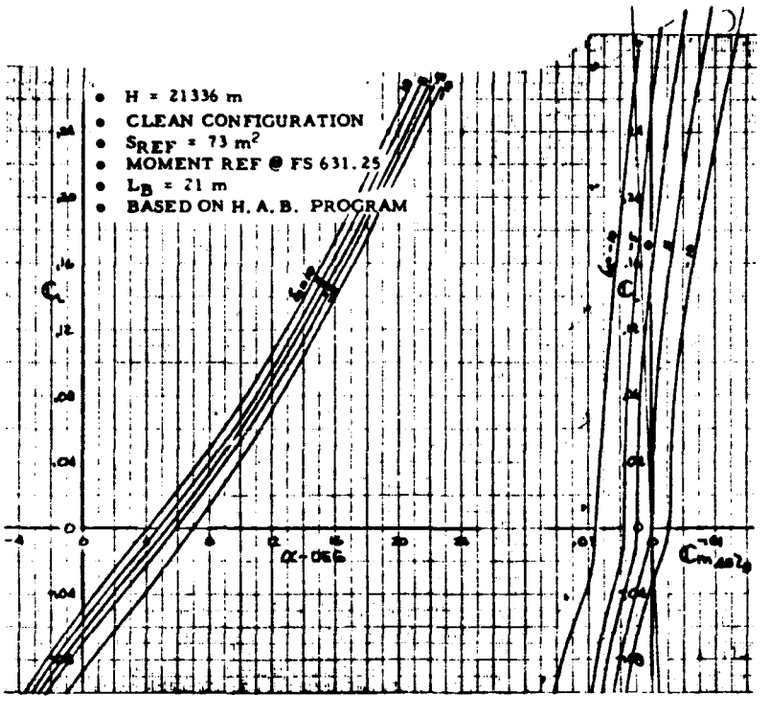

Figure 64 - Pitch Characteristics - M = 4.0

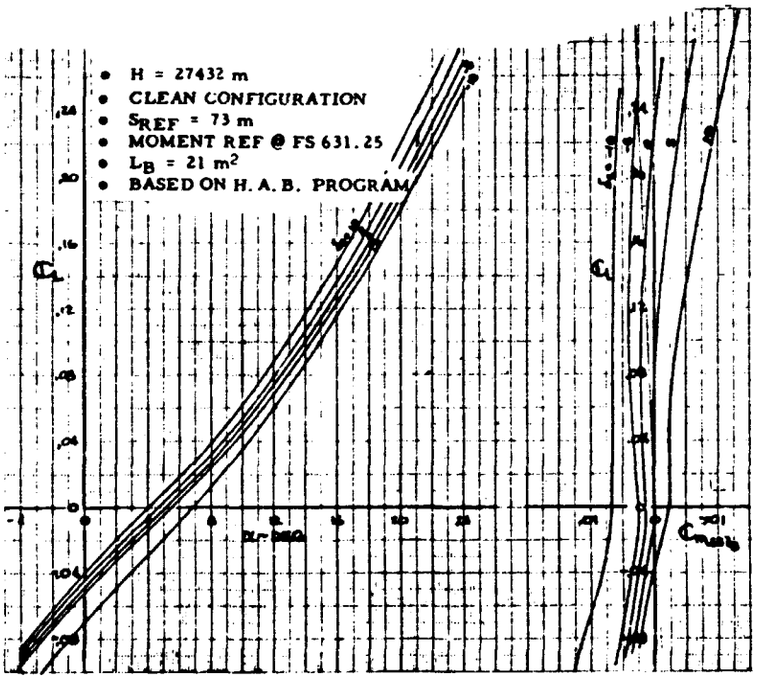

Figure 65 - Pitch Characteristics - M = 6.0

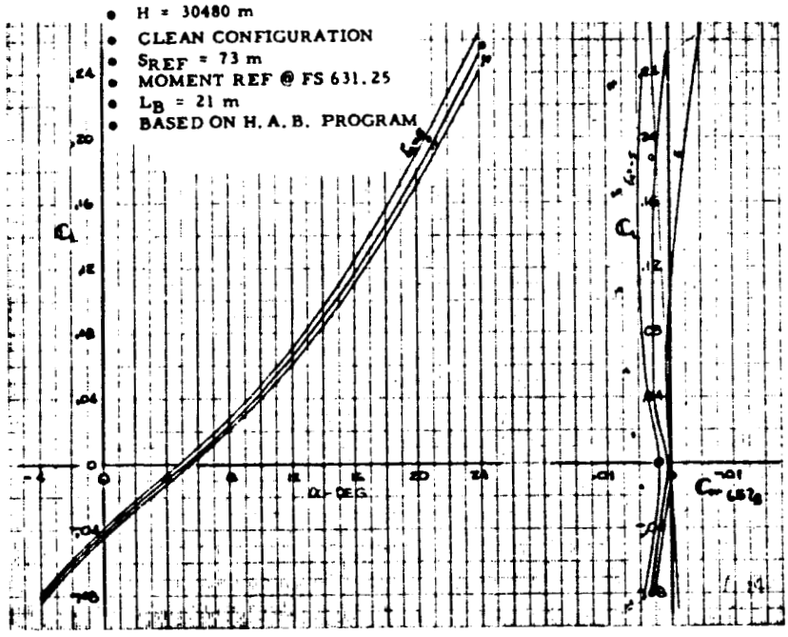

Figure 66 - Pitch Characteristics - M = 8.0

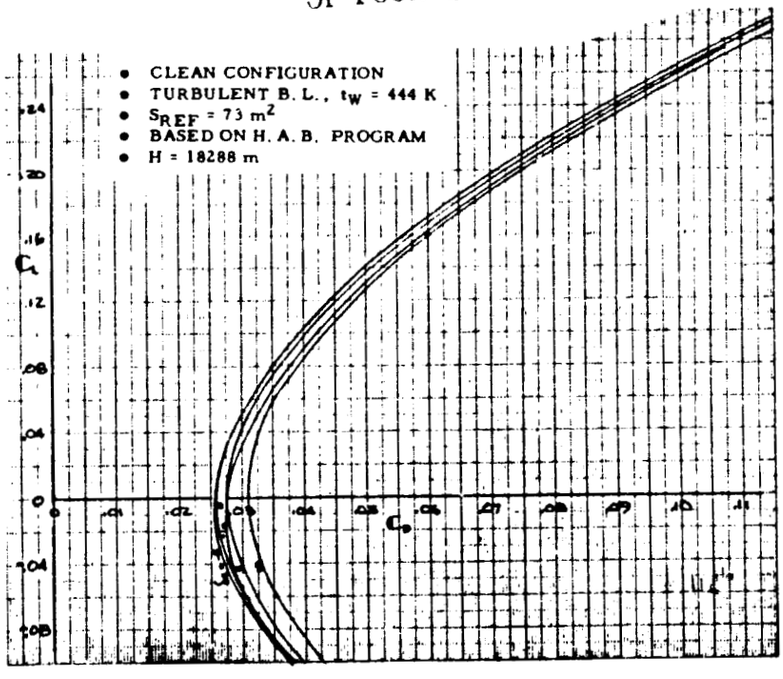

Figure 67 - Drag Polar - M = 3.0

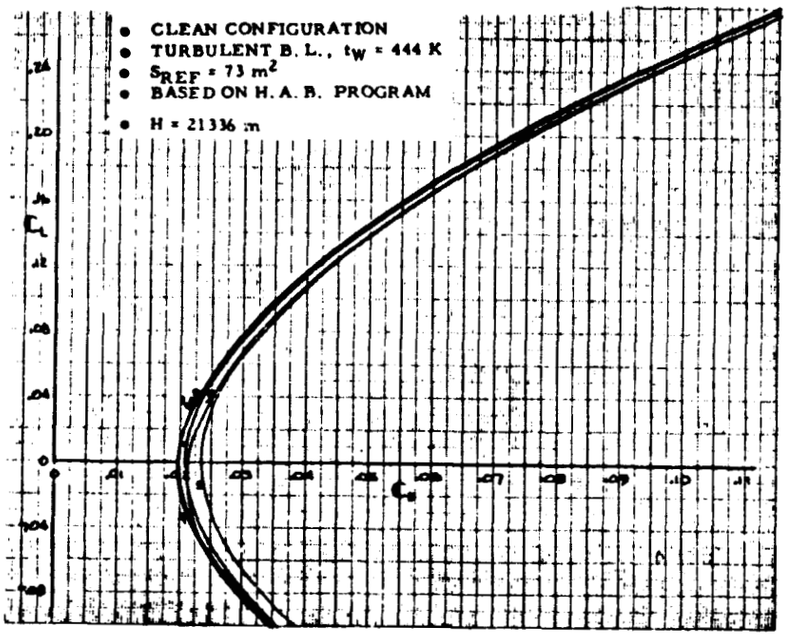

Figure 68 - Drag Polar Drag - M = 4.0

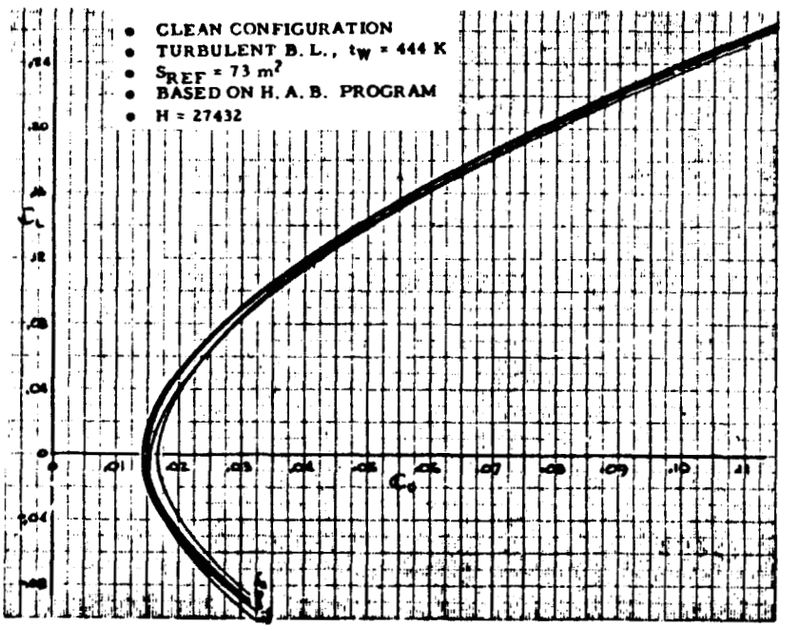

Figure 69 - Drag Polar - M = 6.0

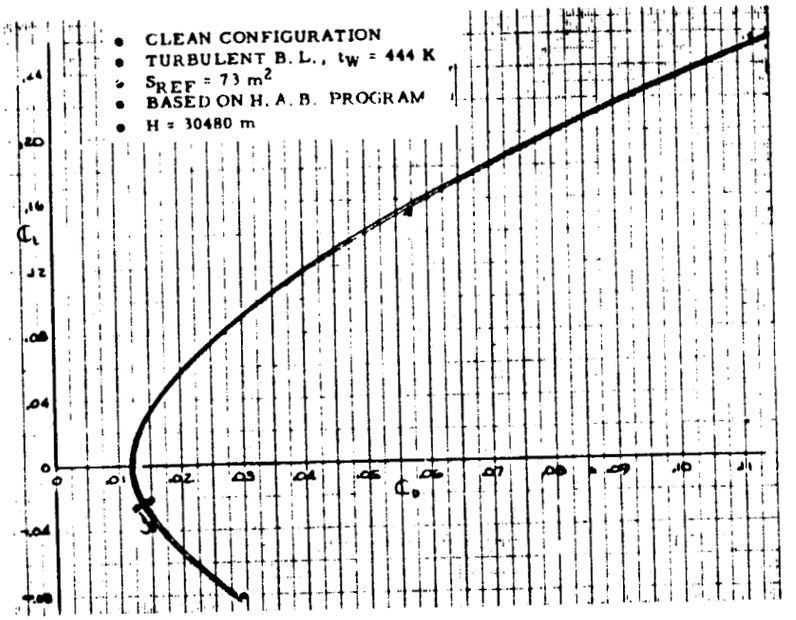

Figure 70 - Drag Polar - M = 8.0

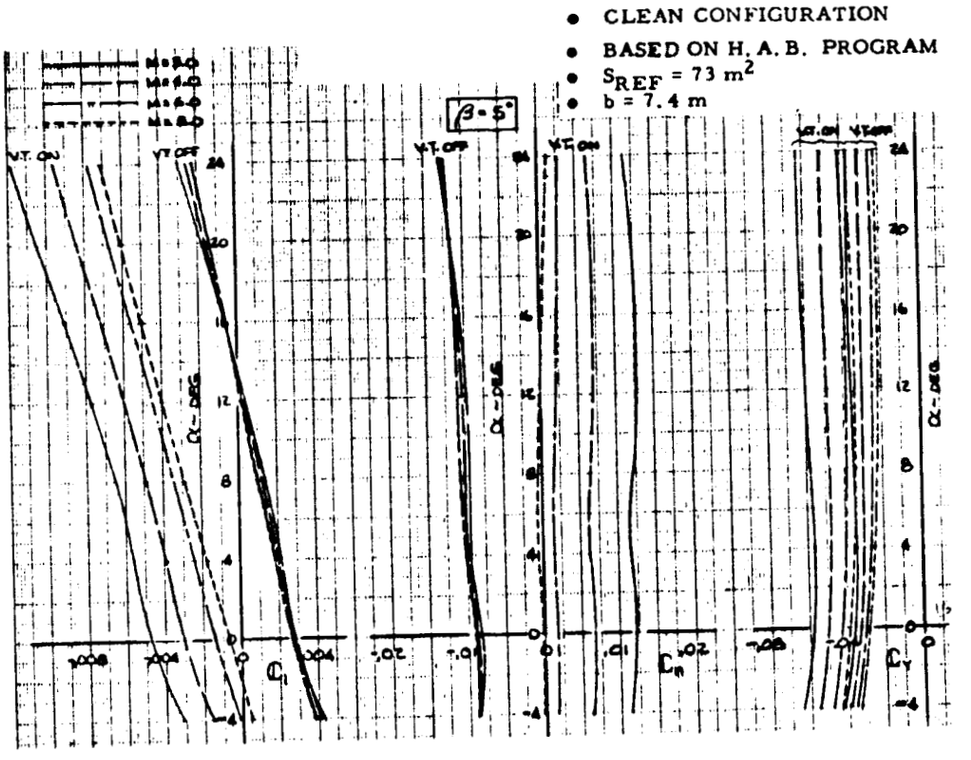

Figure 71 - Sideslip Characteristic

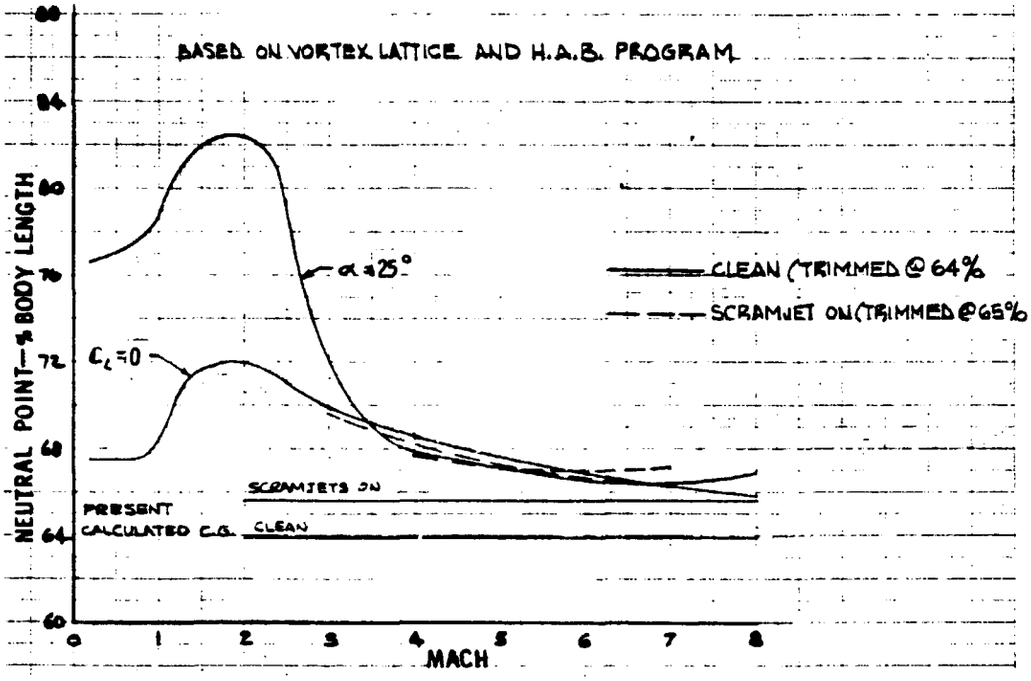

Figure 72 - Longitudinal Stability

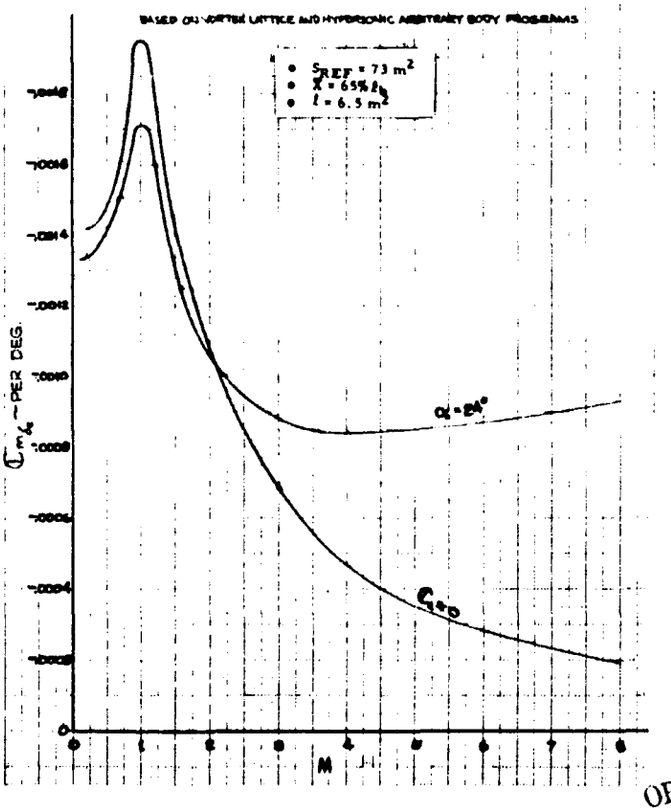

ORIGINAL PAGE IS
OF POOR QUALITY

Figure 73 - Elevon Effectiveness in Pitch

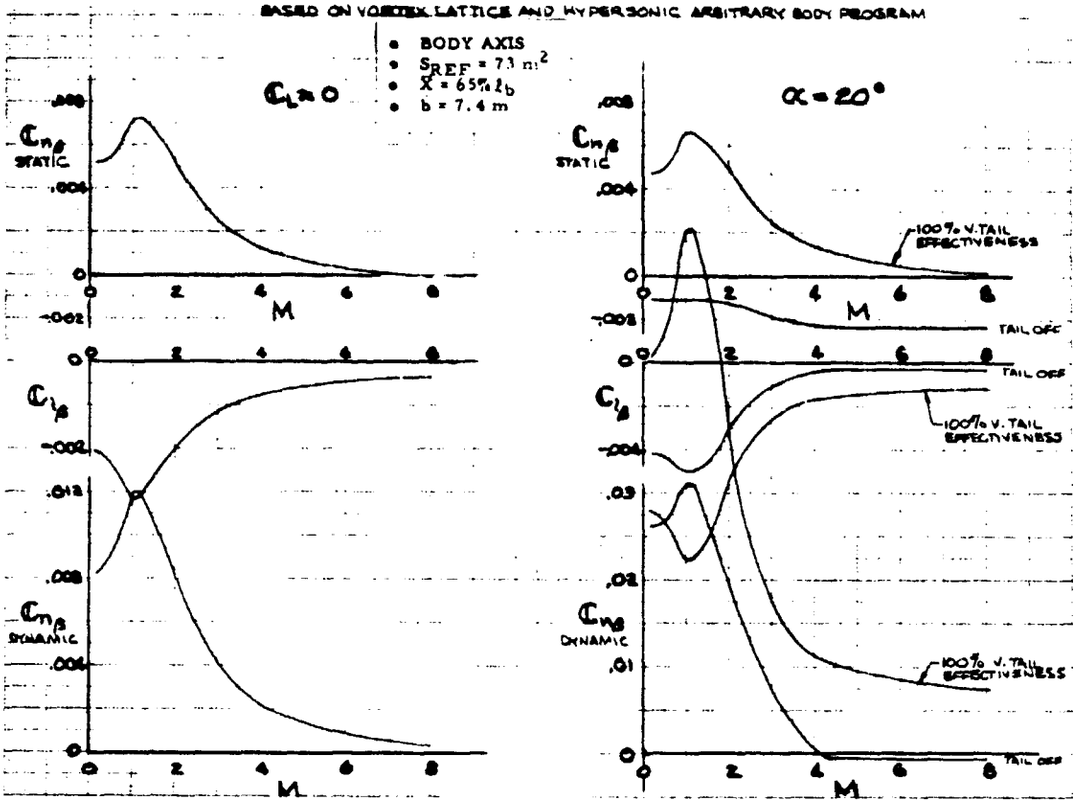

Figure 74 - Lateral Stability

static stability Figure 74 shows dynamic directional stability. The vehicle is statically stable throughout the mach range with vertical stabilizers on. However, due to the "shadowing" effect of the wing at high angles of attack which was not taken into account in this analysis, the vertical stabilizer effectiveness shown here will probably not be realized. The vehicle may be statically unstable at high angles of attack at high Mach numbers. The dynamic directional stability parameter indicates that even for statically unstable flight conditions the vehicle will be dynamically stable.

Aerodynamic Data for Performance - The basic drag data which were used in performance computations are shown in Figures 75 through 82. Total drag for trimmed flight in the clean configuration is shown in Figures 76 and 77. As noted ten percent of zero lift drag must be added to these values for miscellaneous roughness. Skin friction drag was computed using Reynolds numbers corresponding to speeds and altitudes along a nominal flight path.

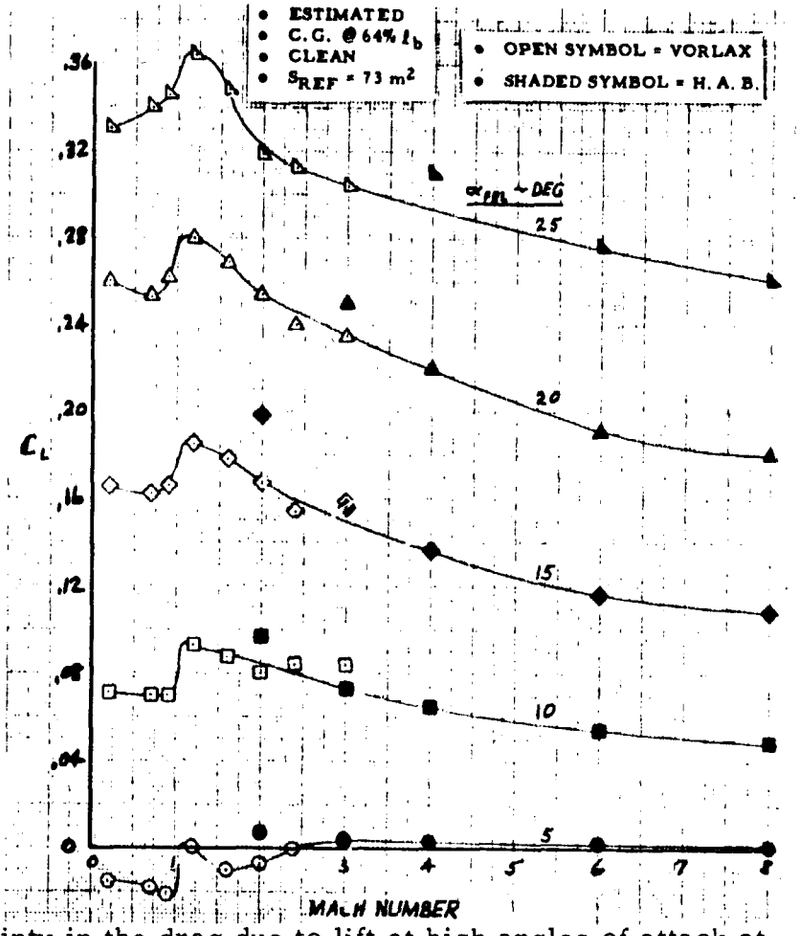

Figure 75 - Trimmed Lift Coefficient

There is some uncertainty in the drag due to lift at high angles of attack at subsonic and transonic Mach numbers because of difficulty in estimating the drag of the deflected elevons. This may have resulted in somewhat optimistic drag levels at high angles of attack below Mach 2. Figure 78 presents low speed drag to be used for landing performance calculations. Skin friction drag for this figure was computed for Reynolds numbers at sea level. Note that the ten percent miscellaneous drag factor is included in these polars.

Scramjet module drag increments, for use during boost, are shown in Figures 79 and 80. These two increments are to be added to the basic drag of Figures 76 and 77 when the scramjet modules are attached to the vehicle. The base drag shown in Figure 81 is already included in Figures 76 and 77 and is presented here for reference only. Component drags for the entire vehicle are presented in Figure 82 at Mach 6 as obtained from the Hypersonic Arbitrary Body Aerodynamic Computer Program. These figures show the relative magnitudes of all the vehicle components.

Figure 76 - Trimmed Drag - C_L = 0 - 0.30

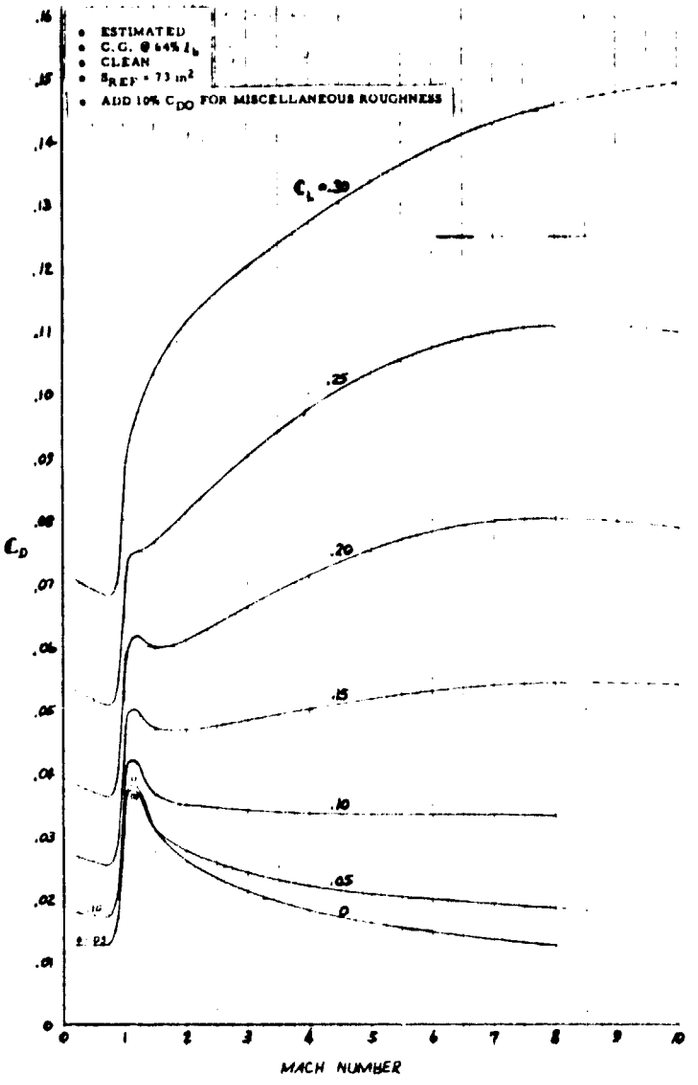

Maximum lift to drag ratio and the angle of attack at which it occurs are presented in Figure 83 as functions of Mach number. A comparison between the Phase III Configuration and the Baseline Configurations shows an improvement in L/D_{max} for the Phase III Configuration over the Baseline. Angle of attack for L/D_{max} is approximately the same for the two vehicles, however, it should be recognized that angle of attack on the Phase III vehicle is measured to the bottom surface. This gives angle readings about 2-1/2° higher than the Baseline (Phase I-II) vehicle.

Performance - The design criteria which had the most effect on this Phase III concept refinement configuration was to cruise on scramjet thrust at M = 6.6

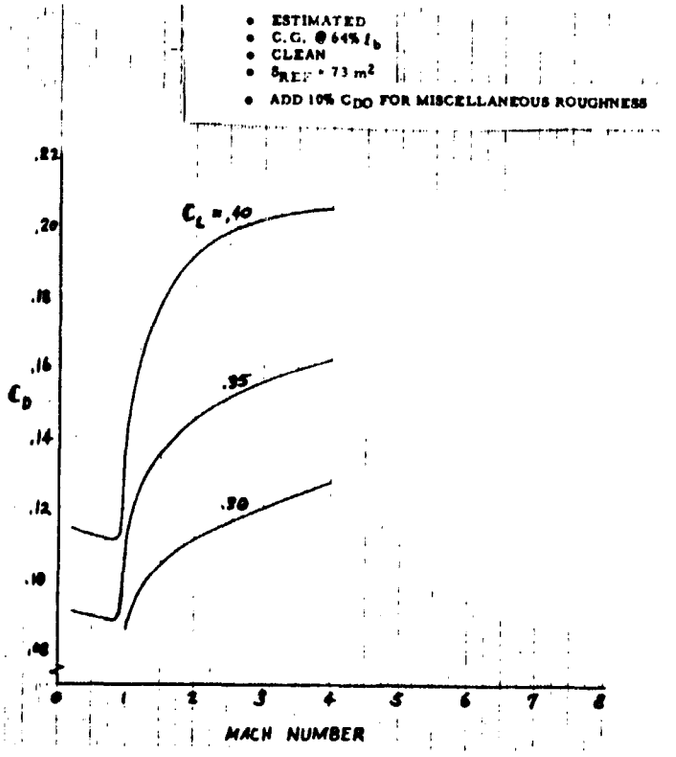

Figure 77 - Trimmed Drag - C_L = 0.35 - 0.40

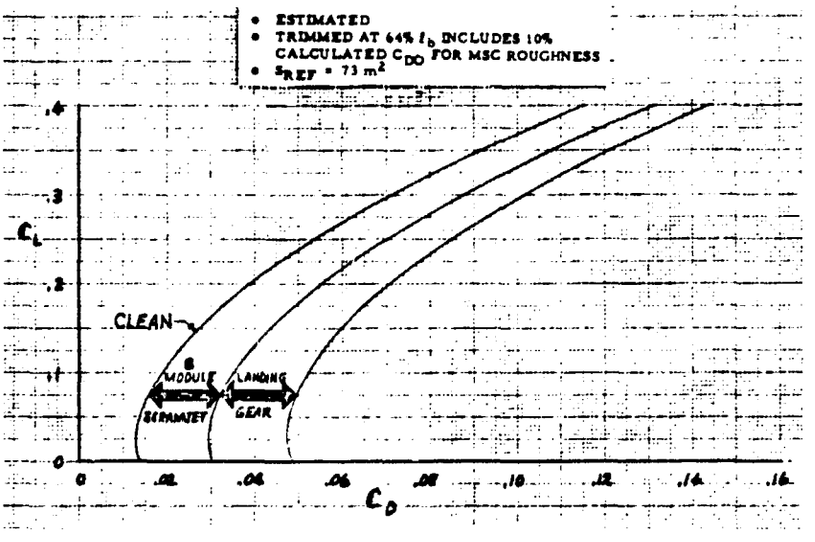

Figure 78 - Low Speed Drag

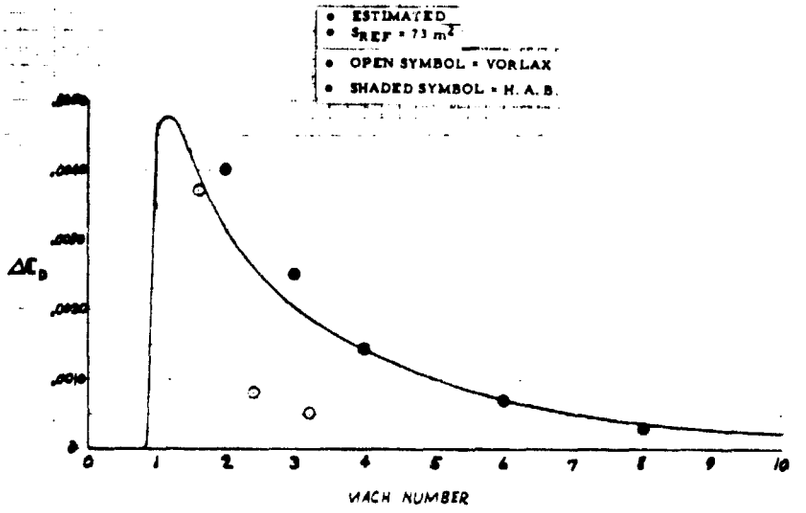

Figure 79 - Scramjet Mount Drag Increment

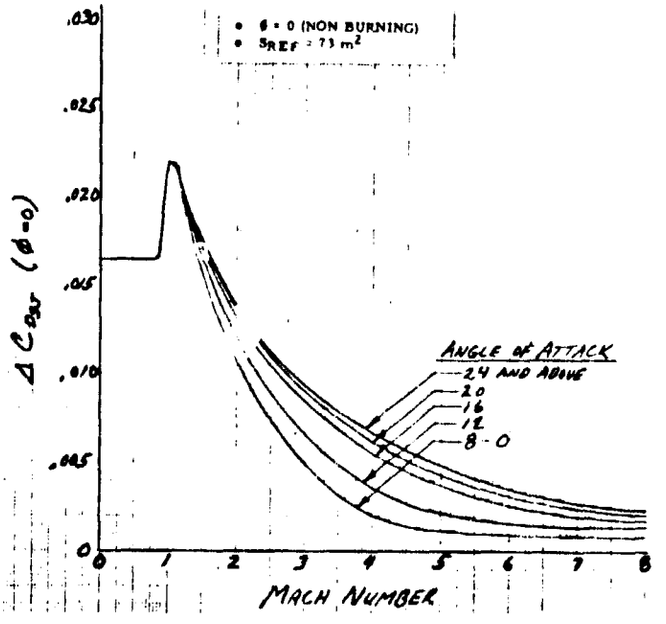

Figure 80 - Scramjet Drag

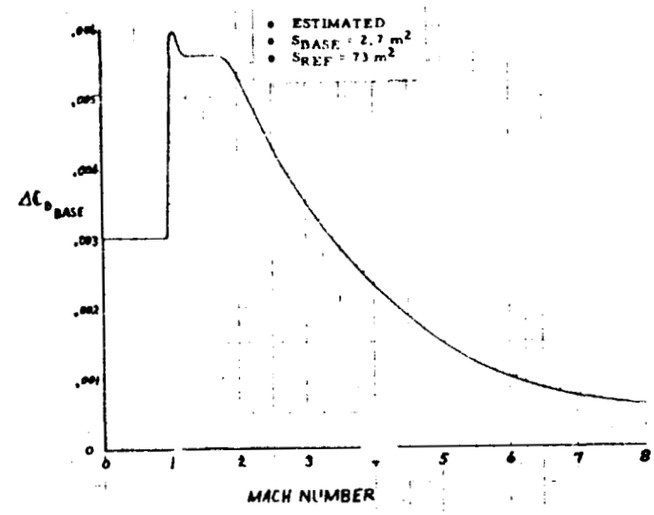

Figure 81 - Base Drag, During Boost

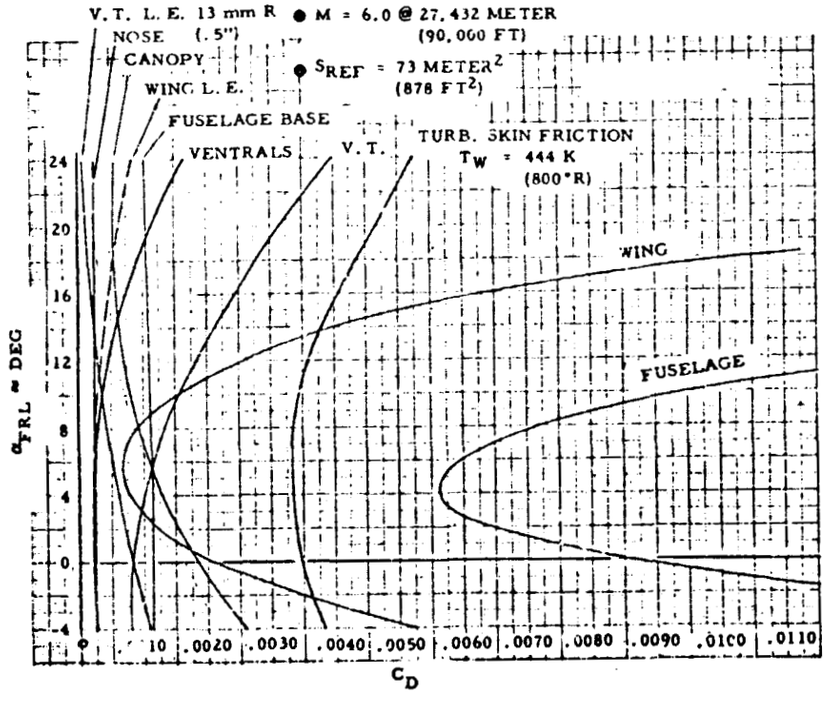

Figure 82 - Component Drag

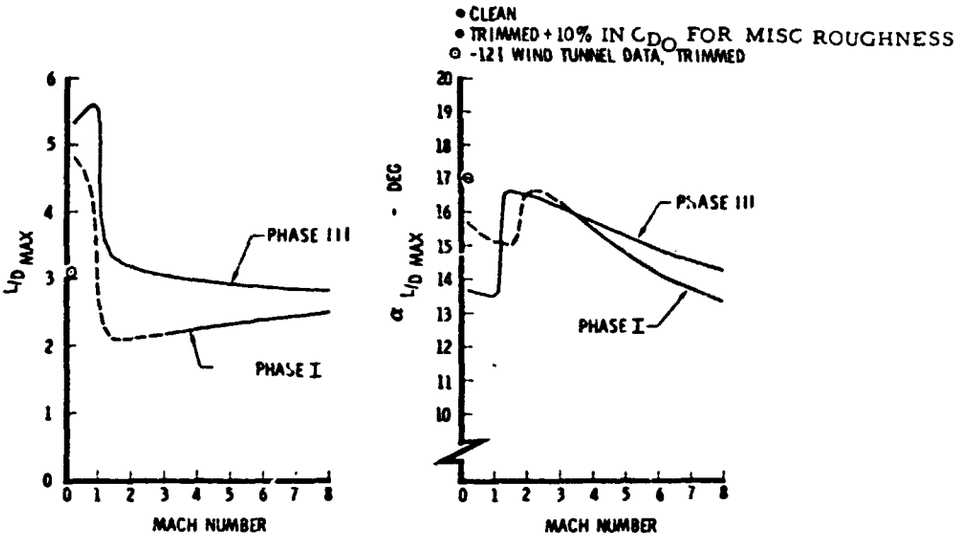

Figure 83 - Lift/Drag Vs Mach Number

and q = 47.9 kPa on 80% of calculated thrust. An evaluation of how well this first configuration iteration did is shown in Figure 84. The installed drag includes all effects, lift, trim, etc. of the 8 - 0.46 m modules at 100% thrust. As can be seen the 80% thrust with 0.46 m modules at C_L for q = 47.9 kPa is 3% short of target.

Scramjets with a cowl angle of 0 were installed for this performance evaluation. With θ_{cowl} = 0, the scramjet height can grow 0.06 m for the same ground clearance as the original θ_{cowl} = 6° scramjets. The resulting 0.5 m modules (same width as the 0.46 m modules) would give an 11% pad on the scramjet cruise criteria. At 100% calculated thrust with either engine size the scramjets could cruise the vehicle at C_L's and q's representative of operational hypersonic cruise aircraft.

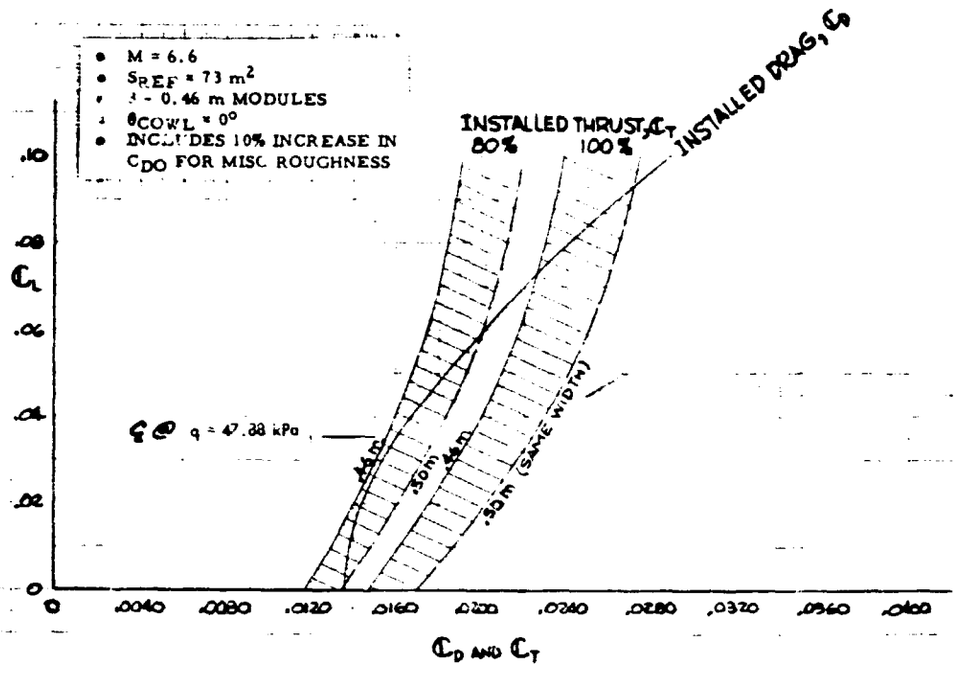

Figure 84 - Scramjet Cruise

The drag for all the calculated performance shown in this repor includes an addition of 10% of the zero lift drag, both friction and pressure, to allow for miscellaneous roughness and protuberances that will evolve as the configuration moves from its present idealized shape to a real vehicle.

For satisfactory landing characteristics, an L/D_{max} greater than 3.5 was specified. Figure 83 shows an L/D_{max} of 5.5 can be obtained for the clean aircraft. The addition of cruise scramjets drops this to 3.6. With cruise scramjets and landing gear extended the L/D_{max} drop to 3.0. A two second gear extension time is proposed such that the landing flare can be mostly completed before adding the gear drag.

At a landing mass of 12.7 Mg, corresponding to a heavy condition with cruise scramjets, 200 KEAS, knots equivalent airspeed, requires a C_L = 0.26. This lift coefficient is slightly above that for L/D_{max} with cruise scramjets indicating a touchdown speed of less than 200 KEAS is possible.

The rocket boosted performance capability with cruise scramjets is shown in Figure 85 and without scramjets in Figure 86. All boosts follow the scheme described in Phase I, Reference 2, terminating in level flight at q = 47.9 kPa.

The capability of the Phase III vehicle is significantly improved over the Phase II configuration. The design point for the Phase III vehicle was for 40 seconds of scramjet cruise at M = 6.6 and a launch mass of 31.75 Mg. The Phase III vehicle is capable of the design performance with a partial propellant load of 17.48 Mg and a launch mass of 30.8 Mg.

At the design launch mass of 31.75 Mg the Phase III vehicle with cruise scramjets can boost to M = 6.82. However, the TPS will not allow 40 seconds of cruise at q = 47.9 kPa. On this first design iteration the Phase III vehicle was sized for 19 Mg of propellant, an intentional excess for contingency. Using the full 19 Mg of propellant gives a launch mass of 32.4 Mg and a boost to M = 6.97. Again, the TPS will not allow 40 seconds of cruise but approximately 25 seconds at q = 47.9 kPa.

The M = 6.6 cruise case carries excess propellant capacity, vehicle size, and structural capability. The M = 6.82 and 6.97 cases are short on TPS and structural capability. A totally consistent vehicle to meet the 40 second cruise criteria is inbetween. Based on Phase II results a consistent vehicle was estimated and scaled to yield scramjet cruise Mach number capability versus launch mass for the improved Phase III configuration. A consistent Phase III vehicle with 31.75 Mg launch mass could cruise for 40 seconds at M = 6.76. A Mach 6.6 cruise vehicle would launch at 30.3 Mg. A Mach 6.0 cruise Phase III configuration could launch at approximately 22.9 Mg.

Without scramjets, the performance capability of the Phase III vehicle with 19 Mg of propellant will provide excellent research potential. Figure 86 shows this in terms of rocket cruise time versus Mach numbers for q = 47.9 kPa. With the full 19 Mg of propellant and 2.3 Mg of payload the vehicle without scramjets would launch at 31.75 Mg. This would give zero cruise time at M = 7.57 or 120 seconds

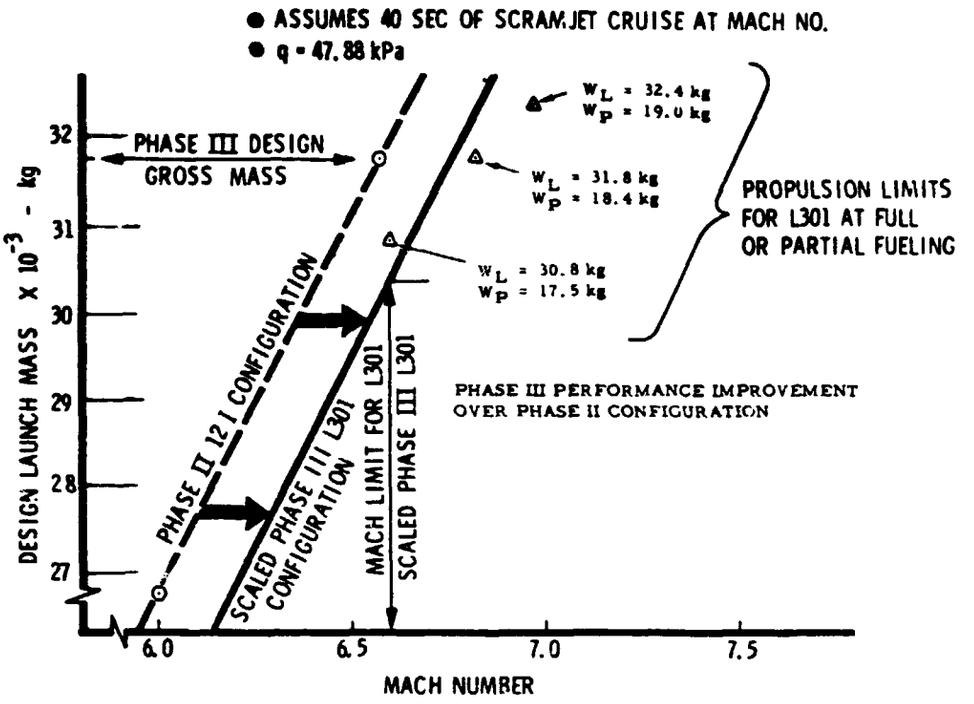

Figure 85 - Performance with Scramjets

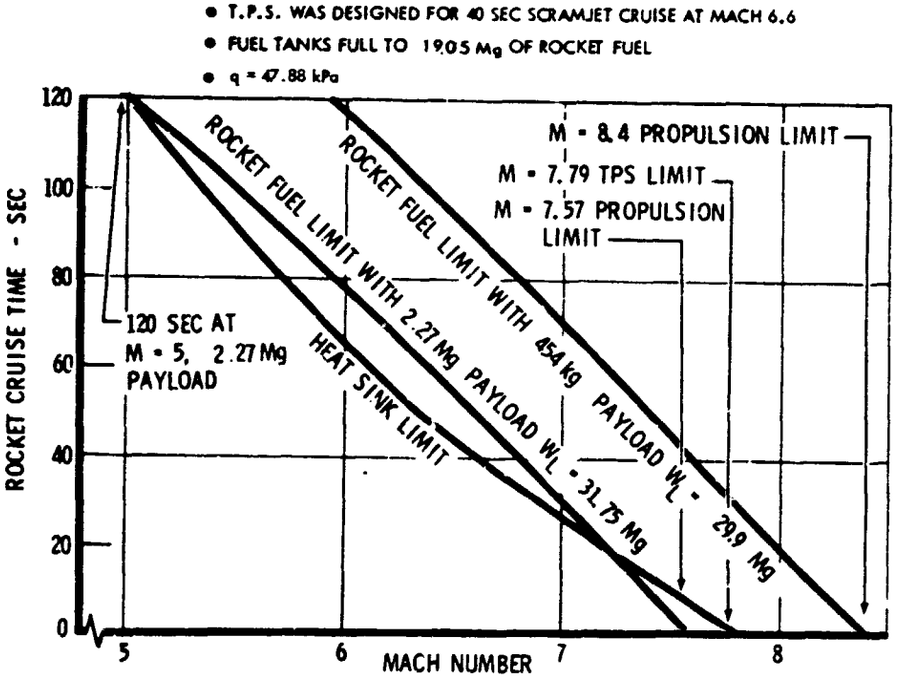

Figure 86 - Performance without Scramjets

at M = 5.0. A TPS limited, zero cruise time, q = 47.9 kPa, Mach number of 7.79 can be attained with approximately 1.81 Mg of payload.

A boost capability with 19 Mg of propellant and 454 kg of payload would be M = 8.4. From Phase II experience, it is estimated that M = 8.4 would be within the TPS capability at approximately q = 23.9 kPa. Even at q = 47.9 kPa the overheating may be found tolerable as flight experience is accumulated, particularly since a factor of safety of 1.25 was used for all heating load calculations.

Scramjet Integration and Performance

Thrust/Drag/Moment Accounting Procedure - The accounting system used for defining scramjet performance was developed in accordance with the desire that scramjet net thrust be defined in the same manner that has been used in the past for jet engines and subsonic combustion ramjets. This establishes engine net thrust as the difference between exhaust nozzle gross thrust and freestream ram drag, where gross thrust is defined as the integral of momentum plus pressure force (referenced to ambient static pressure) over the plane of the scramjet exhaust from scramjet-cowl trailing edge to fuselage trailing edge. Installed net thrust is net thrust minus inlet spillage drag. A summary of the accounting procedure used for thrust, drag, lift, and pitching moment is shown in Tables 1 through 3.

Scramjet Performance Calculation Methods

- Engine Internal Performance - Internal performance of the scramjet module was computed by NASA Langley. Engine flow parameters were defined over the freestream Mach number range from 5.0 to 7.0 and for a range of local Mach numbers at the scramjet inlet station. Performance was defined for stoichiometric and zero fuel flow conditions. Specification of the flow properties, properties of state, and chemical composition at the combustor exits provided initial conditions for subsequent calculations of exhaust nozzle flow.

The installed net thrust in the wind direction if $F_{Net_{inst}} = F_G - F_{R_O} - D_{Spill_{inlet}}$

The installation drag is $\Delta D = D_{Spill_{Fore}} + D_{cowl} - D_1 - D_2 - (F_{R_O} - F_{R_I})$

where F_G = nozzle gross thrust

F_{R_O} = freestream ram drag

$D_{Spill_{Inlet}}$ = inlet stream tube additive drag from initial inlet shock wave to cowl lip

$D_{Spill_{fore}}$ = inlet stream tube additive drag from inlet entrance station to initial inlet shock wave

D_{Cowl} = cowl drag

D_1 = drag of that portion of airframe without scramjets but with scramjet mount which is covered by modules

D_2 = drag of that portion of airframe without scramjets but with scramjet mount which forms the upper nozzle expansion surface

F_{R_1} = ram drag of inlet stream tube evaluated at inlet entrance station

The excess thrust in the wind direction is $F_{net_{inst}} - (D_{airp} + D_{base} + \Delta D)$

where D_{airp} = airplane drag, excluding base drag, without scramjets but with scramjet mount

D_{base} = airplane base drag

Table 1 - Accounting Procedure - Thrust and Drag

- Scramjet Exhaust Nozzle - A two-dimensional method-of-characteristics computer program was used to define flow in the scramjet exhaust nozzle. Typical results are shown in Figure 87, in which divergences of the characteristic lines indicate regions of acceleration in the flow. The example shown is for stoichiometric burning. Typical wall pressure distributions are shown in Figure 88. This example shows the effect of gas properties on static pressure distribution. Both cases were computed with identical properties at the nozzle throat. In one case the

The lift normal to the wind direction due to the scramjet installation and the airframe base pressure is:

$$\Delta L = L_G - L_{R_I} + L_{Spill_{Inlet}} + L_{spill_{fore}} + L_{cowl} - L_1 - L_2 + L_{base}$$

where L_G = nozzle gross lift

L_{R_I} = ram lift of inlet stream tube evaluated at inlet entrance station

$L_{spill_{inlet}}$ = inlet stream tube additive lift from initial inlet shock wave to cowl lip

$L_{spill_{fore}}$ = inlet stream tube additive lift from inlet entrance station to initial inlet shock wave

L_{cowl} = cowl lift

L_1 = lift on that portion of the airframe without scramjets but with scramjet mount which is covered by the scramjet modules

L_2 = lift on that portion of the airframe without scramjets but with scramjet mount which forms the upper nozzle expansion surface

L_{base} = airplane base lift

Table 2 - Accounting Procedure - Lift

The pitching moment due to the scramjet installation is:

$$\Delta M = M_G - M_{R_I} + M_{spill_{inlet}} + M_{spill_{fore}} + M_{cowl} - M_1 - M_2$$

where M_G = nozzle gross moment

M_{R_I} = ram moment of inlet stream tube evaluated at inlet entrance station

$M_{spill_{inlet}}$ = inlet stream tube additive moment from initial inlet shock wave to cowl lip

$M_{spill_{fore}}$ = inlet stream tube additive moment from inlet entrance station to initial inlet shock wave

M_{cowl} = moment on cowl

M_1 = moment on that portion of the airframe without scramjets but with scramjet mount which is covered by the scramjet modules

M_2 = moment on that portion of the airframe without scramjets but with scramjet mount which forms the upper nozzle expansion surface

and the moments, M, are considered positive when they act on the vehicle in a nose-up direction.

Table 3 - Accounting Procedure - Pitching Moment

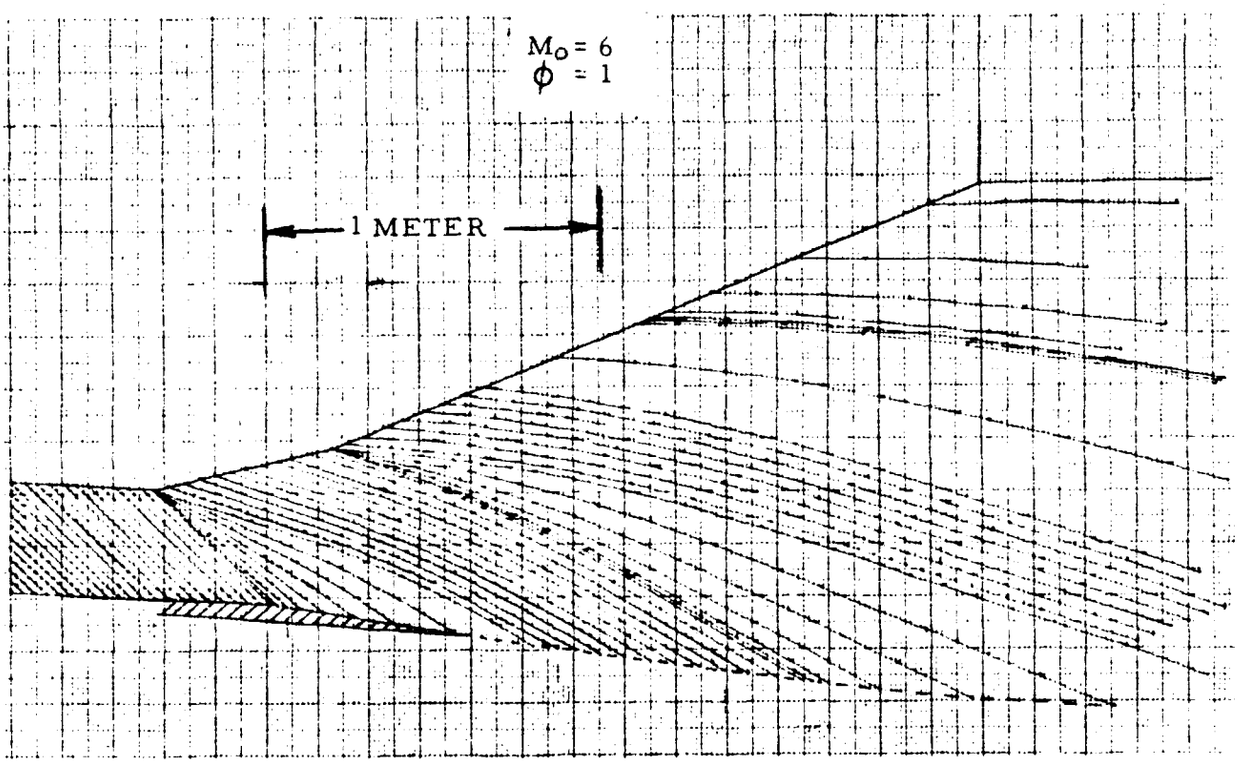

Figure 87 - Typical Scramjet Exhaust Nozzle Characteristics Network

nozzle flow was treated as a real gas with frozen chemical composition, and the other as a perfect gas. As indicated in Figure 88, the resulting pressures, and therefore nozzle thrusts, were nearly the same for the two cases. Subsequent calculations were therefore done using the perfect gas assumption with the ratio of specific heats as specified in the NASA engine performance tables. The true nozzle flow will be somewhere between frozen and equilibrium states; however, the assumption of frozen or perfect gas flow represents a conservative approach at this time.

- Forebody Flow Field - Existing theoretical and experimental results were analyzed to determine the effect of angle of attack on local flow conditions at the scramjet entrance station. Since the scramjet engine

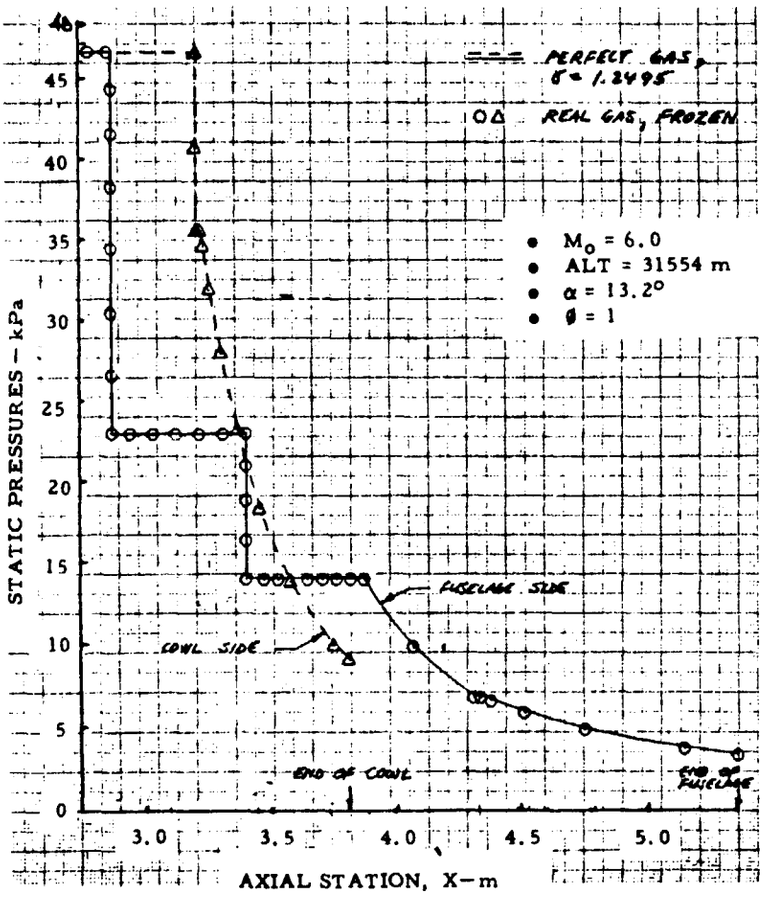

Figure 88 - Effect of Gas Properties on Nozzle Pressure Distribution

data were presented as a function of the effective conical compression angle of the forebody, the flow field data were correlated as shown in Figure 89 so that the effective conical compression angle could be determined knowing the angle of incidence of the lower forebody surface to the freestream direction. At a surface incidence angle of 12 degrees the incidence angles the equivalent conical compression angle is less, whereas at lower incidence angles the equivalent conical compression angle is greater than the incidence angle. With the local forebody ahead of the inlet aligned into the freestream direction, the correlation of Figure 89 indicates about 3.2 degrees of effective conical compression at the inlet entrance stations.

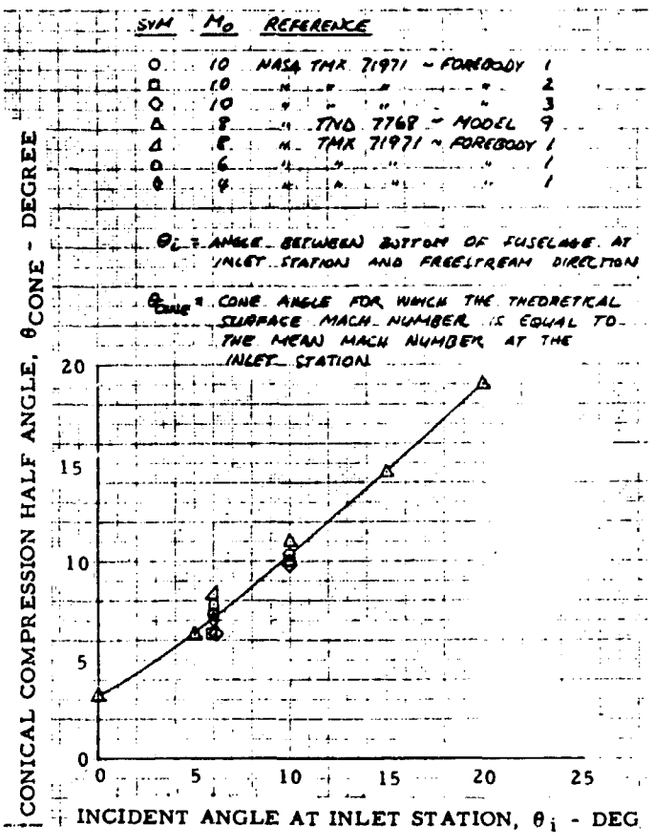

Figure 89 - Effective Conical Compression Angle of Aircraft Forebody

Boundary layer thickness parameters at the inlet entrance station are required for computation of installed scramjet performance. An analytical investigation of the factors affecting boundary layer growth on the aircraft fuselage showed that the most important factor was whether the viscous flow acted in a two-dimensional or three-dimentional manner. Variables of lesser importance appeared to be wall temperature and real gas effects. Bluntness and transition effects, while significant near the forebody nose, had largely disappeared by the time the boundary layer reached the inlet station. A study of NASA boundary layer thickness measurements on the lower surface of the YF-12 aircraft indicated that a two-dimensional prediction technique correlated better with the data than an axisymmetric prediction method. Consequently, the X-24C

centerline boundary layer was computed using two-dimensional flow assumptions. NASA oil flow experiments with an X-24C wind tunnel model indicated that the boundary layer at the outboard edge of the scramjet package might be considerably less thick than that at the centerline, due to a shorter length of run and some three-dimensioned effects. Therefore, the mean boundary layer thickness parameters at the inlet station were estimated to be 75 percent of the computed centerline values.

The two-dimensional boundary layer solutions employed real gas effects, empirical transition locations, sharp leading edges, and wall temperatures equal to the mean value during cruise.

- Scramjet Installation Losses - Scramjet module external surface lift, drag, and moment components were estimated using shock-expansion theory in conjunction with the local Mach number under the fuselage. Forces and moments due to inlet spillage were estimated in a similar manner, allowing for the variation in spillage mass flow with angle of attack. Pressures on the aft fuselage nozzle ramp, without scramjet engines, were taken to be the higher of base pressure or a pressure computed by Prantle-Meyer expansion from local conditions ahead of the ramp.

  Local ram drag at the inlet entrance station was computed using predicted values of the boundary layer thickness parameters. Exhaust nozzle net thrust, lift, and pitching moment were assumed to be proportional to the respective values for inviscid computed from the NASA scramjet engine performance data. The constant of proportionality was assumed in the engine cycle analysis. Fuel flows obtained from the engine cycle data were increased by twenty percent to approximate installation losses.

Scramjet Integration Studies - Integration of the scramjet modules with the airframe proceeded simultaneously with the evolution of the airframe configuration. A summary of the scramjet propulsion system evolution is shown in Table 4. Initial design studies on the Baseline Configuration aircraft indicated that fore and aft translation of the module, with constant nozzle exit area, produced only moderate changes in net thrust minus installation drag, but very dramatic changes in pitching moment due to the scramjet installation. These effects are also shown in Figure 90. Movement of the scramjet package aft to reduce the large nosedown pitching moment introduced new problems in aircraft balancing.

Installation of the scramjet package on a rotating ramp was then considered as a means of alleviating ground clearance problems, reducing scramjet size, and reducing the shift in center of gravity due to installation of the scramjets. As indicated in Table 4, installed thrust minus installation drag did not equal that of the fixed geometry configurations, although the thrust minus drag per square meter of inlet entrance area was greater.

Initial studies on the Phase III airframe configuration determined the effects of nozzle expansion angle (or nozzle area ratio) at constant nozzle length. Table 4 shows that increasing the final nozzle expansion angle from 24.3° to 27.8° resulted in a moderate increase in thrust and a substantial reduction in the large nose-down pitching moment. Moreover, the pitching moment shift, from fuel-on to fuel-off, was greatly reduced by the increase in expansion angle. The primary disadvantage of the increased expansion angle appeared to be the required relocation of the primary rocket engine higher in the airframe.

Variations in nozzle type were then investigated at a constant nozzle length. The upper surface of the NASA scramjet module was recontoured just downstream of the nozzle throat to eliminate the discontinuity in slope at the module/airframe interface. Trends of pitching moment and thrust minus drag with expansion angle were similar to those found previously, but the overall thrust level was higher. A bell nozzle was also investigated. Although thrust minus drag was high, the nozzle upper wall pressure distribution produced nozzle moments which aggravated the nose-down pitching moment problem.

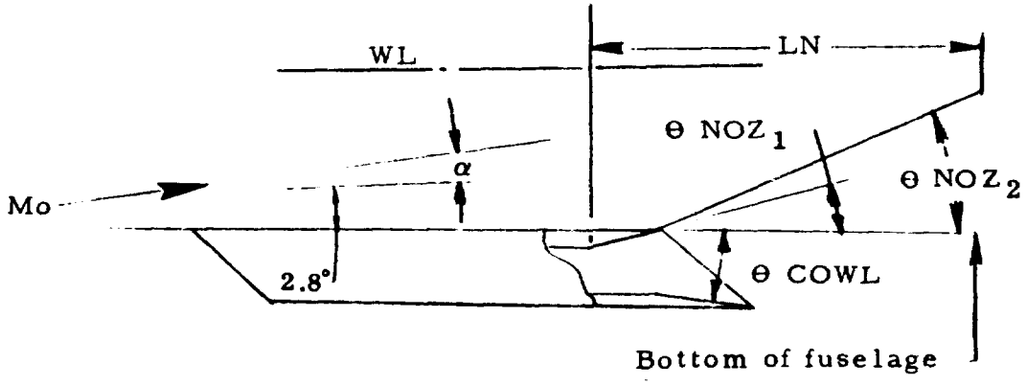

Vehicle	ϕI-II	ϕI-II	ϕI-II	II	ϕ III	ϕ III	ϕ III	ϕ III	ϕ III	ϕ III	ϕ III	ϕ III	ϕ III	ϕ III
α	6.85°	6.85	6.85	7	6.85	6.85	6.85	6.85	6.85	6.85	6.85	6.85	6.85	6.85
No. of modules	8	8	8	7*	8	8	8	8	8	8	8	8	8	8
Cowl height (M)	.457	.457	.457	0.374*	.457	.457	.457	.457	.457	.457	.457	.457	.457	.457
θ_{Noz_1}	15°	15	15	15	15	15	22.395	26.4	30.4	26.4	26.4	26.4	26.4	26.4
θ_{Noz_2}	24.3°	15.5	11.43	24.3	24.3	27.8	22.395	26.4	Bell	26.4	26.4	26.4	26.4	26.4
θ_{Cowl}	6°	6	6	6	6	6	6	6	6	6	6	6	6	0
l_{II} (M)	2.46	3.73	5.00	4.65	3.82	3.82	3.82	3.82	3.82	2.93	2.04	3.82		
F.S. Moment Center	490	490	490		636	636	650	650	650	650	650	650		
W.L. Moment Center	100	100	100		141	141	129.5	129.5	129.5	129.5	129.5	129.5		
ϕ	1	0 1 0	1 0	1 0	1 0	1 0	1 0	1 0	1 0	1 0	1 0	1 0	1 0	1 0
FN_{inst} - AP (Kg)	38.19	-3.94 36.00	31.27	22.60	38.45 3.13	38.95 -2.93	39.86 -3.41	41.18 -3.39	41.05 -3.56	39.67	37.56	42.43	-2.24
ΔN (n.M.)	9145	-6829 -59270	-44362		-45345 -17023	-16705 -17952	-58656 -18225	-19815 -17743	-54288 -18036	2580	41976	-11481	8878

*modules on 6° ramp.

Table 4 - Scramjet Nozzle Installation Study - Summary

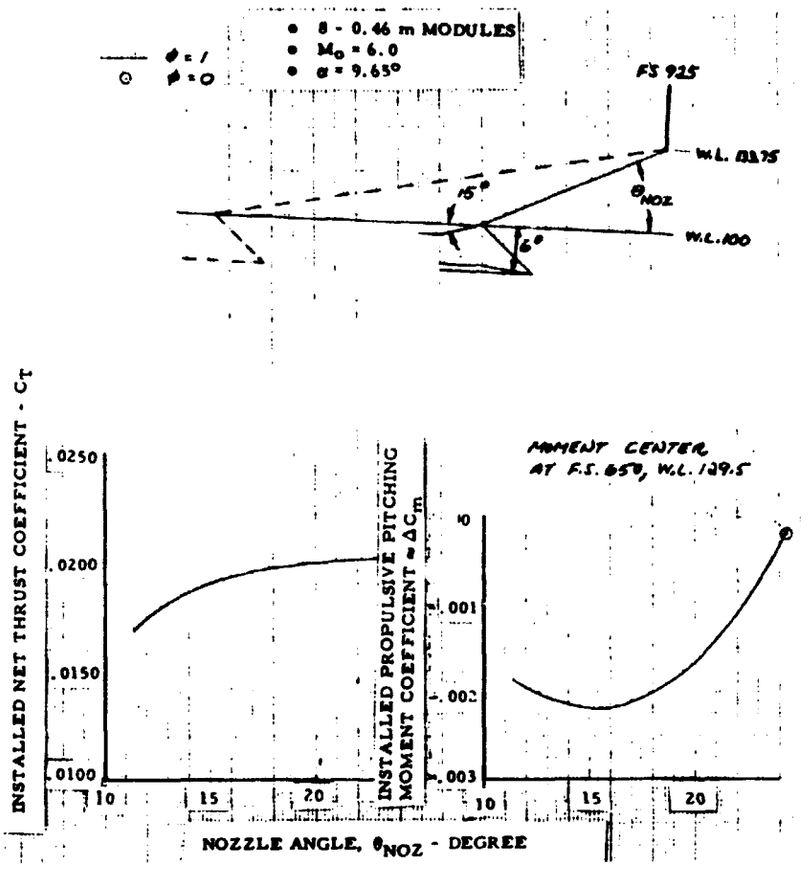

Figure 90 - Effect of Nozzle Angle of Scramjet Performance

As a result of these studies, the 26.4 degree nozzle was selected for the Phase III aircraft. A final translation study was performed with this configuration to determine how far forward the module should be located. Results are shown in Table 4 and Figure 91. The 3.82 m nozzle length was selected on the basis of highest thrust minus drag, acceptable pitching moment characteristics, and least unfavorable effect on aircraft center-of-gravity shift due to scramjet installation.

An analysis of nozzle cowl flap position was the final step in the scramjet/airframe integration study. It was found that generally good performance was obtained with the cowl flap either parallel to or expanding 6 degrees from the bottom of the aircraft. Pitching moment differences between the two configurations varied somewhat with Mach number and angle of attack. Consequently a complete

C-2

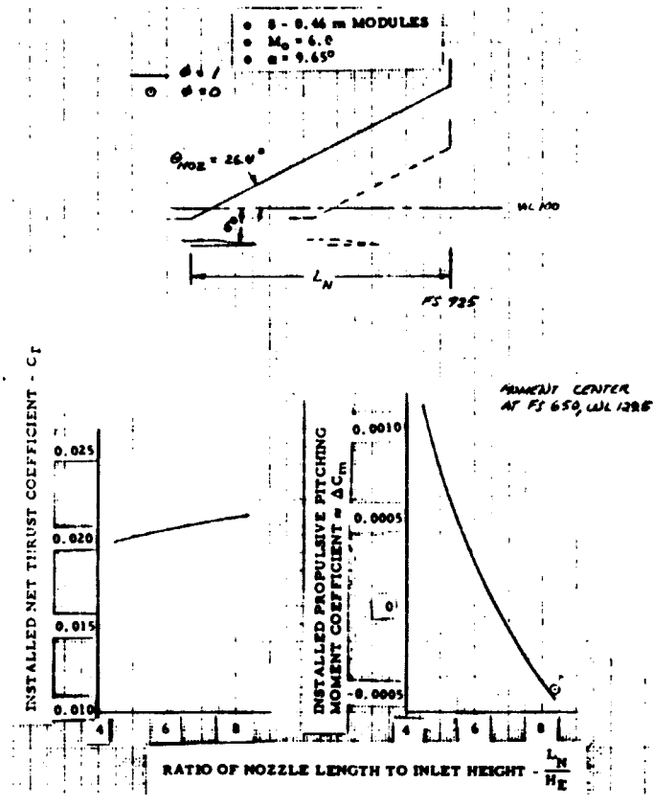

ORIGINAL PAGE IS
OF POOR QUALITY

Figure 91 - Effect of Module Position on Scramjet Performance

map of performance characteristics over the Mach 5 to 7 range was prepared for both configurations. The two configurations are identified in Table 4 by a straight 26.4 degree upper nozzle contour, a 3.82 m nozzle length and nozzle cowl flap internal angles of 6 and 0 degrees. Performance maps are shown in Figures 92 through 97.

Structural Concept

The Phase III vehicle structure is a semi-monocoque construction utilizing the shell as both primary load structure and thermal protector systems.

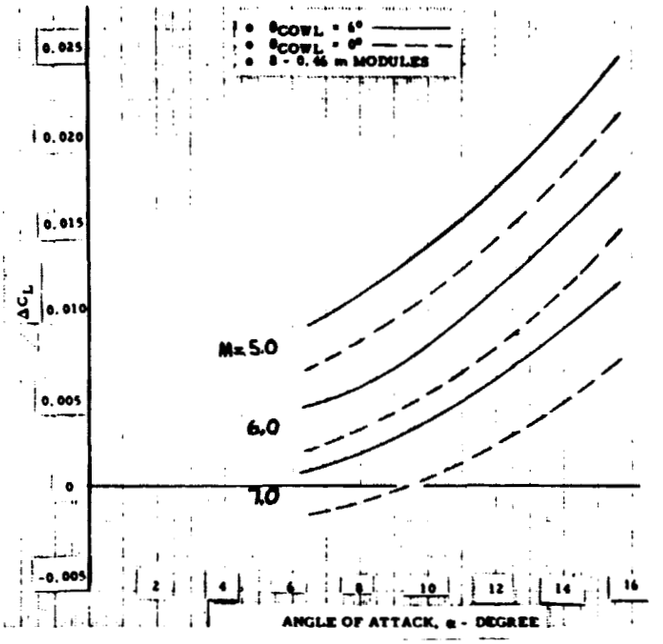

Figure 92 - Effect of Scramjet on Lift - ϕ = 1.0

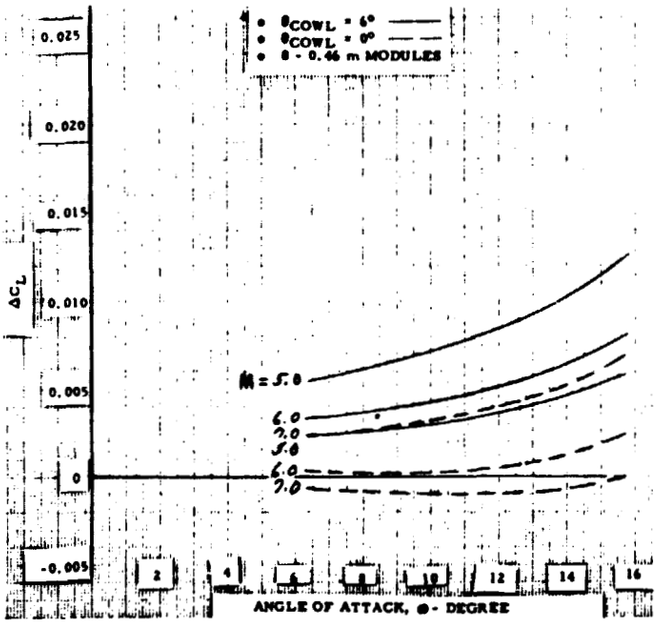

Figure 93 - Effect of Scramjet on Lift = ϕ = 0

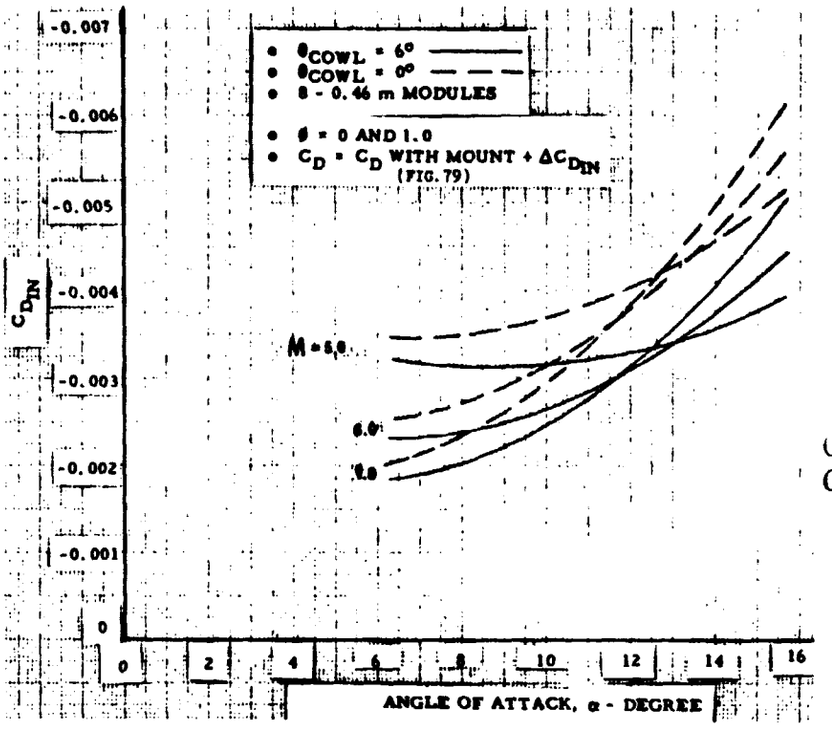

Figure 94 - Installed Drag

Frame spacing, selected as a trade between mass and cost, were set at approximately 0.5 meter centers for an unstiffened shell. Use of longerons was minimized to eliminate secondary loading due to thermal expansion, except in areas where boundary members were required. Frames (bulkheads) were placed at sections of pressure differential and heavy loading. A pressure bulkhead was provided between the payload bay and cockpit area. Main gear and aft launch points carriage loads are supported by a deep frame at F.S. 695, separating the fuel and LOX tanks. Heavy frames were placed at the forward end of the mid-body to carry the forward launch carriage point loads, and at the front of the engine section to provide support for the wing rear beam and vertical side rudder posts.

The wing is configured with eight spars, perpendicular to the main fuselage centerline plane and four streamwise ribs. The wing is configured for easy removal from its pinned joints. Rib and beam webs are corrugated to reduce thermal stresses.

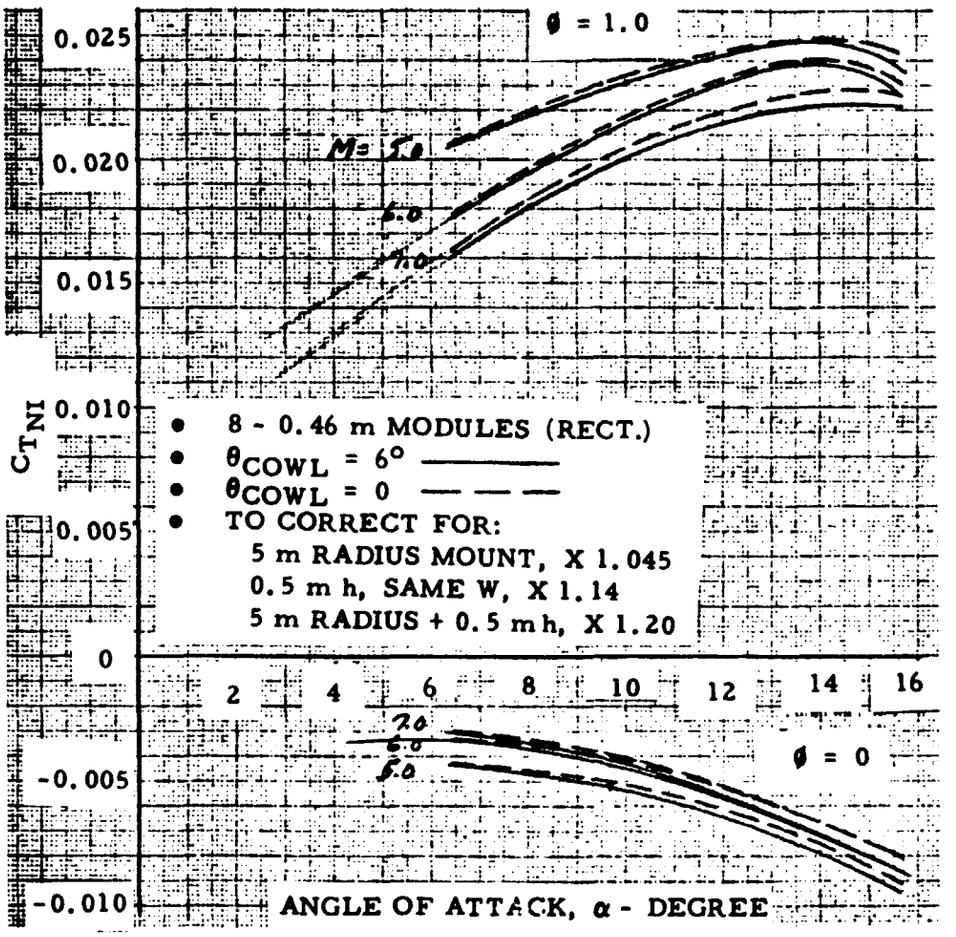

Figure 95 - Installed Thrust

Mission Profiles - Vehicle structure was investigated for loads generated by the missions profiles. A typical profile, shown in Figure 98, for the scramjet cruise mission of 40 seconds at Mach 6.6. The figure reflects the variation of vehicle mass, Mach number, dynamic pressure, altitude and temperature as a function of time. Other mission profiles considered in the vehicle design included; 40 seconds cruise on sustainer rockets, (without scramjets) at Mach 6.6 and zoom to Mach 7.8 with no cruise time.

Each mission starts with a subsonic launch from the B-52 launch vehicle, at 13.7 kM MSL, where boost rocket engine is ignited to accelerate. At this point, the X-24C vehicle is heavy with large loads applied to the structure due to the

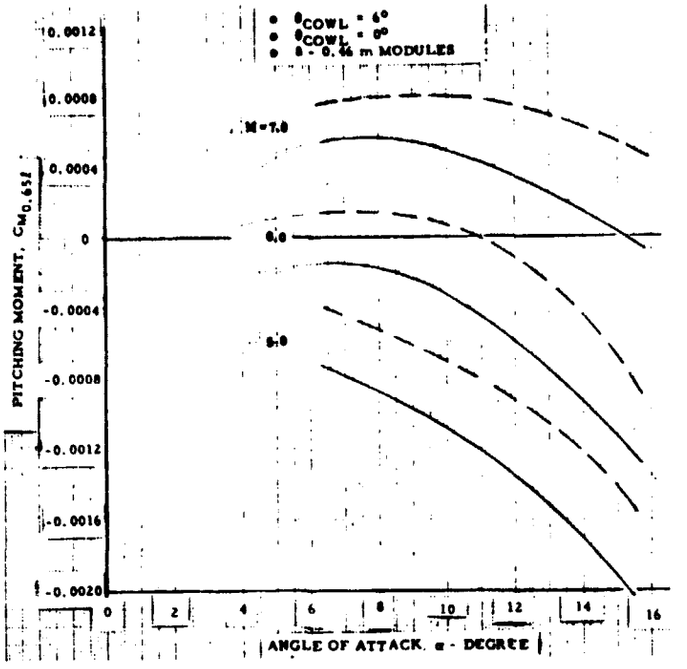

Figure 96 - Effect of Scramjets on Pitching Moment - $\emptyset$ = 1.0

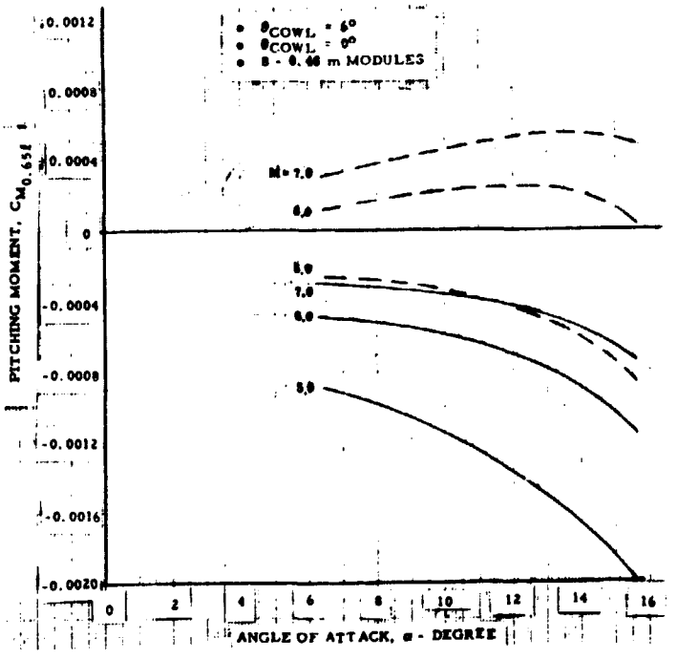

Figure 97 - Effect of Scramjets on Pitching Moment - $\emptyset$ = 0

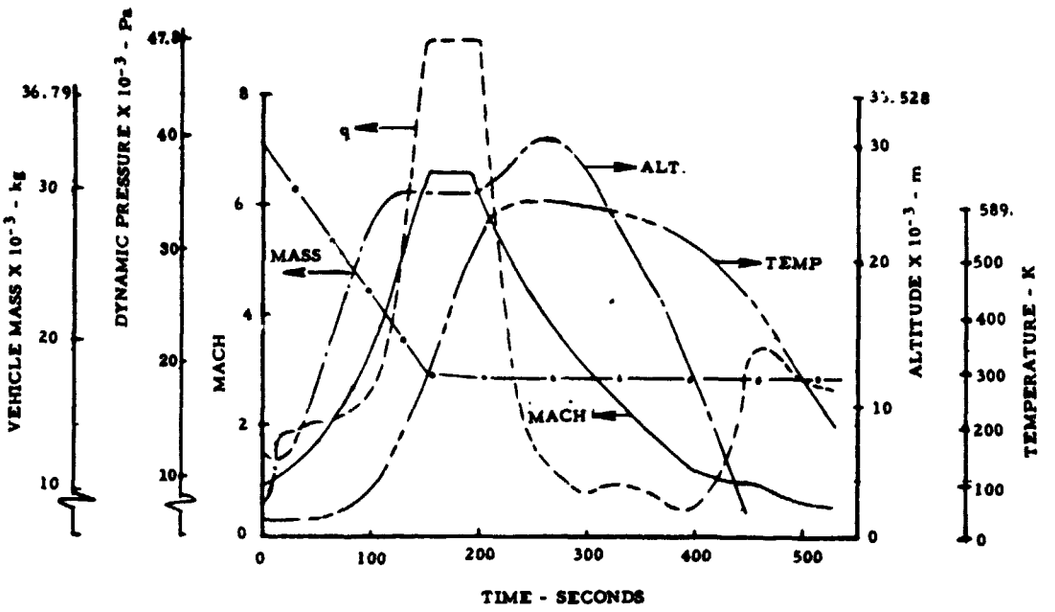

Figure 98 - Mission Profile - M = 6.6, 40 Second Scramjet Cruise

positive 2.5 g limit maneuver and rocket axial thrust. Vehicle structure remains relatively cool during this initial maneuver. At the end of the acceleration phase a 0.0 g push over is initiated to align the vehicle for the desired cruise condition. At start of the cruise phase, the take-off mass has been reduced approximately 50 percent. The structure is increasing in temperature towards a peak shortly after the end of the cruise segment. To stay within the test range constraint, the vehicle performs a high drag 3.0 g pullup combined with a banking maneuver at time of cruise power burnout. Temperatures are combined with flight loads during deceleration. During vehicle descent, the structure begins to cool with the vehicle mass remaining at approximately 12.9 Mg.

The mission for the cruise on sustainer rockets follows the identical flight profile noted above for scramjet cruise. Vehicle structural differences are reflected in the skin panel changes, on removal of scramjet modules, required to

accommodate the thermal gradient difference to the vehicle shell resulting from scramjet removal. (Details on vehicle structural changes from scramjet to the non-scramjet configuration are described in the Scramjet Installation herein.) The dash to Mach mission follows the same profile as for the scramjet mission, except the acceleration phase is extended to Mach 7.8. Level flight is obtained at the end of the acceleration phase followed by the deceleration maneuver identical to the one used in the scramjet mission. Heating peaks occur shortly after the start of deceleration, like in the scramjet mission, but are not as high as in the Mach 6.6 mission due to the shorter mission elasped time involved. Consideration of this mission, however, was made due to the difference in the vehicle shell temperature gradients in the non-scramjet configuration.

Load Conditions - The vehicle structure was investigated for four loading conditions determined by the mission profiles. These include (1) 2.0 g taxi, (2) 2-wheel landing, (3) 2.5 g after launch, and (4) 3.0 g after cruise. Each of the loading conditions was analyzed for the basic mission profiles.

The fuselage was analyzed at four locations corresponding to the frame locations described above. The analysis included calculations of panel (skin) thickness to carry both flight and thermal loads and the investigation of thrust loading during the acceleration phase of the missions.

No analysis was made of the wing structure due to the similarities in loading and arrangement to that of the Phase I vehicle covered in Reference 2.

Load Condition Delineation - Figures 99 through 102 depict each of the load conditions noted above. Important correlation must be made between vehicle configuration and type of loading.

The 2.0 g taxi condition, Figure 99, is given with the X-24C attached to the B-52 launch platform. Peak fuselage bending moments and shears occur at the three attach points to the B-52 vehicle. The moments and shears are relatively large due to the X-24C mass in the launch configuration. Peak bending moment

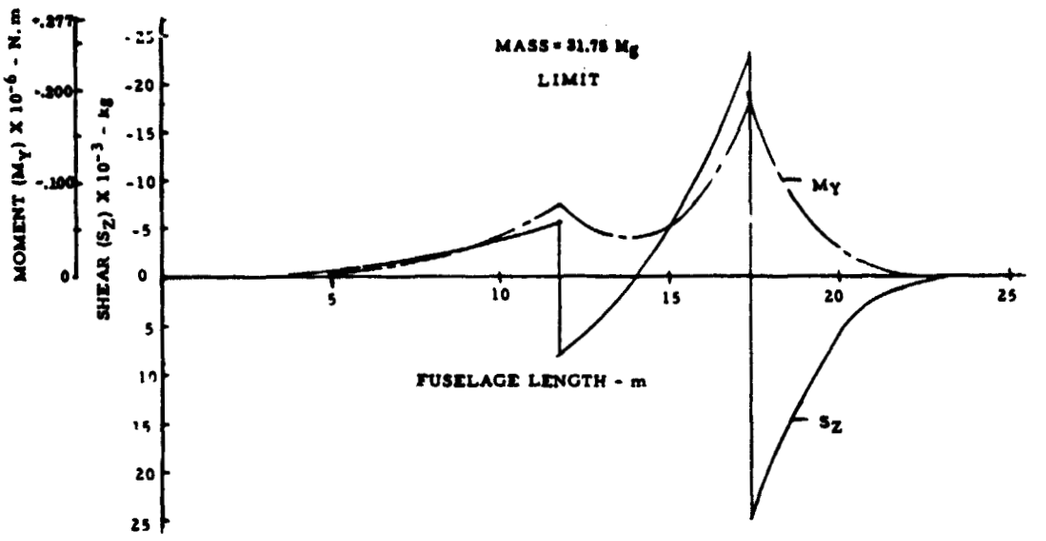

Figure 99 - Net Fuselage Loads - 2.0 g Taxi, Mass = 31.75 Mg, Attached to B-52

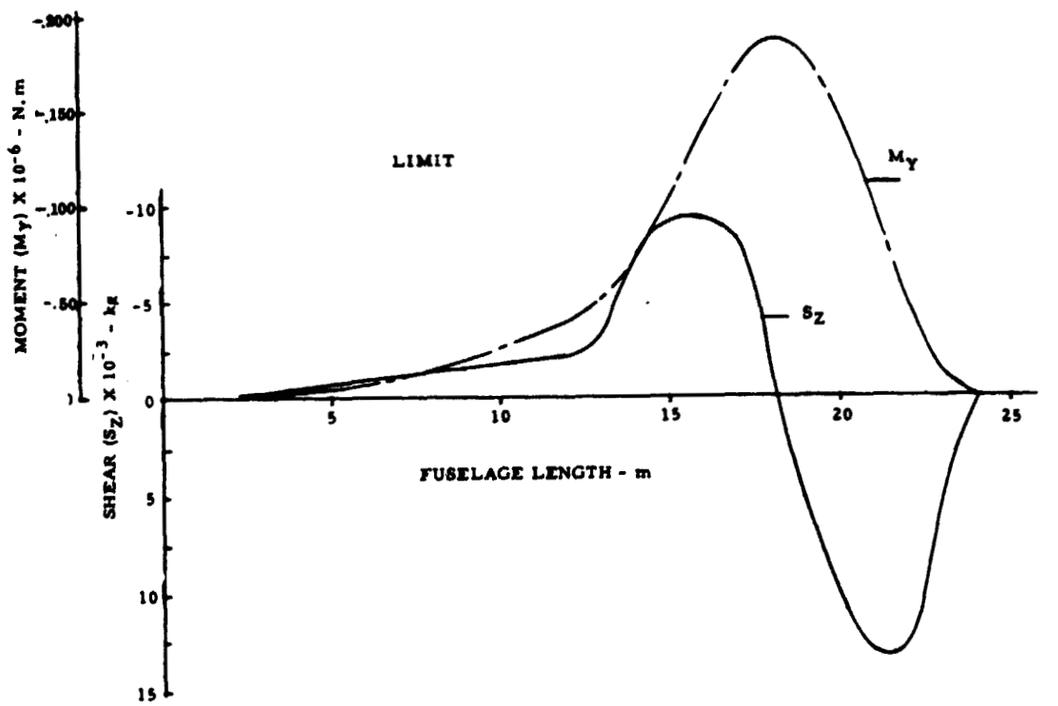

Figure 100 - Net Fuselage Loads - n = 2.5, Mass = 29.5 Mg, Subsonic

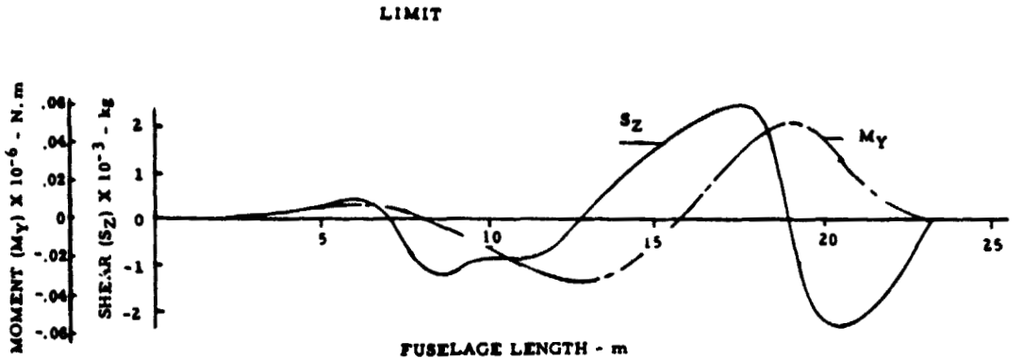

Figure 101 - Net Fuselage Loads - M = 6.6, n = 3.0, Mass = 12.8 Mg

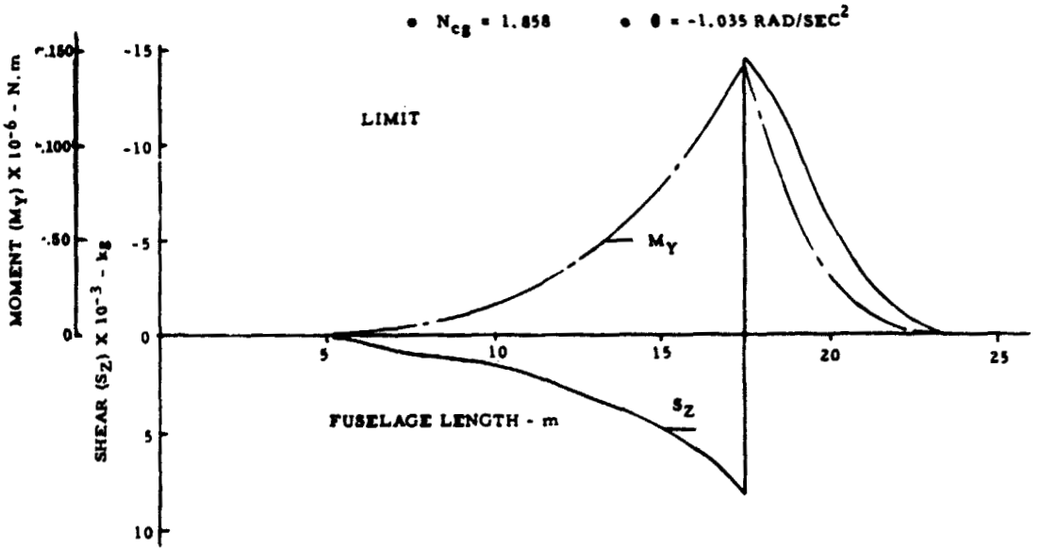

Figure 102 - Net Fuselage Loads - 2-Wheel Landing, Mass = 12.5 Mg

on the aft body is of the same magnitude as the 2.5 g maneuver, but of opposite sense. The structure during both the 2.0 g taxi and the 2.5 g maneuver was basically at ambient temperature.

The 2.5 g positive maneuver is initiated after launch to pull-up the vehicle into the acceleration trajectory. The large fuel load produces peak bending moments on the aft body of the vehicle with a magnitude of 468.9 kN.m (compression on top). During this maneuver the maximum axial thrust of 365 kN is applied to the vehicle and is reacted by inertia and aerodynamic loads. Initially the thrust load is mainly reacted by the fuel load, but as the fuel is consumed a redistribution of the reaction of the remainder of the inertia was considered.

The 3.0 g cruise pull-up maneuver has a maximum bending moment of 51 kN.m on the fuselage station equivalent to the mid-point of the fuel tank, an order of magnitude less than the 2.5 g positive maneuver. This condition designed the fuselage shell within the wing-fuselage section due to the associated high temperatures with the maneuver. The shielding effects of the scramjet modules on the substructure or the replacement panels, in the non-scramjet configuration, were considered with this high temperature-high maneuver loading condition.

The two-wheel landing condition has a maximum bending moment of -356 kN.m at the fuselage station, where the aft launch points are located. Peak shear is of 14.7 Mg acting up. Since the structure is relatively cool during this loading, the 2.0 g taxi condition is comparable and is dominate at this station. The two-wheel landing produces the largest down bending condition coinciding with the section of fuselage housing the LOX tank.

Rocket engine thrust is applied to the fuselage during the acceleration phase. It was conservatively assumed that the load is reacted proportional to the longitudinal distribution of the fuselage volume. Thermal effects are minimal during this segment of the mission and are not accounted for. Thrust loads are added to the 2.5 g positive maneuver loads.

Analysis - Four fuselage stations were investigated as being representative of the fuselage structure. The stations are located at 9.8 m, 31.8 m, 16.4 m, and 19.4 m respectively from the tip of the fuselage. The first station was investigated as being representative of the fuselage forebody in addition to being the forward latch point, to the launch vehicle. The second station was analyzed as being typical of the fuselage mid-body within the scramjet inlet region. Next to last station was analyzed to account for the structural change created by scramjet integration while the last station selected covered the scramjet nozzle region.

Analysis of the first station reveals it to be structurally adequate for a continuous 589 K temperature distribution. This results in the elimination of induced longitudinal thermal stresses and allows more than adequate structure to carry the applied loads of either the 2.0 g taxi or 2.5 g maneuver.

The second station was similarily analyzed as the first station. The resultant shell thickness distribution was analyzed for the 2.0 g taxi and 2.5 g maneuver with positive margins of safety. Some panel stiffening is required in the upper portion of the shell in this region to increase panel compression and shear buckling allowances. Figure 103 provides the skin thickness and stress distribution for the first two stations.

The next to last station was investigated as typical of scramjet thermal effects. During scramjet cruise missions structure above the modules is masked such that considerably lower temperature exist than on the remainder of the shell. Additionally, in the off design missions without the scramjet module, it must also be substantiated without change to the vehicle structure outboard and above the wing. Figure 104 shows the analytical approach used to generate the final temperatures and skin thickness distribution with scramjets. Also included are the calculations of thermal and flight load stresses.

Thermodynamic analysis indicated that the subpanel beneath the scramjet modules would be heated to 361 K peak during the Mach 6.6 mission with scramjets burning. As shown in Figure 104, the first step analyzed the skin thickness and

2.0 g Taxi

$M_Y = 0.19 \times 10^6$ N.m (total vehicle)

+2.5 g Maneuver

$M_Y = 0.10 \times 10^6$ N.m (total vehicle)

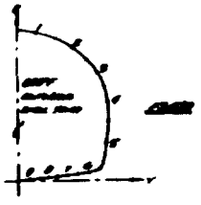

SECTION PROPERTIES ~ cm

Element	t	l	z	A*	Az**	c	$Ac^2 \times 10^{-3}$***
1	0.203	46.74	188.98	9.48	1791.53	134.91	172.54
2	0.208	42.42	171.45	8.84	1515.62	117.38	121.80
3	0.246	40.64	142.24	10.00	1422.40	88.17	77.74
4	0.236	39.62	105.16	9.35	983.25	51.09	24.40
5	0.650	74.68	48.77	48.58	2369.25	-5.30	1.36
6	0.838	25.40	8.89	21.29	189.27	-45.18	43.46
7	0.660	25.40	4.83	16.77	81.00	-49.24	40.66
8	0.610	25.40	2.03	15.48	31.42	-52.04	41.92
9	0.610	25.40	0.76	15.48	11.76	-53.31	43.99
				155.27	8395.50		567.87/side

$\bar{z} = \frac{8395.50}{155.27} = 54.07$*

$I_{Y_{NA}} = 1135.74 \times 10^3$ cm^4 (total vehicle)

FLIGHT STRESSES X 10^6 ~ Pa ~ LIMIT

Element	2g Taxi	+2.5g Man.	+2.5g Man. + fx Thrust
1	22.8	-12.07	-15.31
2	19.83	-10.51	-13.75
3	14.91	-7.89	-11.14
4	8.64	-4.57	-7.81
5	-0.90	0.48	-2.76
6	-7.64	4.05	0.81
7	-8.32	4.41	1.17
8	-8.80	4.66	1.42
9	-9.02	4.77	1.53

2.0 g Taxi

$M_Y = 0.19 \times 10^6$ N.m (total vehicle)

+2.5 g Maneuver

$M_Y = 0.333 \times 10^6$ N.m (total vehicle)

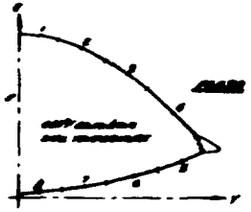

SECTION PROPERTIES ~ cm

Element	t	l	z	A*	Az**	c	$Ac^2 \times 10^{-3}$***
1	0.203	52.32	202.18	10.62	2147.15	139.25	205.93
2	0.203	50.80	187.20	10.31	1930.03	124.27	159.22
3	0.239	48.26	161.04	11.53	1856.79	98.11	110.98
4	0.264	110.74	100.68	29.23	3118.26	43.75	55.95
5	0.592	55.88	40.13	33.08	1327.50	-22.80	17.20
6	0.564	55.88	21.34	31.52	672.64	-41.59	54.52
7	0.485	55.88	8.89	27.10	240.92	-54.04	79.14
8	0.488	55.88	2.79	27.27	76.08	-60.14	98.63
				180.66	11369.37		781.57 (per side)

$\bar{z} = \frac{11369.37}{180.66} = 62.93$*

$I_{Y_{NA}} = 1563.14 \times 10^3$ cm^4 (total vehicle)

FLIGHT STRESSES X 10^6 ~ Pa ~ LIMIT

Element	2g Taxi	+2.5g Man.	+2.5g Man. + fx Thrust
1	17.09	-29.55	-32.43
2	15.25	-26.46	-29.23
3	12.03	-20.88	-23.65
4	5.36	-9.29	-12.06
5	-2.82	4.89	2.12
6	-5.13	8.89	6.12
7	-6.65	11.55	8.78
8	-7.40	12.85	10.08

Note:

* = cm^2
** = cm^3
*** = cm^4

Figure 103 - Section Properties - Station 470 and 630

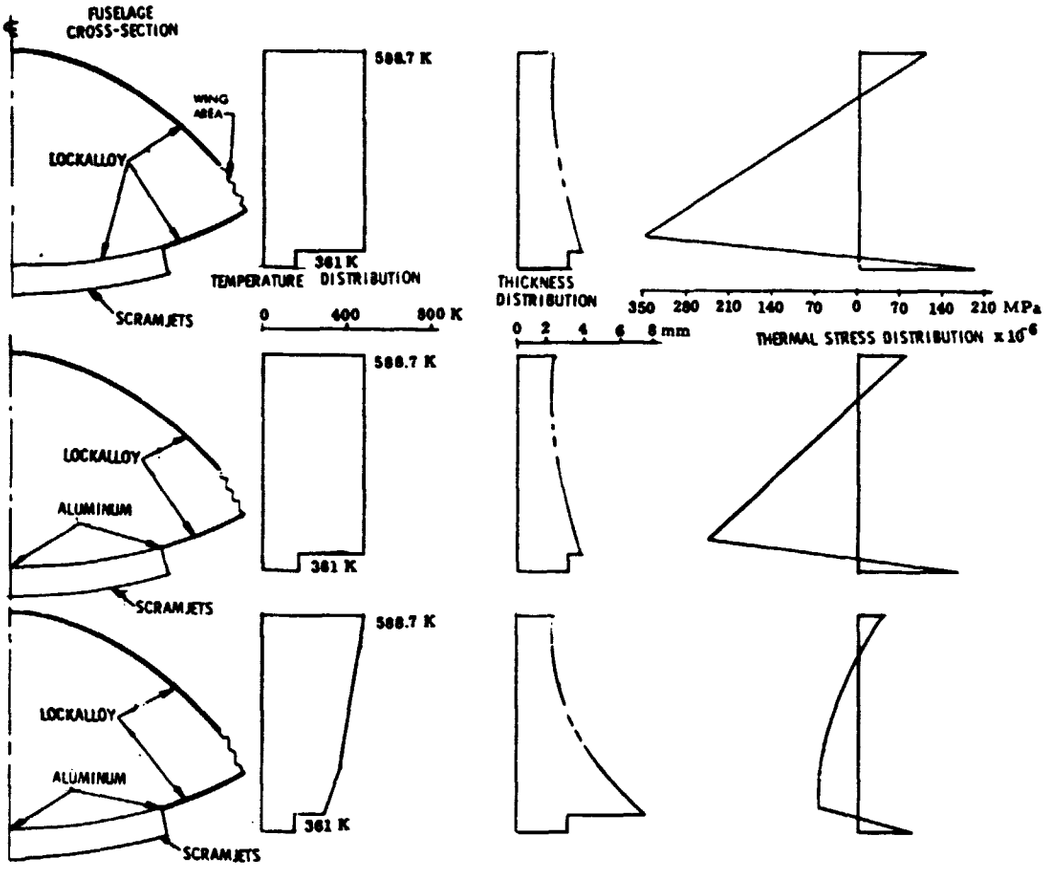

Figure 104 - Typical Stress Analysis

resulting temperature distribution as being a continuous 589 K. The subpanel originally considered was made of Lockalloy which resulted in large thermal stresses on the order of 345 MPa compression. To minimize the effects of the notch in the temperature profile, a low modulus material was next considered for the subpanel.

The wing-fuselage rib has not been considered effective in resisting load. This is felt to be valid in that the rib will be corrugated such that the flexibility of the rib would not carry thermal loads. This approach was employed on the X-15 to eliminate large thermal stresses due to the relatively cool rib.

Aluminum was investigated, as a lower modulus material, for the scramjet subpanel. The temperature distribution was held constant at 589 K on the remainder of the section, with 361 K on the aluminum panel, to determine the relative reduction in thermal stresses. The analysis indicates a 30% reduction in peak compressive stress on the critical panel, just beneath the wing junction. The next step was to modify the shell temperature by the redistribution of panel thickness to further reduce the effects of the scramjet modules.

The shell temperature and thickness distribution were modified to provide a vertical linear variation in temperature. With a peak temperature of 589 K at the crest of the section to 530 K at the upper wing fuselage junction. Beneath the wing, the temperature varied from 505 K to 461 K at the scramjet modules, Figure 104. The temperature profile was thus made linear decreasing, minimizing the stepped temperature profile. The resultant peak thermal stress was 82% less than the original all Lockalloy section. The total section showed an appreciable reduction in the effects of thermal stresses with the addition of the aluminum panel and modification to the temperature profile.

The critical thermal stress condition exists in combination with the limit 3.0 g positive maneuver after cruise. Conservatively applying the peak bending moment of 51.4 kN.m on a 0.6 m band, 0.9 m aft of the rear latch points, resulted in both thermal and thermal plus flight loads giving critical stress levels. Peak

design stress levels were on the order of ±68.9 MPa which are satisfactory at the elevated temperature of the material.

The aluminum panel beneath the scramjets, could have corrugations in the transverse direction, to reduce longitudinal stiffness and thus reduce thermal stresses. This type of panel would be effective in shear but not for longitudinal axial loads which are supported by the Lockalloy panels.

For the off design mission of Mach 6.6 without scramjets, it was considered that the skin beneath the wing could be replaced to establish a more acceptable temperature profile than could be attained by retaining the scramjet cruise outboard panel. Since the above the wing shell remained the same, the under-the-wing panels were selected such as to maintain a constant temperature equal to the minimum of the fuselage temperature above the wing. Thus, the temperature varied linearly, decreasing from a peak at the top centerline to the upper wing - fuselage junction and remaining constant over the underside of the section. This temperature gradient resulted in thermal stresses on the order of ±41 MPa maximum. Analysis of this arrangement for the 2.5 g maneuver without temperature effects produced stress levels of the same order as those due to thermal loads. Calculations are shown in Figures 105 through 107.

The aft station was investigated as being representative of the vehicle aft-body, particularly of the scramjet upper nozzle area. The temperature gradient is linearly decreasing from a peak at the upper centerline to the upper wing fuselage junction with a slope less than established on the prior fuselage station. The Lockalloy skin panel at the bottom of the section varied in temperature from 525 K at the lower wing-fuselage junction to 483 K at the lower centerline. The thermal and flight load bending analysis of the section did not consider the ventral fins to be effective in resisting fuselage loads due to the use of slip joints as attachment of the fins to the fuselage structure. Thermal stress levels generated were in the magnitude of ±27.6 MPa, which is considered acceptable. The combined flight condition with the hot structure, the positive 3.00 g maneuver, produce additive stress of ±13.8 MPa limit. The dash to Mach 7.8 mission had

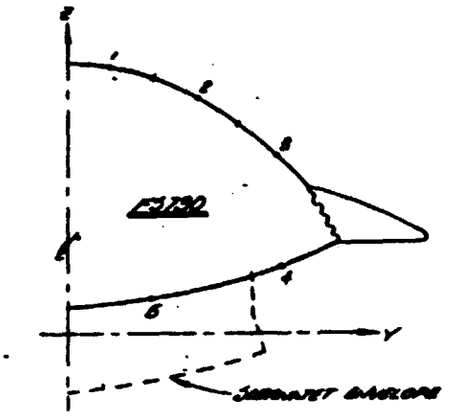

SECTION PROPERTIES (WITHOUT SCRAMJET) ~ cm

Element	t	l	z	A*	Az**	c	$Ac^2 \times 10^{-3}$***
1	0.226	56.90	215.65	12.84	2768.60	124.94	200.42
2	0.216	84.84	194.82	18.32	3569.60	104.11	186.72
3	0.263	87.38	145.80	23.55	3433.26	55.09	71.47
4	0.434	76.20	50.80	33.10	1681.32	-39.90	52.69
5	0.348	152.40	24.89	53.03	1320.14	-65.81	229.68
				140.84	12772.92		740.98 (per side)

$\bar{z} = \frac{12772.92}{140.84} = 90.69$* $I_{Y_{NA}} = 1481.96 \times 10^3$ cm^4 (total vehicle)

SECTION PROPERTIES (WITH SCRAMJET) ~ cm

Element	t	l	z	A*	Az**	c	$Ac^2 \times 10^{3}$***
1	0.226	56.90	215.65	12.84	2768.60	114.96	169.70
2	0.216	84.84	194.82	18.32	3569.60	94.13	162.41
3	0.263	87.38	145.80	23.55	3433.26	45.11	47.95
4	0.689	76.20	50.80	33.10	1681.32	-49.89	130.49
5@	0.305	152.40	24.89	53.03	1320.14	-75.79	124.87
				128.90	12977.27		635.42 (per side)

$\bar{z} = \frac{12977.27}{128.90} = 100.68$ $I_{Y_{NA}} = 1270.84 \times 10^3$ cm^4

Note:

@ = Aluminum
* = cm^2
** = cm^3
*** = cm^4

Figure 105 - Section Properties - Station 730

Thermal Stresses
(M = 6.6, 40 Sec Cruise on Scramjets)

Element	Temp, K	P*	ΔP_{AX}*	P + ΔP_{AX}*	M**
1	587.6	-1008	712	-296	-340.18
2	575.9	-1389	1016	-373	-350.99
3	548.7	-1628	1305	-323	-145.62
4	477.6	-2611	2908	297	-147.86
5	360	-510	1205	695	-526.92
		-7146	7146		-1511.57

	P_M*	P_{TH-TOT}*	f_{TH} x 10^6 ~ Pa
1	351	55.2	42.40
2	410	37.4	20.42
3	253	-70.1	-29.78
4	-622	-32.6	-62.16
5	-332	30.3	65.27

(M = 6.6, 40 Sec Cruise, No Scramjets)

Element	Temp, K	P*	ΔP_{AX}*	P + ΔP_{AX}*	M**
1	587.6	-1008	910	-22	-122.30
2	575.9	-1389	1298	-91	-93.98
3	548.7	-1628	1669	41	22.25
4	548.7	-2288	2345	57	-22.65
5	548.7	-3667	3758	91	-59.90
		-9980	9980		-267.58

Element	P_M*	P_{TH-TOT}*	f_{TH} x 10^6 ~ Pa
1	60	-38	-29.61
2	71	-19	-10.40
3	48	89	37.71
4	-49	7	2.26
5	-130	-39	-7.41

Thermal Stresses
(M = 7.8, No Cruise, with Scramjets)

Element	Temp, K	P*	ΔP_{AX}*	P + ΔP_{AX}*	M**
1	522.0	-803	806	3	3.67
2	518.2	-1127	1150	27	23.19
3	494.3	-1304	1478	174	95.61
4	530.4	-2139	2077	-62	24.56
5	533.2	-3466	3328	-138	90.31
		-8839	8839		237.34

Element	P_M*	P_{TH-TOT}*	f_{TH} x 10^6 ~ Pa
1	-51.4	-48.4	-37.74
2	-61.1	-38.8	-21.19
3	-41.6	131.9	56.05
4	42.3	-19.2	-5.81
5	111.79	-25.4	-4.73

Note:

* = kN
** = x 10^3 N.m

Figure 106 - Thermal Stresses - Station 730

Section Loading - Total Vehicle

- 2.0 g Taxi ~ M_Y = 463.2 x 10^3 N.m Limit
- +2.5 g Maneuver ~ M_Y = 468.9 x 10^3 N.m Limit
- +3.0 g Maneuver @ M = 6.6 ~ M_Y = 50.8 x 10^3 N.m Limit
- 2 Wheel Landing ~ M_Y = -355.9 x 10^3 N.m Limit

Stress Summary x 10^6 ~ Pa ~ Limit

(With Scramjets)

Element	2.0g Taxi	+2.5g + fx Thrust	f_{TH}*	+3.0g Man. + f_{TH}*
1	41.91	-54.50	43.00	38.40
2	34.32	-46.81	20.42	16.66
3	16.44	-28.72	-29.78	-31.58
4	-18.18	6.33	-62.16	-60.17
5 Al	-27.63	15.89	65.27	68.30

(Without Scramjets)

1	39.06	-50.59	-29.61	-33.89
2	32.54	-44.00	-10.40	-13.98
3	17.22	-28.48	37.71	35.83
4	-12.47	1.57	2.26	3.63
5	-20.57	9.77	-7.41	5.16

Element	f_{TH}* @ M = 7.8	+3.0g Man. +f_{TH}* @ M = 7.8
1	-37.74	-42.02
2	-21.17	-24.76
3	56.05	54.16
4	-5.81	-4.44
5	-4.79	7.78

Note:

* = Thermal

Figure 107 - Section Loading - Station 730

thermal stresses of ±27.6 MPa which in combination with flight loads prove to be equivalent to the scramjet cruise mission. Review of the cold structure with applied flight load of a positive 2.5 g maneuver produced stress levels also of ±27.6 MPa limit. Calculations are shown in Figures 108 through 110.

Fuselage shell axial loads due to engine thrust during the acceleration phase were investigated. The thrust load is reacted by inertia and aerodynamic loads. At the start of the acceleration phase, fuel mass represents a large reactance to the thrust loading with the primary structure constructed specifically for this purpose. However, as the fuel is consumed a redistribution of reactive forces requires the fuselage shell to transfer the thrust load of 365 kN. In this analysis it was conservatively assumed that the thrust load was reacted proportional to the summation of the fuselage volume. The distribution is shown in Figure 111. In addition, normal loads of this section were added to the section's 2.5 g limit maneuver panel loads. The combination of these loadings are shown in Figure 112.

Resultant Shell Thickness and Temperature - Vehicle skin thickness for the design missions delineated under Mission Profiles herein are shown in Figure 113. Installation of the scramjet modules, for the scramjet role, requires replacement of the Lockalloy panel, directly above the module, with a 3 mm aluminum panel and the Lockalloy panel outboard of the module to the lower wing-fuselage junction with a 7 mm panel.

Temperature distribution during the Mach 6.6 cruise for 40 seconds, without scramjets based on the above analysis are shown in Figure 114.

Vehicle Mass Analysis

The Phase III vehicle is designed at 31.75 Mg maximum launch mass with thermal protection for Mach 6.6 at 40 second cruise time on scramjets and at maximum q of 47.9 kPa. This design consideration allows the primary substructure and applicable systems to be scaled from the Phase I vehicle at a launch mass of 25.85 Mg to the 31.75 Mg Phase III vehicle.

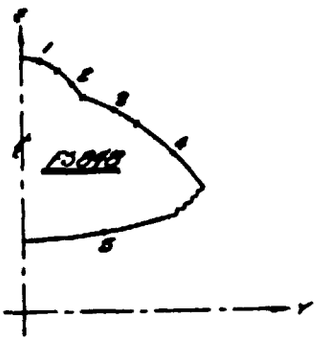

SECTION PROPERTIES (WITHOUT SCRAMJET) ~ cm

Element	t	l	z	A*	Az**	c	$Ac^2 \times 10^{-3}$***
1	0.236	35.05	277.37	7.68	2129.37	108.41	90.24
2	0.224	47.75	257.05	10.65	2736.32	88.09	82.62
3	0.216	69.09	224.79	14.90	3350.18	55.83	46.45
4	0.330	101.60	175.77	33.55	5896.73	6.81	1.54
5	0.610	167.64	85.85	34.06	2924.44	-83.11	235.25
				100.84	17037.04		456.11 (per side)

$\bar{z} = \frac{17037.04}{100.84} = 168.95$* $I_{Y_{NA}} = 912.22 \times 10^3$ cm^4 (total vehicle)

SECTION PROPERTIES (WITH SCRAMJET) ~ cm

Element	t	l	z	A*	Az**	c	$Ac^2 \times 10^{-3}$***
1	0.236	35.05	277.37	7.68	2129.37	139.04	148.43
2	0.224	47.75	257.05	10.65	2736.32	118.74	150.05
3	0.216	69.09	224.79	14.90	3350.18	66.46	111.43
4	0.330	101.60	175.77	33.55	5896.73	37.44	47.03
5	0.610	152.40	85.85	92.90	7980.96	-52.48	255.82
				159.68	22088.66		712.75 (per side)

$\bar{z} = \frac{22088.66}{159.68} = 138.33$* $I_{Y_{NA}} = 1425.5 \times 10^3$ cm^4 (total vehicle)

Note:

* = cm^2
** = cm^3
*** = cm^4

Figure 108 - Section Properties - Station 848

Thermal Stresses
(M = 6.6, 40 Sec Cruise on Scramjets)

Element	Temp, K	P*	ΔP_{AX}*	P + ΔP_{AX}*	M**
1	588.7	-605	586	-19	-26.5
2	580.9	-819	812	-7	-8.16
3	566.5	-1095	1137	42	36.16
4	551.5	-2345	2560	215	80.46
5	588.7	-7319	7088	-231	121.11
		-12182	12182		203.07

Element	P_M*	P_{TH-TOT}*	f_{TH} x 10^6 ~ Pa
1	-30	-49	-64.45
2	-36	-43	-40.28
3	-37	5	3.43
4	-36	179	53.39
5	139	-92	9.89

(M = 6.6, 40 Sec Cruise, No Scramjets)

Element	Temp, K	P*	ΔP_{AX}*	P + ΔP_{AX}*	M**
1	588.7	-605	508	-97	-104.58
2	580.9	-819	705	-114	-100.58
3	566.5	-1095	987	-108	-60.53
4	551.5	-2345	2221	-124	-8.39
5	489.9	-1813	2256	443	-367.64
		-6677	6677		-641.72

Element	P_M*	P_{TH-TOT}*	f_{TH} x 10^6 ~ Pa
1	117.1	20.6	26.87
2	131.9	17.7	16.67
3	117.1	8.7	5.81
4	32.1	-91.2	-27.17
5	-393.3	44.0	12.93

Thermal Stresses
(M = 7.8, No Cruise, Without Scramjets)

Element	Temp, K	P*	ΔP_{AX}*	P + ΔP_{AX}*	M**
1	549.8	-533	433.5	-99.5	-107.54
2	538.7	-710	602	-108	-95.21
3	510.9	-889	843	-46	-26.06
4	502.6	-1930	1896.5	-33.5	-2.28
5	466.5	-1639	1926	287	-238.81
		-5701	5701		-469.84

Element	P_M*	P_{TH-TOT}*	f_{TH} x 10^6 ~ Pa
1	85.7	-13.5	-17.55
2	96.6	-11.5	-10.79
3	85.7	39.1	26.26
4	23.5	-10.0	-2.96
5	291.6	-4.3	-1.25

Note:

* = kN
** = x 10^3 N.m

Figure 109 - Thermal Stresses - Station 848

Section Loading - Total Vehicle

- 2.0 g Taxi ~ M_Y = 11.00 x 10^3 N.m ~ Limit
- +2.5 g Maneuver ~ M_Y = 197.00 x 10^3 N.m ~ Limit
- 3.0 g Maneuver @ M = 6.6 ~ M_Y = 14.688 x 10^3 N.m ~ Limit
- 2-Wheel Landing ~ M_Y = 14 x 10^3 N.m ~ Limit

Stress Summary x 10^6 ~ Pa ~ Limit
(With Scramjets)

Element	2-Wh Land	+2.5g Man.	+3.0g Man. + f_{TH}^*	f_{TH}^*
1	2.21	-19.28	-65.89	-64.45
2	1.88	-16.46	-41.50	-40.28
3	1.37	-11.99	2.54	3.43
4	0.59	-5.19	53.01	53.39
5	-0.83	7.28	-9.36	-9.83

(Without Scramjets)

1	2.63	-23.49	25.12	26.37
2	2.18	-13.09	15.25	16.57
3	1.34	-12.10	4.91	5.81
4	0.155	-1.475	-27.28	-27.17
5	-2.05	18.02	14.27	12.93

Element		+3.0g Man. f_{TH}^* @ M = 7.8	f_{TH}^* @ M = 7.8
1		-19.29	-17.55
2		-21.21	-10.79
3		25.37	25.25
4		-3.08	-2.95
5		0.033	-1.25

Note:

* = Thermal

Figure 110 - Section Loading - Station 848

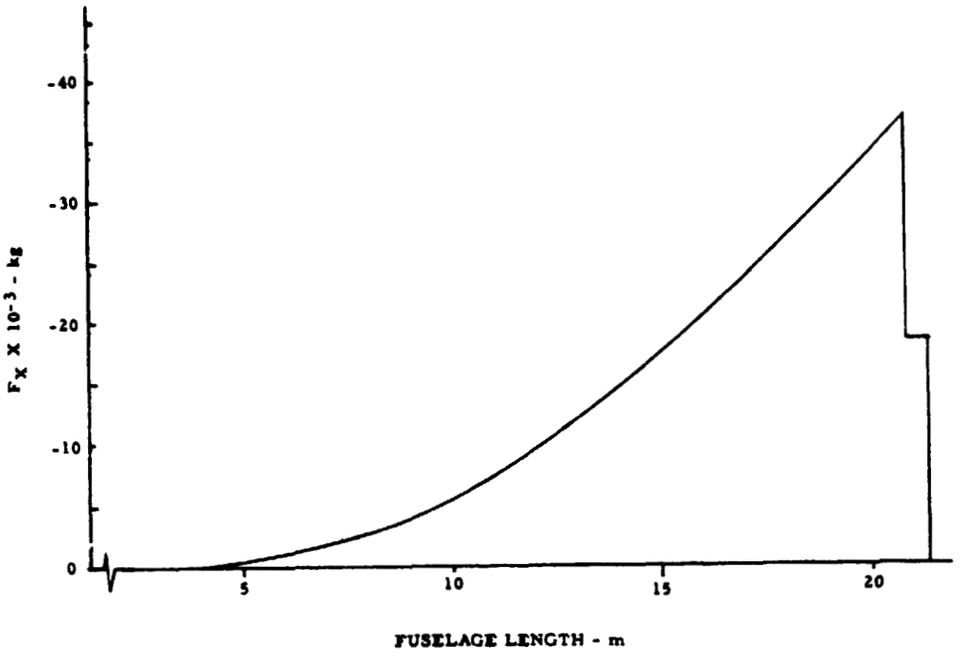

Figure 111 - Fuselage Thrust Distribution

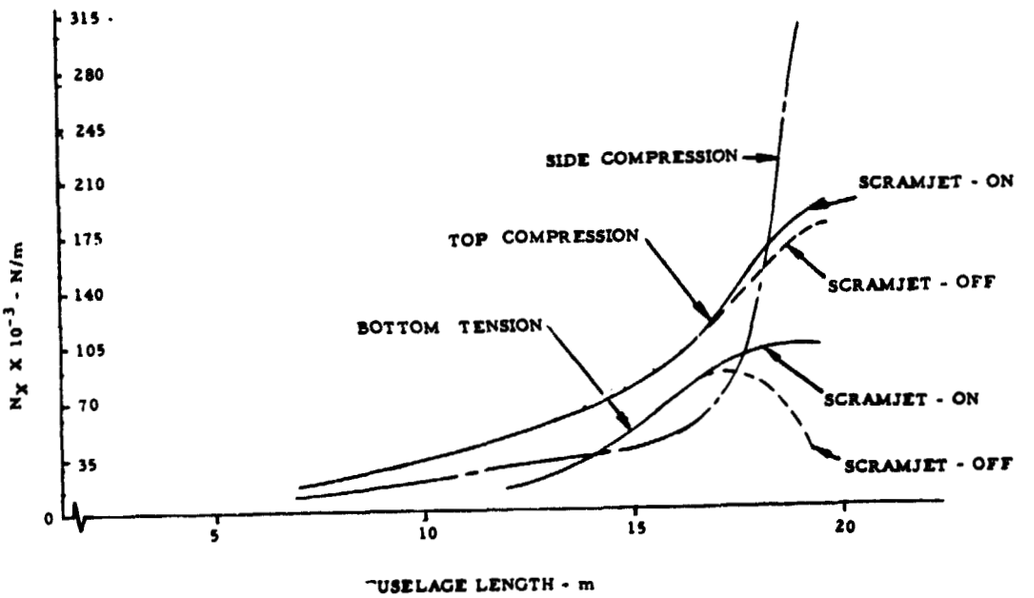

Figure 112 - Ultimate Panel Normal Running Load - 2.5 g Pullup + Max Thrust

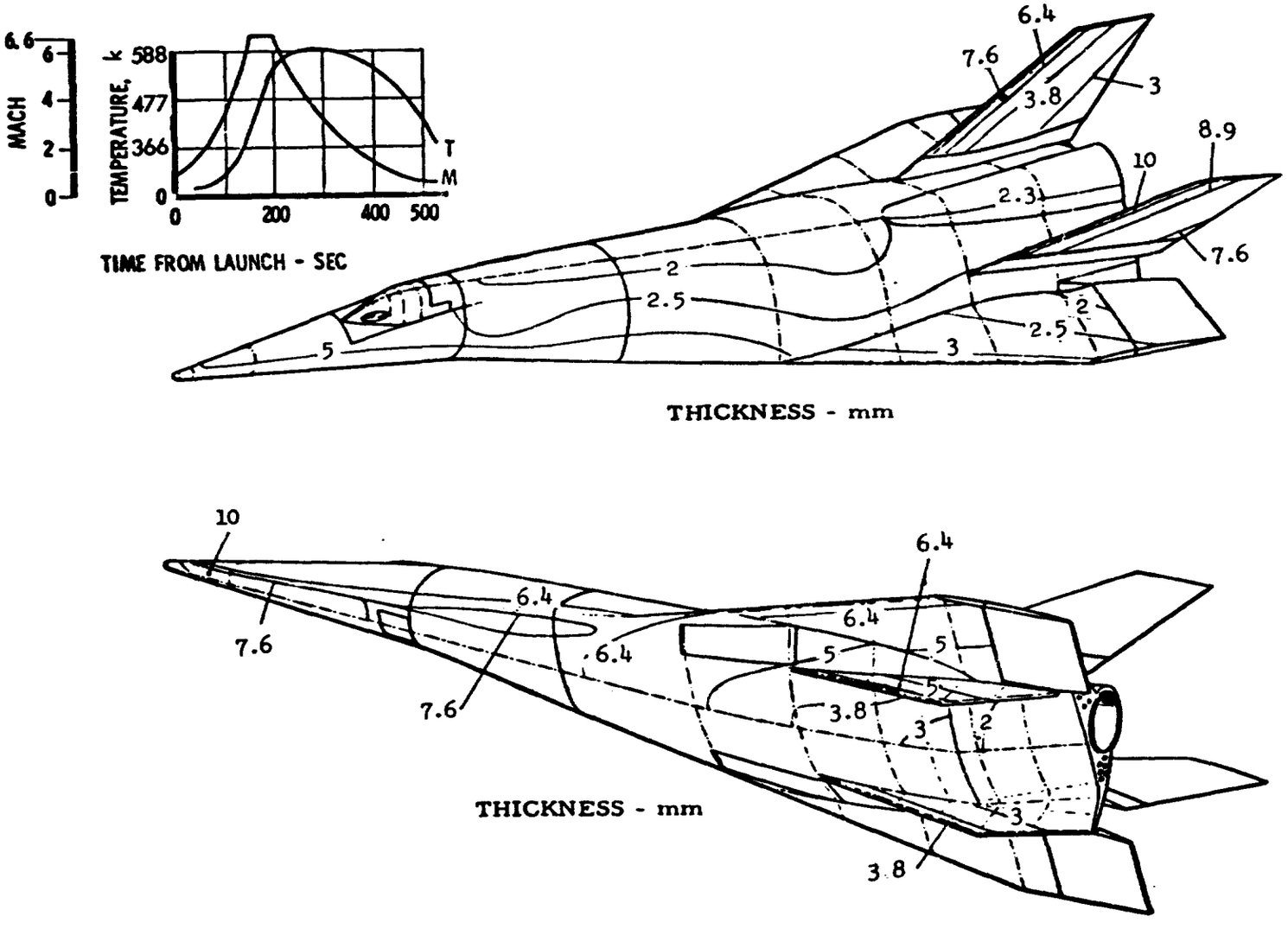

Figure 113 - Shell Thickness Distribution - Heat Sink + Structural Requirements

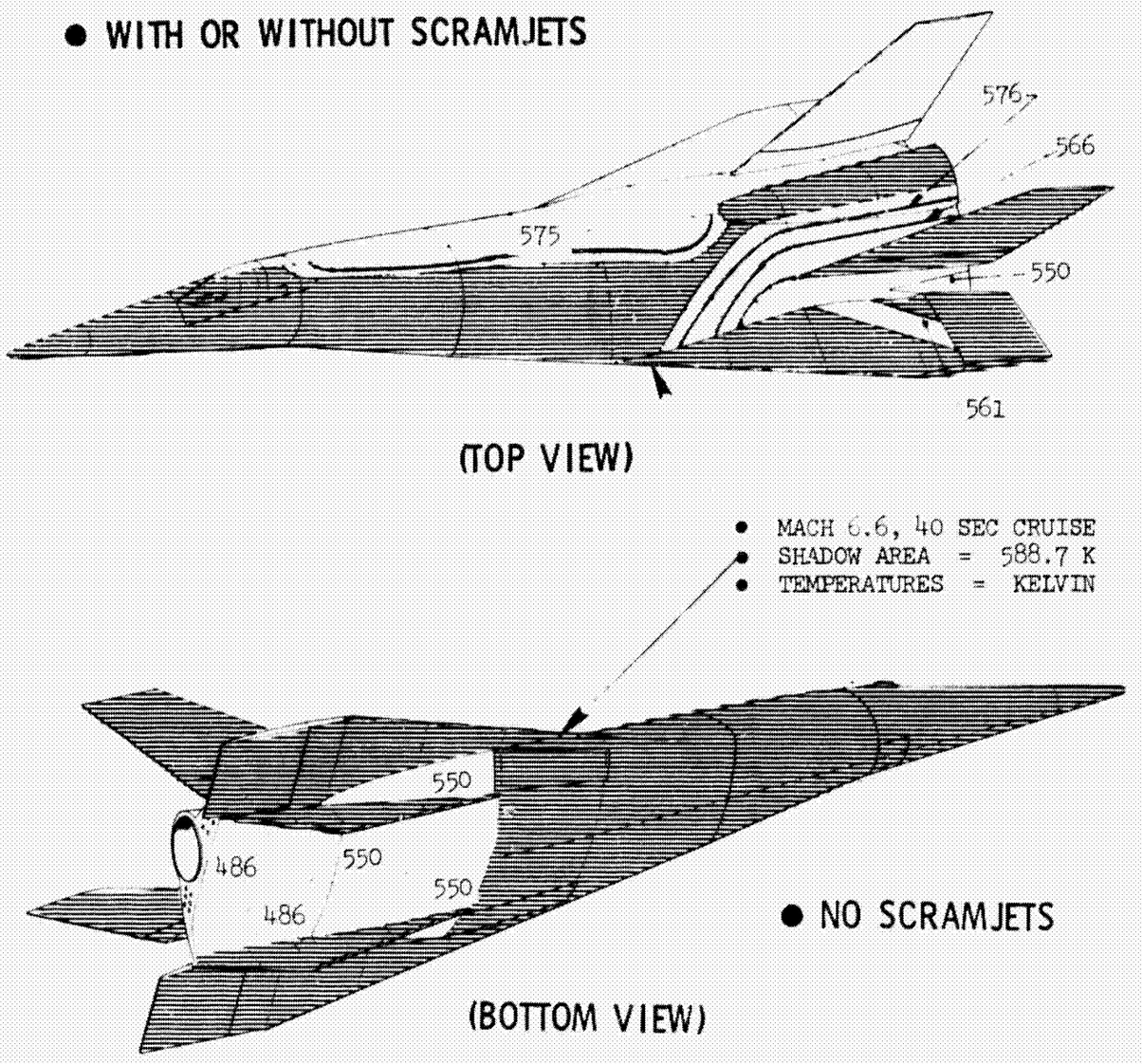

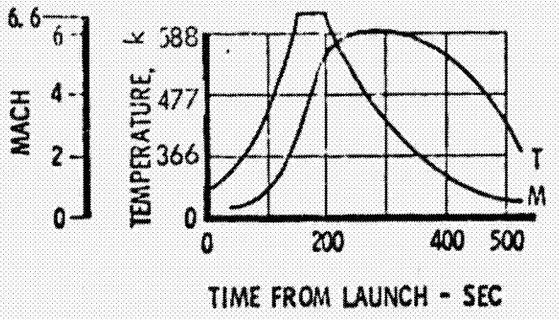

Figure 114 - Shell Temperature Distribution - Heat Sink + Structural Requirements

The skin panel gages on the Phase III vehicle had to be reevaluated because of the different heating pattern produced by the blended wing vehicle concept as described in the Thermal Analysis herein. The panel re-sizing was done in the same manner of acquiring the skin panel gages on the Phase I vehicle. Both thermal and stress requirements are accounted for in the skin panel mass of the Phase III vehicle.

The group mass statement, Table 5, shows the mass breakdown for two candidate configurations. The application of the various payload masses, cruise times and Mach numbers are described in the Aerodynamic Analysis under the section on Performance herein. Note that the fuselage mass on the scramjet configuration is changed by the restructuring of the aft body lower skin panels to accept the scramjet module as described under the Structural Concept herein.

Figure 115 depicts the center of gravity for the two missions, of the Phase III vehicle, presented in mass (weight) vs percent of body length. The percent of body length is determined by:

$$\% \text{ body } \ell = \frac{\text{body station} - 2.18}{21.3} \times 100$$

VEHICLE COST

Cost Premises - The study contract Statement of Work provides that at the start of Phase III "the contractor shall be supplied with a total initial cost figure. With this cost figure, the contractor shall apply the 'design to cost' approach to the Phase III conceptual design." This value, based on data derived in Phase II, was established at $63.4 mission for two vehicles. It is based on the following premises and exclusions:

Phase III Vehicle	Basic (Kg)	Scramjet (Kg)
Wing	749	749
Tail	722	722
Fuselage	4 403	4 576
Landing Gear	612	612
Propulsion	829	829
Propellant System	1 197	1 197
Surface Controls	354	354
Instruments	45	45
Hydraulics	141	141
Electrical	231	231
Avionics	91	91
Furnishings	136	136
Air Conditioning	181	181
Mass Empty	9 691	9 865
Flight Test Instrumentation	454	453
Pilot	129	129
Oxygen	11	11
Residual Fluids	45	45
Operating Mass Empty	10 330	10 503
Payload:		
Scramjet System		2 381
Payload Bay Package	453	
Inert Mass	10 783	12 884
Expendables:		
Pressurization System (Helium)	56	56
Propellant	(19 051)	(18 430)
LOX	13 114	12 687
PR-1	5 937	5 743
Purge and Cold Start Fluids (GN_2)	43	43
Scramjet System:		(338)
Fuel (LH_2)		283
Purge Fluid (Helium)		5
Turbine Drive Fuel (N_2H_4)		50
Launch Mass	29 934	31 751

Table 5 - Group Mass Breakdown

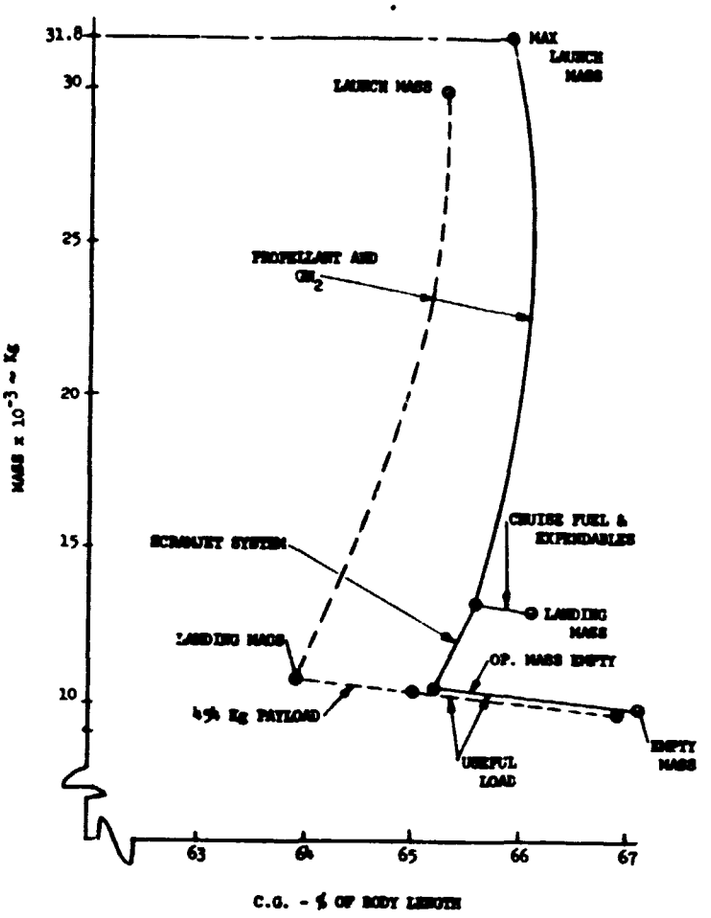

Figure 115 - Center of Gravity

- Includes initial spares, AGE and tech data
- Stated in January 1976 dollars
- Excludes:
  - Aero configuration development wind tunnel program
  - Flight test instrumentation and payload/experiment development
  - B-52 modification
  - Flight test and vehicle support after delivery
  - Rocket propulsion systems

It should be noted that these exclusions are cost estimating premises only and all of these items must be provided for in the funding for an X-24C development program. In particular, the wind tunnel test program, excluded from prior cost studies by definition, must be conducted by the airframe contractor and will be added to Phase III costs.

As in prior phases of this study, cost estimates have been prepared in the same manner and with the same degree of accuracy and confidence as for a firm priced CPFF contract proposal. We believe that we have met or bettered our objective which was to provide cost estimates in a range of plus or minus ten percent.

Complexity Factors - Table 6 provides a side-by-side comparison of many of the factors which were analyzed in developing the cost of the Phase III vehicle vs. those used for the Phase II and Phase I study vehicles. The "plus" symbol indicates the item of greater complexity with a resultant effect of increasing vehicle or program cost. A "plus" to the right hand side indicates increased complexity and cost for the Phase III vehicle as compared to the Phase II vehicle. A "plus" to the left represents reduced complexity. A "plus" on the centerline indicates no change. It should be noted that two items, the complete wind tunnel test program and a fuel system functional mockup for rocket engine testing at the Edwards AFB Rocket Propulsion Lab, are added to the program costs as requested by NASA. These are tasks that must be performed by the airframe contractor.

In addition to consideration of the foregoing complexity factors, all significant purchased equipment and Lockalloy pricing has been updated by revised supplies quotations as of August 1976.

Lockalloy Material Considerations - Because Lockalloy material cost and supplier capability are vital to the ability to produce the Phase III vehicle, these factors have been carefully reconsidered in Phase III. The more advanced aerodynamic shape and reduced thermal stress requirements of the Phase III vehicle permit the use of thinner gage Lockalloy skin material as follows:

ITEM	PHASE II	PHASE III
AERODYNAMIC CONFIGURATION	X-24C - 12 I	X-24C - L301
THERMAL PROTECTION SYSTEM	LOCKALLOY HEATSINK SKIN ⊕	SAME AS PHASE II
PROPULSION SYSTEM	MAIN BOOST - LR 105 CRUISE - 12 LR 101'S	SAME AS PHASE II EXCEPT ADD: ⊕ • IN FLIGHT PURGE • COLD START
LAUNCH MASS (WITH 8 CRUISE SCRAMJETS)	31.75 Mg ⊕	SAME AS PHASE II
DCPR MASS	8.07 Mg	8.47 Mg ⊕ (BASIC A/C WITH SCRAMJET PROVISIONS ONLY - 8.30 Mg)
SURFACE WETTED AREA	204.4 m^2	233.0 m^2 ⊕
VERTICAL CONTROL SURFACES	⊕ THREE	TWO
SPEED BRAKES	⊕ SEPARATE SPLIT FLAP AND ACTUATOR SYSTEM ON CENTER VERTICAL	INCLUDED IN ALL MOVEABLE VERTICAL TAIL SYSTEM
PAYLOAD BAY STRUCTURE	⊕ DUAL WALL CONSTRUCTION	SINGLE WALL - COMPARABLE TO MAIN FUSELAGE STRUCTURE
COMPOUND CONTOUR LOCKALLOY SKIN PANELS	NIL	⊕ APPROX. 50 (7% OF TOTAL)
TOOLING FOR LOCKALLOY	⊕ FORMED ON HEATED CERAMIC DIES	COLD FORMING SINGLE CURVATURE
FUNCTIONAL SYSTEMS (CONTROLS, AVIONICS, FUEL, ECS, ELECTRICAL, HYDRAULICS GEAR, COCKPIT FURNISHINGS, ESCAPE)	ESSENTIALLY THE SAME ⊕ ⊕	
PARTS COUNT	ESSENTIALLY THE SAME	
SCRAMJET INSTALLATION	ESSENTIALLY THE SAME ⊕	
CONTRACTOR PERFORMS COMPLETE AERO DEVELOPMENT WIND TUNNEL TESTING (USING GOVT FACILITIES)	SUPPLEMENTAL TESTING ONLY	INCLUDED ⊕
CONTRACTOR SUPPLIES "BOILER PLATE" FUEL RIG FOR POWER PLANT TESTING AT RPL	EXCLUDED	INCLUDED ⊕
GOVERNMENT FURNISHED ITEMS AND SUPPORT	⊕ SAME, EXCEPT AS NOTED ABOVE	

Table 6 - Phase II vs Phase III Complexity Factor Comparison

Phase II		Phase III	
Maximum	Minimum	Maximum	Minimum
15 mm	4 mm	10 mm	2 mm

The higher cost per kilogram of the thinner material is confirmed by the supplier, Kawecki Berylco Industries, and included in the Phase III vehicle cost. While the cost per kilogram increases substantially with gage reduction, the actual cost per unit of vehicle surface area does not, and the use of thinner gages is cost effective. Gages below 4 mm are achieved by grinding (rather than progressive rolling) a technique well established in the manufacture of thin gages of other metals as well as Lockalloy.

There are no processes or techniques in the manufacture of Lockalloy material and the fabricating of parts for the Phase III vehicle which have yet to be demonstrated.

Phase III Vehicle vs Design-to-Cost Objective - Did the vehicle as initially configured meet the design-to-cost objective? The requirement to meet the Phase III constraints imposed by scramjet integration, B-52 compatibility, drag reduction and stability improvements which, in turn, created the increased complexity previously described, has caused the initial vehicle to exceed the design-to-cost objective by 7 percent. However, this vehicle also exceeds the Phase III performance target. The comparison is summarized as follows:

	Design-to-Cost Objective	Phase III Vehicle	Cost Increase From Complexity Factors
Two vehicles plus initial spares, AGE and data	$63.4M	$67.9M	$4.5M (7%)
Added Elements:			
Wind Tunnel Test		$ 1.5M	
Fuel Test rig for RPL		.5M	
Adjusted Total		$69.9M	

Although the basic vehicle did not meet the design-to-cost objective, subsequent sections of this report will address a vehicle that will meet the objective.

Cost Breakdown by Element - Table 7 is a breakdown by major cost element for one or two scramjet vehicles. Engineering includes design, design support, wind tunnel testing, mockups, materials/structures and functional system development testing, flight test planning, the functional mockup for rocket testing and all required engineering test parts and materials. Tooling includes planning and quality assurance as well as fabrication and assembly labor. Lockalloy material cost is included under Manufacturing Material and Equipment. GFAE includes the landing gear, communications systems and an allowance to refurbish other GFAE from the X-15 and X-24B programs. Spares and AGE are provisioned on the same basis as for Phase I and Phase II of this study. All estimates except for GFAE include an allowance for contractor fee of 10 percent.

Vehicle Cost Vs Launch Mass - Trade-off studies in Phase II have established a relationship between cost and launch mass for X-24C vehicles of the same configuration. This relationship remains valid even though the vehicle changes. Figure 116 displays the cost vs launch mass relationship. The design-to-cost objective for Phase III is $63.4 million for two vehicles, a value established

	(JAN 1976 DOLLARS IN THOUSANDS)	
	ONE VEHICLE	TWO VEHICLES
ENGINEERING	$18,036	$18,582
TOOLING	12,055	12,611
MFG LABOR	11,785	21,213
MFG MATL AND EQUIP	7,500	12,369
GFAE	344	688
SUB-TOTALS	$49,720	$65,463
INITIAL SPARES, AGE AND DATA	3,900	4,400
TOTAL - PHASE III	$53,620	$69,863

Table 7 - Phase III Vehicle Cost Estimates

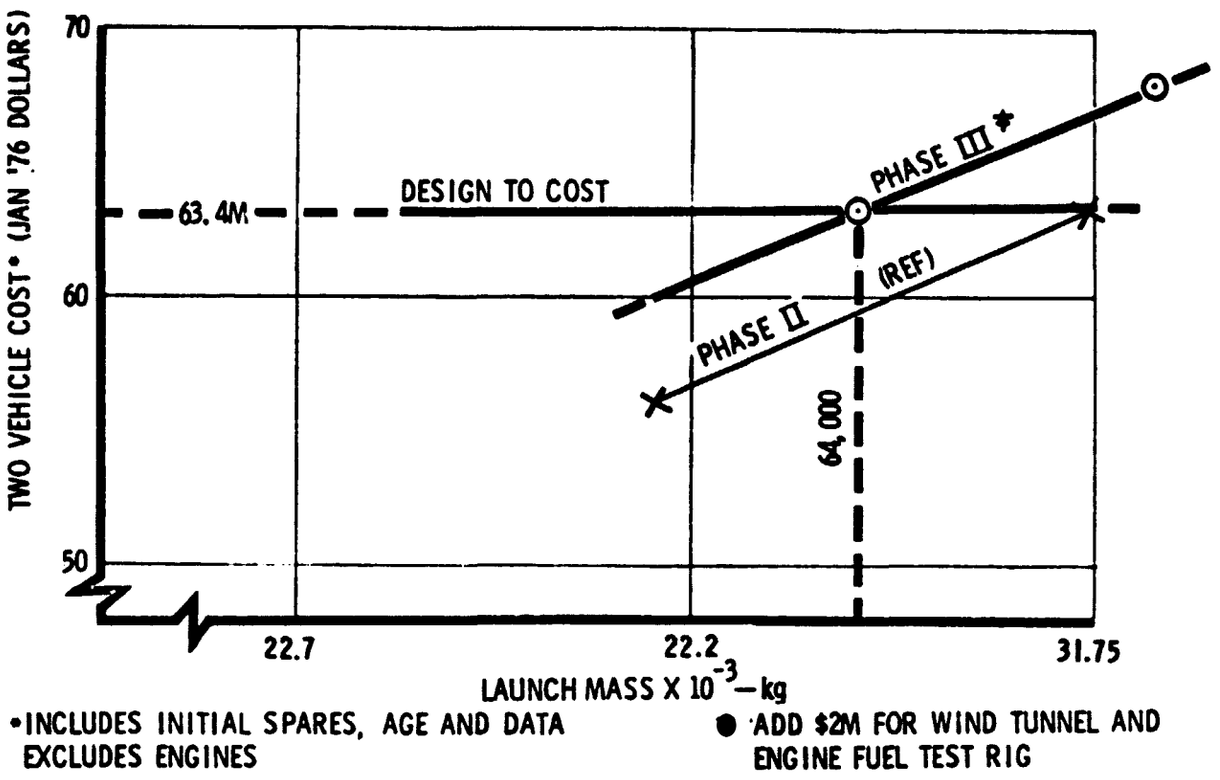

Figure 116 - Phase III Scramjet Vehicle Cost vs Launch Mass

based on a 31.75 Mg mass/8 scramjet/Mach 6.57 Phase II vehicle. (It should be observed that the Phase II vehicle was not viable for the required mission.) Cost vs launch mass from the Phase II study is shown for reference. For a given launch mass the Phase III vehicle will cost approximately 7 percent greater than the vehicle from Phase II.

Two plot points are significant on the Phase III cost line. The upper point is the Phase III vehicle which actually has a capability of a 32.39 Mg mass when fully fueled. The vehicle which meets the design-to-cost objective will have a launch mass of 29.03 Mg.

Vehicle Cost Vs Mach Number - Figure 117 shows the relationship between vehicle cost and Mach number, a relationship also validated in Phase II of the study. In this case the upper point on the Phase III cost line is the Phase III vehicle

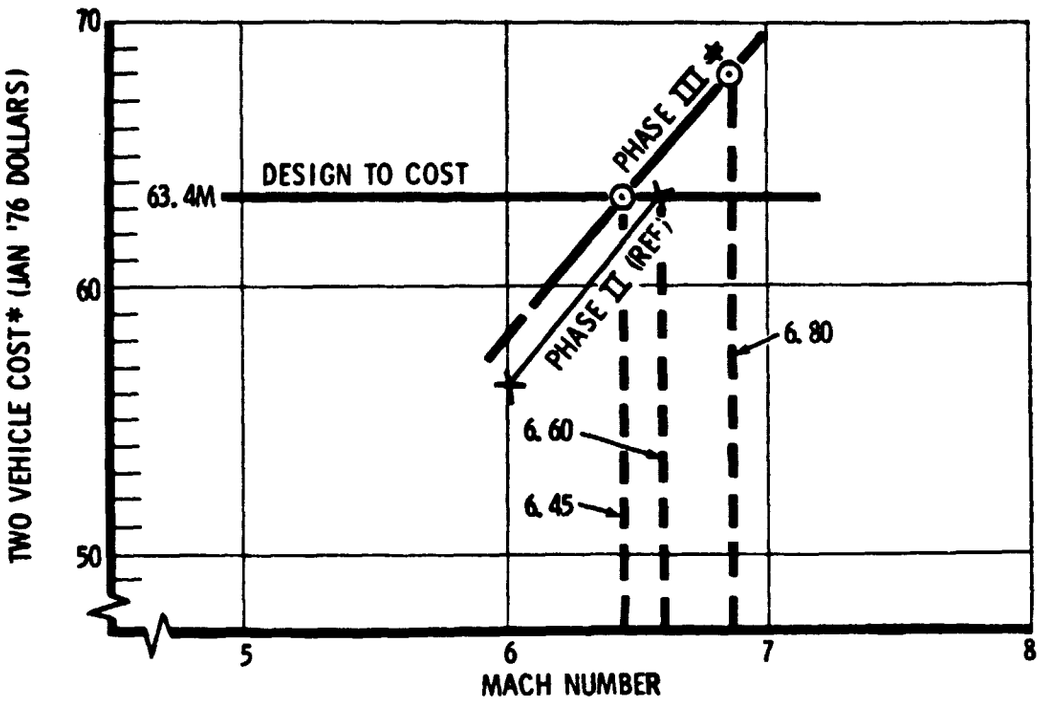

Figure 117 - Phase III Scramjet Vehicle Cost vs Mach Number

which has a capability of Mach 6.85 cruise for 40 seconds with 8 scramjets. For a given Mach number the vehicle cost is only 3 percent greater than the cost of the X-24C Phase II vehicle. The "design-to-cost" vehicle will have a capability of Mach 6.45 for 40 seconds at a launch mass of 29.03 Mg. Two Mach 6.0 vehicles can be produced for approximately $58 million.

It should be noted on both Figure 116 and Figure 117 that the $2 million for wind tunnel tests and engine fuel test rig are excluded in order to make a direct comparison to Phase II data.

Scramjet Installation Costs - All cost estimates presented to this point are based on the Phase III vehicle as configured with scramjets installed, although the cost of the scramjet package (including fuel tanks and plumbing normally supplied

by the airframe manufacturer) is excluded. In actuality, it is anticipated that the X-24C vehicle will be initially constructed in a basic configuration with the scramjet engine package and conversion kit added later. This, of course, depends on the availability of the scramjet relative to the basic vehicle development. The basic vehicle will have aerodynamic and structural provisions for later scramjet conversion. This approach will result in a $1.1 million lower cost for the basic vehicles. The subsequent cost to convert two vehicles later in the program may be considered as part of the scramjet engine experiment cost if desired. These estimates are summarized as follows:

	Two Vehicles (Jan. 1976 Dollars)
X-24C Phase III Basic vehicle as configured without scramjets for initial flight testing	$68.6M
X-24C Phase III Scramjet vehicle as developed and manufactured for scramjet installation at initial flight	$69.9M
Cost for conversion kit and installation (for adding scramjets to basic vehicle)	$ 3.4M

Note: In all cases the scramjet engine package including related pumps, computer and controls are assumed to be GFE.

Other Cost Factors - Other factors which can affect the total X-24C program cost have also been addressed in the Phase III study. These include the method of development program management and contracting and performing the program to an optimum schedule pace.

One of the premises supplied by NASA at the inception of this study specified that "prototype or model shop type management and methods" should be utilized in the vehicle development program. To illustrate how the Lockheed Skunk Works views the importance of this aspect of the proposed X-24C program and its potential impact on cost, Table 8 lists data from two other studies and Lockheed ADP's

DEVELOPMENT CONTRACT COST RATIOS

DATA BASED ON:			
LOCKHEED-CALIFORNIA CO. STUDY	"PROTOTYPE"	"MINIMAL"	"NORMAL"
USN/CARRIER ONBOARD DELIVERY (COD) (JAN 1972)	1.0	1.77	2.03
	"CO. FUNDED"	"FLY-BEFORE-BUY"	"CONCURRENCY"
ROCKWELL STUDY			
NASA REPORT CR114368-UTX/T-39 (SEPT 1971)	1.0	1.45	1.72
	"SKUNK WORKS"	STANDARD GOVT DEV. CONTRACT	FULL MIL-SPEC PRODUCTION
SKUNK WORKS ESTIMATE (AUGUST 1976)	1.0*	1.5	NOT APPLICABLE FOR NHFRF

*BASED ON C-130, U-2, JETSTAR, YF-12, SR-71 AND PROPOSED NHFRF

Table 8 - Other Factors Affecting Cost

estimate of "Skunk Works" vs a more standard Government contracting and management approach. Data is based on actual cost performance on the models listed.

It should be noted that, while there are differences in the terminology used by various organizations, there is a correlation between the cost relationships. The Skunk Works believes that costs can increase as much as 50 percent over the Phase III estimates in this study if full standard procedures are used.

The optimum schedule for the X-24C Phase III first vehicle is 24 to 27 months from go-ahead to delivery to NASA/USAF. A second vehicle can be delivered 6 months later. Funding limitations which cause program schedules to be significantly stretched from the optimum have an adverse effect on cost. This results from both the economic escalation normally encountered and the inefficiencies of retaining a design team and other specialists for longer periods. Stretching the

X-24C schedule by 12 months will add 8 to 10 percent to X-24C Phase III costs. Skunk Works experience strongly indicates that a contractor should be permitted to design and develop a new aircraft at his own optimum pace for maximum effectiveness.

Optional Cost Items - Two items represent an opportunity to consider alternative installation costs for either one or both X-24C Phase III vehicles. These are the single vs dual walled payload bay and the scramjet conversion kit approach.

Single Wall vs Dual Wall Payload Bay - The X-24C Phase III design provides for a 3.7 meter long interchangeable payload bay. The basic design and cost estimates for the Phase III vehicle are shown in this report based on a "single wall" construction. This saves 190 kg of airframe structure which equates to approximately 680 kg of vehicle launch mass with its attendent loss of performance.

To provide for versatility of experiments a "dual wall" payload bay construction can be utilized. This adds complexity and cost as follows:

Incremental increase for one vehicle . . . . . $ 764,000

Incremental increase for two vehicles $1,111,000

To summarize the options available for alternative payload bay costs refer to Table 9.

The total cost to design and manufacture separate interchangeable 3.7 meter single wall payload bays at a later time (presumably as a part of the scramjet experiment) is estimated at:

For one vehicle $2,044,000

For additional payload bays . . . . . Approx. $1,000,000 each

(January 1976 Dollars in Thousands)			
	1st Vehicle	2nd Vehicle	Total
1st Vehicle - Single Wall 2nd Vehicle - Single Wall	$53,620 ———	——— $16,243	$69,863
1st Vehicle - Dual Wall 2nd Vehicle - Dual Wall	$54,384 ———	——— $16,590	$70,974
1st Vehicle - Dual Wall 2nd Vehicle - Single Wall	$54,384 ———	——— $17,265	$71,649
1st Vehicle - Single Wall 2nd Vehicle - Dual Wall	$53,620 ———	——— $18,029	$71,649

Table 9 - Alternate Payload Bay Costs

Scramjet Conversion Options - Depending on program requirements, it is possible that only one X-24C vehicle will be required to be dedicated to scramjet engine testing with the second vehicle assigned to other hypersonic research testing (while retained as a backup to the scramjet test aircraft). The design of the X-24C Phase II permits this approach.

The incremental costs previously stated in this report for scramjet installation are summarized as follows:

	(January 1976 Dollars in Thousands)		
	First Vehicle	Second Vehicle	Total For Two
X-24C Basic Vehicle	$52,890	$15,910	$68,800
Δ for Scramjet installation provisions at initial delivery	$ 730	$ 333	$ 1,063
Phase III Scramjet Vehicle	$53,620	$16,243	$69,863
For conversion kits and scramjet engine installation	$ 2,534	$ 866	$ 3,400

Therefore, to provide an option with one vehicle configured for scramjets and the other as a basic hypersonic test bed with only aerodynamic and structural provisions for scramjets:

	First Vehicle (With Scramjets)	Second Vehicle (No Scramjets)	Total For Two
Vehicle	$53,620	$15,910	$69,530
Scramjet Installation	2,534		2,534
Total Program	$56,154	$15,910	$72,064

CONCLUSIONS

As a result of this study, it is evident that it is practical to design and build a high performance NHFRF vehicle with today's state of the art.

- The vehicle launched at 31.75 Mg from the B-52, can cruise for 40 seconds at Mach 6.78 on scramjets.

- The vehicle as designed for scramjet cruise at Mach 6.6 has a capability of approaching Mach 8 with 453.6 Kg of payload in lieu of scramjets.
- This same vehicle has the capability of cruising on rockets, without scramjets, for approximately 70 seconds with 2.27 Mg payload at Mach 6.

The X-24C two vehicle cost can be kept within $70M in January 1976 dollars, including spares, AGE, and Data, but excluding engines and other GFE.

In order to reduce cost the X-24C vehicle can be scaled to lesser launch mass and lesser capability.

- For a Mach 6 maximum scramjet cruise capability the two vehicles can be produced for under $60M.

Design-to-cost capability is Mach 6.45, 40 seconds scramjet cruise at a launch mass of 29.03 Mg.